SKELETAL DEVELOPMENT AND BONE HEALING IN HIV-1 TRANSGENIC ANIMAL MODELS

A Dissertation
Presented to
The Academic Faculty

by

Jason Lee Wang

In Partial Fulfillment
of the Requirements for the Degree
Doctor of Philosophy in
Bioengineering

Georgia Institute of Technology
December 2018

SKELETAL DEVELOPMENT AND BONE HEALING IN HIV-1 TRANSGENIC ANIMAL MODELS

Approved by:

Dr. Robert E. Guldberg, Advisor
School of Mechanical Engineering
Georgia Institute of Technology

Dr. Manu O. Platt
Department of Biomedical Engineering
Georgia Institute of Technology

Dr. M. Neale Weitzmann
School of Medicine
Emory University

Dr. Johnna S. Temenoff
Department of Biomedical Engineering
Georgia Institute of Technology

Dr. Rudolph L. Gleason
School of Mechanical Engineering
Georgia Institute of Technology

Date Approved: June 12, 2018

To my friends, family, and most of all, my wife for their unending support.

Especially to my wife for her patience, perseverance, support, and love through it all.

ACKNOWLEDGEMENTS

God, grant me the serenity
To accept the things I cannot change,
Courage to change the things that I can,
And the wisdom to know the difference.

Reinhold Neibuhr

Reflecting on my PhD inevitably leads me to reflecting on the entirety of my time in the Guldberg Lab. I cannot adequately capture in words the deep gratitude and respect that I have for my advisor, Dr. Robert Guldberg. Through the many years that I have struggled in his lab and under his guidance, I have grown tremendously, and for that, I cannot thank him enough. I would be remiss if I did not also acknowledge the significant support, input, and understanding that my committee has provided me during my PhD. To Dr. Neale Weitzmann, Dr. Rudy Gleason, Dr. Manu Platt, and Dr. Johnna Temenoff, a far too inadequate but sincere 'Thank You' to all of you for being a part of my PhD committee through it all.

A special thank you to Angela and Hazel for being the anchors of our lab and a source of fun conversation and distraction through the stresses of life and research. Of course, I must thank Vivian Johnson not just for helping all of us administratively, but also for her honesty and genuine spirit that helped me to stay grounded. I must also thank all the Guldberg lab members that I have had the privilege of working with – both past and present – without whom the completion of this PhD would not have been possible. The importance of the relationships and interactions for me remain more valuable unwritten

and unspoken and the following list captures the weight of this far more than my words could. Thank you all.

Angela Lin	Ashley Allen, PhD	Lina Maria Mancipe Castro
Hazel Stevens	Lauren Priddy, PhD	Ryan Akman
Jessica Green, PhD	David Reece, PhD	Gilad Doron
Tamim Diab, PhD	Brennan Torstrick, PhD	Casey Vantucci
Joel Boerckel, PhD	Albert Cheng, PhD	Ramesh Subbiah, PhD
Chris Dosier, PhD	Marian Hettiaratchi, PhD	Vivian Johnson
Nick Willett, PhD	Giuli Salazar-Noratto, PhD	Rose Brito
Brent Uhrig, PhD	Andrew Miller, PhD	Blair Naples
Laxmi Krishnan, PhD	Olivia Burnsed, PhD	Alex Cavallaro
Alice Li, PhD	Marissa Ruehle	Yazdan Raji
Tanushree Thote, PhD	Brett Klosterhoff	

I must also acknowledge the PRL staff and IBB staff who were integral to my success. Thank you to Dr. Laura O'Farrell, Kim Benjamin, Ogeda Blue, Altair Rivas, and the rest of the PRL staff for keeping our animals well cared for and our research as smooth as possible. Thank you to Laura Paige for making sure I stick to my deadlines and for always providing a firm but friendly presence for the BioE students. A special thank you to Aqua Asberry not just for her help in the histology core, but for her friendship and support through all the many years we have known each other.

A special thank you to all those who have helped me as I worked to develop and hone my passion and skills for teaching: the CTL staff past and present (especially Dr. Damon Williams, Dr. Dia Sekayi, Dr. Daniel Haynes, and Dr. Chaohua Oh), Dr. Antonia

Antoniou, Dr. Larry Jacobs, Dr. Roberta Berry, Dr. Wendy Newstetter, Dr. Michael Miller, Dr. Scottie-Beth Fleming, Dr. Alexandra Strong, and Dr. Matthew Priddy.

Finally, no words can possibly capture my gratitude for the support and love my friends and family provided me through my whole graduate career at Georgia Tech. Thank you all.

TABLE OF CONTENTS

ACKNOWLEDGEMENTS **v**

LIST OF TABLES **x**

LIST OF FIGURES **xi**

LIST OF SYMBOLS AND ABBREVIATIONS **xiii**

SUMMARY **xvi**

CHAPTER 1. SPECIFIC AIMS **1**
1.1 Introduction **1**
1.2 Aim I **2**
1.3 Aim II **3**
1.4 Aim III **4**
1.5 Significance and Scientific Impact **5**

CHAPTER 2. BACKGROUND **7**
2.1 Bone Physiology **7**
2.1.1 Bone Structure and Function 7
2.1.2 Bone Development and Healing 9
2.2 HIV-1 Pathology **11**
2.2.1 Virus and Infection 11
2.2.2 Epidemiology 13
2.2.3 HIV-Associated Comorbidities 14
2.3 HIV and Bone **15**
2.3.1 Low Bone Mass 15
2.3.2 Bone Healing 20
2.4 HIV and Animal Models **21**

CHAPTER 3. SKELETAL PHENOTYPE AND FRACTURE HEALING IN AN HIV-1 TRANSGENIC MOUSE **24**
3.1 Introduction **24**
3.2 Materials and Methods **26**
3.2.1 HIV-1 Transgenic Mouse Model 26
3.2.2 X-Ray Radiographs and MicroCT 28
3.2.3 Mechanical Testing 29
3.2.4 Vascular Perfusion and Analysis 30
3.2.5 Statistics 31
3.3 Results **31**
3.3.1 Bone Microarchitecture 31
3.3.2 Bone Biomechanical Phenotype 39
3.3.3 Radiographic and MicroCT Evaluation of Fracture Healing 43
3.3.4 Fracture Callus Biomechanical Properties 46

3.3.5 Early Vascularization of Fracture Callus Analysis 47
3.4 Discussion 49

CHAPTER 4. SKELETAL PHENOTYPE OF GROWING HIV-1 TRANSGENIC RAT 56
4.1 Introduction 56
4.2 Materials and Methods 58
4.2.1 HIV-1 Transgenic Rat Model 58
4.2.2 Microcomputed Tomography 59
4.2.3 Blood Collection and Serological Analysis 60
4.2.4 Mechanical Testing 60
4.2.5 Statistics 61
4.3 Results 61
4.3.1 General Observations 61
4.3.2 Longitudinal Bone Microarchitecture 62
4.3.3 Bone Turnover Markers 71
4.3.4 Bone Biomechanical Phenotype 72
4.4 Discussion 75

CHAPTER 5. BONE HEALING IN HIV-1 TRANSGENIC RAT 81
5.1 Introduction 81
5.2 Materials and Methods 83
5.2.1 Surgical Procedure 83
5.2.2 Radiography and Microcomputed Tomography 84
5.2.3 Biomechanical Testing 84
5.2.4 Statistics 80
5.3 Results 85
5.3.1 Segmental Defect Surgery 85
5.3.2 Radiographic and MicroCT Evaluation of Bone Healing 86
5.3.3 Biomechanical Testing 89
5.4 Discussion 91

CHAPTER 6. SUMMARY AND FUTURE DIRECTIONS 96
6.1 Overall Summary 96
6.2 Skeletal Development and HIV 98
6.3 Bone Healing and HIV 103
6.4 Bone, ART, and HIV 106
6.5 Final Conclusions 107

APPENDIX A. PROTOCOLS 109
A.1 Mouse Fracture Surgery Protocol 109
A.2 Rat Tail Ventral Artery Blood Collection and Serum Isolation Protocol 112

APPENDIX B. SUPPLEMENTAL DATA 116

REFERENCES 120

LIST OF TABLES

Table 5-1	Pearson's Correlation Coefficient (*r*) between biomechanical properties and microCT measures (n = 5 WT, n = 8 HIV).	90
Table B-1	MicroCT Bone Microarchitecture - HIV-1 tg Male Mouse (FVB/N)	116
Table B-2	Bone Biomechanical Properties - HIV-1 tg Male Mouse (FVB/N)	117
Table B-3	Mechanical Properties of Contralateral Intact Femurs - HIV-1 tg Male Mouse Fracture Study	118
Table B-4	MicroCT Bone Microarchitecture - FVB/N administered AZT or Water	119
Table B-5	MicroCT Bone Microarchitecture – HIV-1 tg Rat (Male, 14 months old)	122

LIST OF FIGURES

Figure 3-1: (A) Representative microCT 3D reconstructions of femur mid-diaphysis. (B) MicroCT evaluation of femur mid-diaphysis. 33
Figure 3-2: (A) Representative microCT 3D reconstructions of distal femur epiphysis. (B) MicroCT evaluation of trabecular bone at distal femur epiphysis. 35
Figure 3-3: (A) Representative microCT 3D reconstructions of distal femur metaphysis. (B) MicroCT evaluation of trabecular bone at distal femur metaphysis. 36
Figure 3-4: (A) Representative microCT 3D reconstructions of L6 vertebra. (B) MicroCT evaluation of trabecular bone at L6 vertebra. 38
Figure 3-5. Biomechanical properties of whole femurs tested in three-point bending. (A) Measured structural properties. (B) Estimated derived material properties. .. 40
Figure 3-6. Biomechanical properties of L6 vertebrae tested in compression. (A) Measured structural properties. (B) Estimated derived material properties. .. 42
Figure 3-7. Representative 2-D radiographs of fracture healing 44
Figure 3-8. MicroCT evaluation of fracture healing. 45
Figure 3-9. Biomechanical properties of fractured femurs. 46
Figure 3-10. MicroCT analysis of Week 1 fracture callus vascularization. (A) Representative 3-D microCT reconstruction. (B) Quantitative evaluation of callus vasculature. 48
Figure 4-1. Body mass of WT and HIV rats. 62
Figure 4-2. Femur lengths of WT and HIV animals. 63
Figure 4-3. MicroCT evaluation of cortical bone morphology at the femur mid-diaphysis. 64
Figure 4-4. MicroCT evaluation of trabecular bone architecture at the distal femur epiphysis. 66
Figure 4-5. MicroCT evaluation of trabecular bone architecture at the distal femur metaphysis 68
Figure 4-6. MicroCT evaluation of trabecular bone architecture at the L6 vertebra. 70
Figure 4-7. Bone turnover markers in HIV and WT rats. 71

Figure 4-8. Mechanical properties of the femur. (A) Measured structural properties. (B) Estimated derived material properties. 73
Figure 4-9. Mechanical properties of the L6 vertebra. (A) Measured structural properties. (B) Estimated derived material properties. 74
Figure 5-1. Representative longitudinal 2-D radiographs of bone healing in WT and HIV animals. 87
Figure 5-2. MicroCT analysis of bone healing response. (A) Representative Week 12 *ex vivo* 3-D reconstructions of defect area. Cortical bone ends have been included for orientation. (B) Longitudinal evaluation of new bone growth. 88
Figure 5-3. Biomechanical properties of bone defects. n = 6 WT; n = 8 HIV. 90

Figure B-1. Effect of AZT on biomechanical properties of whole femurs tested in three-point bending. (A) Measured structural properties. (B) Estimated derived material properties 120
Figure B-2. Effect of AZT on biomechanical properties of L6 vertebrae tested in compression. (A) Measured structural properties. (B) Estimated derived material properties. 121
Figure B-3. Biomechanical properties of bones from HIV-1 tg male rats. (A) Measured structural properties of whole femurs tested in 3-point bending. (B) Measured structural properties of L6 vertebrae tested in compression. 123
Figure B-4. Growth of HIV-1 tg female rats and littermates. 124

LIST OF SYMBOLS AND ABBREVIATIONS

AIDS	Acquired immunodeficiency syndrome
ALP	Alkaline phosphatase
ANOVA	Analysis of Variance
ART	Antiretroviral therapy
BA	Bone area
BMD	Bone mineral density
BMP	Bone morphogenetic protein
BMP-2	Bone morphogenetic protein-2
BV/TV	Bone volume fraction (Bone volume/Total volume)
CCR5	Chemokine receptor 5
Conn.D	Connectivity density
Ct.Th	Cortical thickness
CTx	C-terminal telopeptides of type I collagen
CXCR4	Chemokine receptor 4
DNA	Deoxyribonucleic acid
DXA	Dual energy X-ray absorptiometry
FEA	Finite element analysis
GLM	General linear model
HAART	Highly active antiretroviral therapy
HCV	Hepatitis C virus
HIV	Human Immunodeficiency Virus
HIV-1	Human Immunodeficiency Virus 1

HR-pQCT	High resolution peripheral quantitative computed tomography
IACUC	Institutional Animal Care and Use Committee
LTR	Long terminal repeat
MA	Marrow area
M-CSF	Macrophage colony-stimulating factor
microCT	Microcomputed tomography
MOI	Moment of inertia
MSM	Men who have sex with men
OPG	Osteoprotegerin
PBS	Phosphate buffered saline
pMOI	Polar moment of inertia
pQCT	Peripheral quantitative computed tomography
RANK	Receptor activator of NF-κB
RANKL	Receptor activator of NF-κB ligand
rhBMP-2	Recombinant human bone morphogenetic protein-2
RNA	Ribonucleic acid
ROI	Region of interest
SEM	Standard error of the mean
SHIV	Simian-human immunodeficiency virus
SIV	Simian immunodeficiency virus
SMI	Structure model index
Tb.N	Trabecular number
Tb.Sp	Trabecular spacing
Tb.Th	Trabecular thickness
TDF	Tenofovir disoproxil fumarate

tg	Transgenic
VOI	Volume of interest
WT	Wild Type
SIV	Simian immunodeficiency virus
SMI	Structure model index
Tb.N	Trabecular number
Tb.Sp	Trabecular spacing
Tb.Th	Trabecular thickness
TDF	Tenofovir disoproxil fumarate
tg	Transgenic
VOI	Volume of interest
WT	Wild type

SUMMARY

HIV and AIDS have drastically compromised the quality of life and lifespan for millions of people worldwide. The increasing effectiveness of and access to antiretroviral therapy has dramatically increased the life expectancy of those infected with HIV to nearly that of the general population. Once considered a death sentence, a positive HIV diagnosis with appropriate treatment is now a chronic condition bringing with it the premature onset of disorders traditionally associated with the natural aging process including cardiovascular disease, neurocognitive decline, kidney disease, and osteoporosis. It is well understood that HIV infection is a risk factor for osteopenia and osteoporosis and subsequently for fragility fractures. More recently, studies have established an increase in fracture prevalence in the HIV-infected population. However, the effects of HIV infection on bone are difficult to investigate in the clinical setting. Traditional risk factors for osteoporosis – such as vitamin D deficiency, drug use, smoking, and alcohol use – can complicate any observed effects that HIV may have. Despite the increased risk for fracture and fracture prevalence in the HIV-infected population, relatively few clinical studies and no pre-clinical studies have investigated the potential for HIV infection to adversely affect fracture healing.

The main goal of this work was to investigate the effects of HIV on skeletal growth and bone healing as exhibited by HIV-1 transgenic rodent models, specifically the mouse and the rat. In addition to the extensive body of bone research conducted in mouse and rat models, the transgenic rodent models offer significant advantages for pre-clinical research over the more recognized non-human primate and humanized mouse models, including less time and expense. Additionally, HIV-1 transgenic rodent models have been used to

study various comorbidities associated with HIV infection. Thus, we first characterized the skeletal phenotype in the HIV-1 transgenic mouse model by evaluating bone microarchitecture and biomechanics. We further assessed whether HIV mice present with impairment in long bone fracture healing. Second, we characterized the longitudinal skeletal changes in the growing HIV-1 transgenic rat. Finally, we investigated alterations to bone healing in the HIV-1 transgenic rat using a critically-sized segmental bone defect model.

This work presents findings supporting an HIV associated skeletal phenotype that is exhibited by both HIV-1 transgenic mice and rats that reflects the clinical literature. Specifically, HIV animals have reduced cortical and trabecular bone mass and altered bone microarchitecture at multiple skeletal sites. These deleterious effects on bone structure resulted in decreased whole bone mechanics and may be age-dependent in HIV-1 transgenic rodents. More significantly, we present the first pre-clinical investigation into fracture healing in the HIV-1 transgenic rodents showing impaired bone healing in both HIV-1 transgenic mice and rats. Our findings support the clinical need to monitor skeletal health in the HIV infected population and further emphasize the unmet need for robust clinical studies to investigate bone healing in this growing and aging population.

CHAPTER 1. SPECIFIC AIMS

1.1 Introduction

An estimated 36.7 million people worldwide are infected with the human immunodeficiency virus (HIV) and 1.8 million people were newly infected in 2016 [1]. Without treatment, HIV infection typically progresses to end-stage acquired immune deficiency syndrome (AIDS) and eventually death. The effective administration of antiretroviral therapy (ART) has drastically improved the life expectancy of the HIV infected population [2, 3]. Once considered a death sentence, a positive HIV diagnosis with appropriate treatment is now a chronic condition bringing with it the premature onset of disorders traditionally associated with the natural aging process including cardiovascular disease, renal (kidney) disease, hepatic (liver) disease, neurocognitive decline, and bone disorders [4-7].

It is commonly recognized that HIV infection is associated with low bone mineral density (BMD) and consequent risk for osteoporosis and fragility fractures [8]. In recent years, it has been shown that the prevalence of fracture with HIV infection is also increased, further emphasizing HIV's negative effect on skeletal health [9, 10]. However, the effects of HIV infection on bone are difficult to investigate in the clinical setting and to-date poorly understood [11]. Additionally, there is a paucity of robust studies investigating the potential adverse effects of HIV on bone repair despite the increased risk for and prevalence of fracture [12, 13].

The most commonly used animal models in HIV/AIDS research – non-human primates, humanized mice, and felines – have been utilized heavily in the search for a cure [14]. These models, while more applicable to HIV cure research, are disadvantaged for investigations into non-AIDS-related comorbidities by the considerably more resource intensive nature of the animal models as well as the inherent risk in using active viral infection specifically with humanized mice [15]. In contrast, the HIV-1 transgenic (tg) mouse and rat are noninfectious and colonies are easily maintained [16, 17]. Both have also been used in studies on the various HIV-associated comorbidities [16-24]. Additionally, laboratory mouse and rat models have been used extensively in both osteoporosis [25] and bone healing research [26, 27]. Considering this information, the HIV-1 transgenic rodent models are attractive vehicles for examining bone-related disorders in the context of HIV as presented by these animals. Therefore, the *overall objective* of this work was to investigate the effects of HIV on skeletal growth and bone healing as exhibited by two noninfectious HIV-1 transgenic rodent models, specifically the mouse and the rat. The *central hypothesis* of this project was that HIV-1 transgenic animals will present with significant deficiencies in skeletal development and bone repair. We tested this hypothesis via the following three aims:

1.2 Aim I

Characterize the skeletal phenotype and fracture healing of the HIV-1 transgenic mouse.

Despite the evidence for use of HIV-1 tg mice in the study of select HIV-associated comorbidities, there are very few research studies using the models for bone-relevant

research. The opportunity to utilize one of these noninfectious models to investigate bone abnormalities was generously provided by Dr. Rudy Gleason and Dr. Roy Sutliff as a part of their ongoing research studies. Thus, the goals of this aim were to characterize the structural and biomechanical phenotype of HIV-1 tg mouse bone and to investigate fracture healing differences between HIV and control (WT) mice. First, to test the hypothesis that HIV mice would have impaired bone structure and function compared to WT mice, we analyzed the femur and L6 vertebra using microcomputed tomography (microCT) for bone microarchitecture and mechanical testing procedures to determine effects on biomechanical properties. Second, to test the hypothesis that HIV mice would have impaired bone healing, we implemented a closed femur fracture model using intramedullary stabilization to compare the fracture healing response in HIV-1 tg and WT mice.

1.3 Aim II

Investigate the longitudinal skeletal phenotype in the growing HIV-1 transgenic rat.

The noninfectious HIV-1 provirus used to generate the HIV-1 tg mouse from Aim I is the same used to create the HIV-1 tg rat. However, significant differences exist between the two species including more efficient HIV gene expression in the rat resulting in the presence of viral proteins in multiple lymphatic tissues. Although one study in the literature established that male HIV-1 tg rats present with an osteoporotic phenotype starting at 8-9 months of age, no studies have shown skeletal changes over time or bone biomechanics in this model. Therefore, the goal of this aim is to characterize the changes to the skeleton in the growing HIV-1 tg rat and the subsequent aged bone biomechanical properties at the

end of the study. Changes in cortical and trabecular bone architecture were assessed using microcomputed tomography (microCT). Serum levels of bone turnover markers were assessed for global changes in bone remodeling. Finally, bone biomechanical properties were determined for femurs and vertebrae. We hypothesized that alterations to bone morphology and function would occur in the 5- to 9-month period of HIV/AIDS symptomatic onset leading to an osteoporotic phenotype and impaired biomechanics in HIV-1 tg animals.

1.4 Aim III

Evaluate bone healing in the HIV-1 transgenic rat using a long bone segmental defect repair model.

Much of the clinical investigations into fracture healing in the HIV infected population have looked at closed and open fractures with a special interest in wound infection and clinical management. However, no clinical or preclinical studies have looked at the significant challenge that large bone defects may pose in the HIV infected population. The results from Aim I and Aim II provide support for the hypothesis that bone healing in HIV-1 tg rats would be impaired. Thus, the objective of this aim was to investigate whether the HIV condition of the HIV-1 tg rat influences BMP-2 mediated segmental bone defect repair using a well-established rat femur segmental bone defect procedure. A critically sized 8 mm mid-femoral bone defect was used in conjunction with a biomaterials-based therapeutic utilizing BMP-2 to induce bone healing. The bone healing process was assessed using qualitative x-ray radiographs and quantitative microCT scans. Functional restoration was evaluated via ex vivo biomechanics. We hypothesized that repair of the critically-sized

large bone defect would be impaired in the HIV-1 transgenic rats despite therapeutic intervention.

1.5 Significance and Scientific Impact

Millions of people continue to live with HIV infection, and although significant improvements to life expectancy and quality of life have been achieved, this growing and aging population is faced with many new challenges including greater risks for osteoporosis and fractures. While considerable progress has been made towards elucidating the connections between HIV and bone, there is yet more work to do to unravel this complex relationship. The use of animal models for HIV/AIDS research is especially difficult given that HIV is a human-specific virus and the current state-of-the-art in animal models for cure research are resource intensive. However, in addition to the extensive body of bone research utilizing both mice and rats, the HIV-1 transgenic rodent models are noninfectious and require less expertise and resources. Additionally, these models have been shown to be useful for researching HIV-associated comorbidities including cardiovascular disease, renal dysfunction, and neurocognitive decline. There remains a continued need for a useful small animal model to study bone disorders with HIV.

The work put forth here is significant because it has characterized the skeletal phenotype and bone healing response in the HIV-1 tg mouse and rat models in order to validate them for use in further research into the alterations to normal skeletal structure and function. This adds to the body of work investigating the clinically relevant HIV-associated comorbidities manifested in the HIV-1 tg rodent models. Additionally, it presents the first pre-clinical research on the effects of HIV-1 on bone healing as exhibited in the HIV-1 tg

rodent models. Specifically, this project has shown both rodent models exhibit a skeletal phenotype characterized by negatively altered bone microarchitecture and bone mechanics that agrees with clinical findings in HIV infected individuals. More importantly, the HIV-1 tg mouse and rat models both present with impairment of the normal bone healing process emphasizing the need for further clinical attention to fracture management in the HIV positive patient, especially with older patients.

Animal models are inherently disadvantaged when it comes to translating findings to the human condition. However, the opportunities they provide towards increasing understanding of disease mechanism and the significant impact on quality of life in humans is not trivial. As the HIV infected population continues to grow and to age, the once considered homogeneous demographic has become a far more epidemiologically diverse population of concern that will require a similarly diverse body of research. By presenting the HIV-1 tg rodent models as functional surrogates for orthopedic and HIV research, this work has provided the ground work for further exploration of the association between HIV and bone disorders.

CHAPTER 2. BACKGROUND

2.1 Bone Physiology

2.1.1 Bone Structure and Function

Bone is a fascinatingly complex and critical organ of our bodies. As the fundamental component of the skeletal system, bone serves multiple metabolic and structural roles including a repository of calcium and phosphate for mineral metabolism; supporting hematopoiesis in the bone marrow; protecting internal organs; and providing a rigid yet flexible structure for stability and movement. Commonly perceived as a static material, bone is dynamic in nature, constantly adapting to changes in its mechanical and physiological environment. It develops into specialized shapes and sizes during rapid growth and repairs itself to optimize mechanics and prevent catastrophic failure [28].

Bone can be divided into two types: cortical (compact) and trabecular (cancellous). These bone types are present in varying ratios throughout the skeleton providing different degrees of mechanical support. Cortical bone is dense with very low porosity and makes up approximately 80% of the adult human skeleton [29]. Primarily found in the diaphysis of long bones like the femur, cortical bone is present as the outer wall of all bones. Trabecular bone makes up the remaining 20% of the human skeleton and can be found in the epiphysis and metaphysis of long bones and in the inner compartment of vertebrae. It is characterized by a highly interconnected network of trabecular structures called plates and rods. Macroscopically, the highly porous trabecular structure provides considerable shock absorption and facilitates load transfer to cortical bone [28, 30]. Cortical bone, on

the other hand, is stiffer and can support greater ultimate stresses than trabecular bone but is more brittle [31].

The unique mechanical contributions of cortical and trabecular bone can be highlighted by comparing bones from different skeletal sites, specifically the femur and the vertebra. In the femur, the ratios of cortical and trabecular bone range from no trabecular bone at the mid-diaphysis to predominantly trabecular bone at the femoral head-neck junction [28, 31]. Here, cortical bone provides significant support under shear forces and bending moments and the trabecular bone contributes considerably less to the mechanical integrity of the femur. In the vertebra, the trabecular compartment provides the bulk of the mechanical strength supporting the predominantly compressive loads seen in the spine.

Irrespective of the bone type, bone is composed primarily of inorganic mineral (~65%) and organic protein (~25%) elements with the organic components made up primarily of type I collagen (90%) [32]. The mineral phase of bone consists mainly of a nanocrystalline called hydroxyapatite [$Ca_{10}(PO_4)_6(OH)_2$] whose greater solubility compared to geologic hydroxyapatite crystals allows support of mineral metabolism [29]. While the mineral side provides the stiffness of bone and the organic side imparts ductility, it is the combination of the two in varying amounts and arrangements that dictate the mechanical properties of bone from the nanoscale to the whole bone.

Bone is able to adapt to changes in stresses and strains through the processes of modelling and remodelling thereby adjusting bone composition and morphology [28]. Modelling is characterized by an activation signal followed by either resorption or formation of bone at a particular location [33]. This process seeks to optimize the shape of

the bone in response to the rapid growth towards adulthood. Unlike modelling, remodelling is a tightly regulated sequential progression of activation, resorption, and formation that replaces a specific volume of bone. There are three bone cell types involved in these processes: osteoblasts, osteocytes, and osteoclasts. Osteoblasts are the bone forming cells that derive from mesenchymal progenitors. As osteoblasts lay down new bone matrix, some of them remain behind and eventually become embedded in the bone tissue to differentiate into osteocytes. Osteocytes are the most common bone cell type and play a critical role in sensing mechanical strain and microdamage. Osteoclasts are the bone resorbing cells of the monocyte-macrophage lineage recruited from the bone marrow or potentially from circulation. Together, the osteocytes, osteoblasts, and osteoclasts work in concert to maintain healthy and functional bone tissue.

2.1.2 Bone Development and Healing

Skeletal development and growth follows two distinct processes known as endochondral and intramembranous ossification [34, 35]. Development and growth of long bones occurs through endochondral ossification and is characterized by the formation and subsequent replacement of cartilage with bone tissue. Proliferating chondrocytes differentiate into hypertrophic chondrocytes which initiates the process of cartilage resorption by osteoclasts, bone deposition by osteoblasts, and blood vessel formation. In flat bones such as in the skull, intramembranous ossification occurs when osteochondroprogenitor cells differentiate into osteoblasts which subsequently lay down bone matrix, bypassing the cartilage phase present in endochondral ossification. The newly formed bone from either process is characterized by a disorganized arrangement of collagen fibers and is referred to as primary, immature, or woven bone [32]. This bone is a

placeholder, formed rapidly to provide temporary stability and structure to the surrounding tissues. It is quickly remodelled and replaced by lamellar (also secondary or mature) bone, a more mechanically competent mineralized tissue with highly organized collagen fibers.

Bone is unique in its ability to heal without scar tissue through a process combining endochondral and intramembranous ossification [36]. Bone healing can be categorized into primary (direct) and secondary (indirect) healing. Primary fracture healing is not common and requires strict stability of the injury site with little to no gap between fractured bone ends. Secondary fracture healing is the most common path towards bone healing and does not require strict stable fixation or contact between fractured bone ends. In fact, some degree of instability and micromotion is necessary for proper bone healing. The fracture healing cascade follows a continuum of processes starting with the bone injury and progressing to formation of a hematoma, an inflammatory phase, soft callus formation, transition to hard callus, and remodelling phase.

Bone injury causes significant damage to the vasculature in and around the bone resulting in an influx of blood and the formation of a hematoma [37]. The subsequent acute inflammation involves multiple inflammatory cells including polymorphonuclear leukocytes, monocytes, macrophages, T cells, and B cells [38]. This phase clears out debris and necrotic tissue, promotes angiogenesis, and initiates recruitment of osteochondroprogenitors via a variety of inflammatory and chemotactic cytokines as well as key growth factors including bone morphogenetic proteins (BMPs) [37]. As a result of the injury, the local environment closest to the central region of the injury site has become more hypoxic, avascular, and mechanically unstable than the regions further from the fracture site. This fracture site microenvironment encourages chondrogenesis and

formation of a cartilaginous soft callus that stabilizes the area and sets the stage for endochondral ossification. Concurrently, primary bone healing via intramembranous ossification begins some distance away from the soft callus and advances towards the region of injury. Subsequently, the soft callus chondrocytes differentiate into hypertrophic chondrocytes and eventually undergo apoptosis, leaving behind a calcified cartilage matrix and promoting vascular ingrowth. The process of endochondral ossification proceeds as the cartilage is resorbed by osteoclasts and primary bone formation by osteoblasts begins leading to the formation of a hard callus. This mineralized cartilage and woven bone matrix is then remodelled and replaced by lamellar bone which continues to be remodelled until the native bone structure and mechanical strength is restored.

2.2 HIV-1 Pathology

2.2.1 Virus and Infection

The human immunodeficiency virus 1 (HIV-1) is a member of genus Lentivirus under the family of Retroviridae [39]. The life cycle of HIV-1 can be summarized as infection of a cell, integration of viral genome, viral gene expression, and production of viral particles [39, 40]. HIV-1 infection of a cell begins with a sophisticated interaction of viral surface proteins with host cell surface receptors. Initially, the glycoprotein gp120 on the HIV particle surface binds to the CD4 receptor of CD4+ cells which include T helper cells, macrophages, dendritic cells, and astrocytes. Subsequent conformational changes and binding to co-receptors – chemokine receptor 5 (CCR5) or chemokine receptor 4 (CXCR4) – results in the fusion of the virus and host cell membrane. The viral contents are released into the cytoplasm and the viral RNA is reverse transcribed into DNA which

is subsequently transported to the nucleus for random integration into the host cell's genome. Utilizing the host cell's transcriptional and translational machinery, the HIV genes are transcribed into mRNA which is then translated to produce the various viral proteins needed for a mature HIV particle. Finally, the virus is assembled, buds, and is released from the host cell membrane to mature and infect more cells. The whole process from HIV-cell attachment to release of new viral particles takes approximately 24 hours [39].

The HIV-1 genome consists of nine genes that code for the structural and regulatory proteins necessary for HIV-1 replication and infection [39, 40]. Three of these genes – *gag*, *pol*, and *env* – are common to all retroviruses while the remaining six are regulatory proteins unique to HIV-1. The proteins encoded by *gag* make up the structure of the viral core. The *pol* gene codes for the major viral enzymes including reverse transcriptase and integrase. The surface proteins gp120 and gp41 critical for virus-cell attachment are encoded by *env*. The regulatory proteins Tat, Rev, and Nef are the first produced after infection and are essential for accelerating viral gene transcription, facilitating transport from the nucleus to the cytoplasm, and reduction of cytoplasmic CD4 levels, respectively. The additional accessory proteins Vif, Vpr, and Vpu influence the infectiousness, maturity, and production of viral particles.

As described by the Centers for Disease Control and Prevention (CDC), HIV infection progresses through three stages: acute infection (Stage 1), clinical latency (Stage 2), and AIDS (Stage 3) [41]. Initial HIV infection (Stage 1) results in rapid viral replication and, within 2 to 4 weeks, flu-like symptoms that can last anywhere from several days to a few weeks [42]. In response to the sharp rise in viremia, HIV-1 specific cytotoxic T cells attempt to eliminate the virus from the body, lowering the viral load to what is called a

viral load set-point. The actual HIV-1 viral load oscillates about this steady value and can vary significantly from individual to individual [43]. This phase of steady viral load characterizes the asymptomatic phase (Stage 2) wherein the infected individual may or may not present with symptoms, a state that can last up to ten years or more [41]. During this time, the viral infection is slowly depleting the body of a functional immune system [44]. As stated previously, HIV can infect multiple cell types but the eventual progression to AIDS is a consequence of a dramatic loss in CD4+ T cells [45]. These T cells are critical to the immune system, modulating other immune cell function and recruitment through the secretion of various cytokines and chemokines [46]. A Stage 3 AIDS diagnosis is defined by a CD4+ T cell count that is below 200 cells/mm^3 or, as a consequence of a compromised immune system, the presence of opportunistic illnesses [41]. Individuals with AIDS survive around three years without treatment.

2.2.2 Epidemiology

The HIV/AIDS epidemic continues to impact the quality of life of millions of people worldwide. In 2016, over 36 million people in the world were living with HIV with an estimated 2.1 million under the age of 15 [1] and in 2014, 4.2 million over the age of 50 or about 13% of the adult population living with HIV [47]. In the early 1980s in the United States, HIV infection was associated with young, white, men who have sex with men (MSM), but this demographic has since diversified across race/ethnicity, gender, and age [48]. In fact, the highest prevalence of HIV infection at the end of 2015 by race was among blacks/African Americans; by age group was among those 45-54 years old; and by sex was among males [49]. Additionally, an estimated 14.5% of those living with HIV over the age of 13 years in the United States did not know they were HIV positive. UNAIDS reported

that the rate of infections globally is on the decline, but 1.8 million new infections were estimated for 2016 [1] with nearly 40,000 people receiving a new HIV diagnosis in the United States [50].

Early in the HIV/AIDS epidemic, a positive HIV diagnosis was almost certainly a death sentence. With the advent of effective treatment initially called highly active antiretroviral therapy (HAART) and now simply antiretroviral therapy (ART), patients infected with HIV can expect to live considerably longer and to nearly that of the uninfected population [3, 51]. Efforts to develop a cure and to prevent new HIV infections have been substantial, however neither has yet been successful in removing HIV/AIDS as a both an acute and chronic healthcare concern. Consequently, living with HIV infection requires a strict adherence to ART regimens which, over a lifetime, can result in adverse side effects from ART itself, drug interactions from polypharmacy, drug resistance, or significant pill burden [51, 52].

2.2.3 HIV-Associated Comorbidities

Living with HIV has become a chronic condition so long as patients adhere to their therapeutic regimen [53]. Unfortunately, longer lifespans have brought with it unexpected complications including traditionally age-related comorbidities such as cardiovascular disease, renal disease, liver disease, neurocognitive decline, and osteoporosis [4, 51, 54]. The onset of these complications has also been suggested to occur at a younger age compared to the uninfected population leading to the hypothesis that individuals with chronic HIV infection and effective ART have a syndrome of premature aging [55, 56]. This syndrome may be a combined consequence of chronic immune activation and latent

viral reservoirs, functional HIV that is "hiding" in resting cells [57, 58]. These HIV reservoirs may continue to replicate at low levels in part due to low concentrations of antiretroviral drugs in various tissues [58]. Additionally, it is suspected that viral proteins continue to be produced despite effective therapy as found in the blood and tissues of HIV patients on ART [59-62].

2.3 HIV and Bone

2.3.1 Low Bone Mass

Osteoporosis is the most common bone disease afflicting millions of people in the world. It is characterized by significantly low bone mass and poor bone quality and consequently an increased risk for fragility fractures such as those that occur from falls [63, 64]. According to the World Health Organization (WHO) guidelines, if an individual's bone mineral density (BMD) – measured using dual energy x-ray absorptiometry (DXA) – falls at or below 2.5 standard deviations from the mean peak BMD of young adults, then they are diagnosed as having osteoporosis [65]. Low bone mass has been found to be a significant concern in the HIV positive population. In a meta-analytical review, Brown and Qaqish found an increased prevalence of reduced BMD and osteoporosis in the HIV positive population whether patients were ART-naive (odds ratio, OR, of 6.4 and 3.7, respectively) or ART-treated (OR of 2.5 and 2.4, respectively) when compared to respective uninfected controls [66]. In a more recent meta-analysis, Goh and colleagues found that HIV-infected individuals had a comparatively lower but still significant 2-fold increased prevalence of osteopenia/osteoporosis compared to uninfected controls regardless of ART treatment status [67]. More specifically, HIV positive men have

significantly decreased BMD at the femoral neck and lumbar spine compared to uninfected controls with prevalence of osteopenia or osteoporosis in the study cohorts ranging from 51% to 82% [68-72]. Similarly, lower BMD is more prevalent in women infected with HIV with rates of osteopenia or osteoporosis ranging from 23% to 78% [73-78]. Although much of this evidence comes from research from resource rich settings, the impact on bone health is similarly deleterious if not more so in resource limited settings [79]. Additionally, the prevalence of low bone mass afflicts children and adolescents infected with HIV. The risk of mother-to-child transmission of HIV is very high without ART, but treatment can reduce this risk considerably. However, maternal HIV infection is associated with a higher risk of preterm birth, low birth weight, and small-for-gestational-age whether the mother is ART-naïve or not [80, 81]. Premature birth, low weight at birth, or poor growth early in life may lead to below normal peak bone mass and bone strength [82, 83]. Whether infected perinatally or behaviorally, multiple studies have shown that HIV infected children and adolescents have reduced bone mass [84-86]. In a study of HIV infected males in their early 20s, Yin and colleagues showed that early infection results in a subnormal peak bone mass [87]. Given that peak bone mass is a critical predictor of osteoporosis and fracture risk [88, 89], HIV positive youth may be at a greater risk for skeletal complications later in life. Although comparisons between studies can be difficult to make given differences in cohort characteristics including sample size, alcohol consumption, smoking, drug use, BMI, age, race/ethnicity, and menopausal state, there is significant evidence for a high risk of low bone mass in HIV infected individuals regardless of various demographic characteristics.

In addition to bone mass concerns, skeletal fragility in osteoporosis is a consequence of an imbalance in the bone remodelling process whereby bone resorption is at a level that bone formation is not matching [90]. How bone remodelling is unbalanced in the context of HIV depends on many factors including severity of HIV infection, level of immune dysfunction, effects of ART, comorbidities, and behavioural risk factors [91]. Much of the research looking at bone turnover in HIV patients is concerned with ART effects which can vary by drug. Overall, there is evidence for increased bone turnover in HIV positive individuals initiating ART that remains at elevated levels compared to pre-treatment levels [91-95]. In ART-naïve HIV patients, bone formation appears to be suppressed with resorption levels equal to or greater than uninfected controls [78, 96]. Changes in bone turnover markers in HIV infected children vary as a consequence of study cohort characteristics but suggest a significant association between increased bone turnover markers and low bone mass [86, 97, 98]. Additionally, i*n vitro* research has suggested that the HIV-1 virus and its proteins may alter bone turnover by directly influencing osteoclastogenesis [99-101], osteoclast activity [102, 103], osteoblast activity [104-107], and mesenchymal stem cells [105, 108-112].

A relatively new field known as osteoimmunology has highlighted the interactions between the immune system and the skeletal system. Applying this lens to the study of HIV and bone loss has provided considerable insight into the mechanism underlying this pathophysiology. Osteoclastogenesis requires permissive concentrations of macrophage colony-stimulating factor (M-CSF) and binding of receptor activator of NF-κB (RANK) ligand (RANKL) with its receptor, RANK, on osteoclast precursors. Osteoprotegerin (OPG) acts as a physiological decoy receptor for RANKL thereby inhibiting osteoclast

differentiation. The ratio of RANKL and OPG is therefore a key factor in determining the downstream levels of bone resorption. Recent work has shown that T cells and B cells are both sources of OPG and instrumental in moderating bone resorption via the RANKL/OPG ratio [113]. With HIV infection, it has been suggested both pre-clinically [24] and clinically [114, 115] that bone loss in the HIV infected population is due in part to loss of or dysfunctional T cells and reduction in OPG production by B cells. The mechanism of ART-mediated bone loss is not clear but suggested to be a consequence of early immune reconstitution whereby a rapid recovery of T cells induces bone loss [116]. The exact role that chronic immune activation plays in bone loss in the setting of successful ART treatment remains unclear [117].

Changes in bone remodelling dynamics influence bone microarchitecture and can negatively impact bone strength. In an early study looking at bone histomorphometry of transiliac bone biopsies from HIV infected individuals, Serrano et al. found a difference in trabecular spacing with greater spacing in HIV bone accompanied by histomorphometric measures indicating decreased bone turnover that worsened with HIV disease severity [118]. Recently, a method known as trabecular bone score (TBS) was introduced that takes two-dimensional DXA images of the lumbar spine and extracts a gray-level textural index, and it has been shown to correlate to 3D measures of bone microarchitecture and predict fracture risk [119]. Using TBS, Sharma and colleagues found that women infected with HIV were more likely to have lower TBS even after adjusting for age and menopausal status but no difference in percent change in TBS per year was found over the 5 years of the study when compared to uninfected women [120]. Although TBS provides more information than BMD, it still falls short in quantifying bone microarchitecture. Using

high-resolution peripheral quantitative computed tomography (HR-pQCT) can provide a more accurate assessment of BMD than DXA as well as microstructural level detail of trabeculae. Calmy et al. utilized HR-pQCT with HIV positive and negative premenopausal Swiss Caucasian women to analyse the bone at the distal tibia and the distal radius [121]. They found decreased trabecular BMD and number and increased trabecular separation at the distal tibia as well as significantly reduced cortical BMD at the distal radius with similar but non-significant reductions in trabecular measures. HIV positive women also had lower lumbar spine BMD but no differences in proximal femur BMD. Similarly, in a group of postmenopausal Hispanic and African American women, Yin and colleagues found reduced BMI-adjusted aBMD *Z*-scores at the lumbar spine, total hip, and ultradistal radius in the HIV group with higher levels of bone resorption markers [122]. However, in this cohort, they only found differences in the tibia with HIV women having decreased cortical bone area and thickness with a trend towards decreased cortical BMD. Given the differences in the demographics in the two studies, it is difficult to make useful comparisons. Nevertheless, the results suggest altered bone microarchitecture in HIV infected women that may predispose this population to fragility fractures.

In young men aged 20-25 years on ART, Yin et al. used HR-pQCT to scan the non-dominant distal radius and distal tibia and found significantly lower trabecular BMD, cortical thickness, and trabecular thickness at both sites as well as greater trabecular spacing at the distal tibia [87]. Using a technique for HR-pQCT called individual trabeculae segmentation (ITS)-based morphological analysis [123-125], they reported significantly reduced trabecular plate measures in HIV infected groups with no differences in trabecular rod measures. Using micro finite element analysis (FEA), they further found whole bone

(i.e., cortical and trabecular bone) stiffness to be reduced in the HIV infected groups at the radius and reduced trabecular bone stiffness at both sites. Importantly, this study highlights that early life infection with HIV – whether perinatally or behaviorally – compromises bone mass, microarchitecture, and mechanics at the time of peak bone mass attainment. Studies on older men have found that middle-aged [126] and elderly [127] men infected with HIV have similarly disrupted cortical and trabecular morphologies. Additionally, Co-infection with the hepatitis C virus (HCV) was shown in both men [128] and women [129, 130] to exacerbate the deficits to bone morphology more than HIV infection alone. Although bone microarchitecture is known to contribute to bone strength, little research – aside from micro FEA estimations – has been done to assess bone mechanical properties in HIV infected persons. Güerri-Fernández et al. used microindentation to assess tissue level bone material properties in ART-naïve HIV infected patients and controls in Spain and found that bone material strength index (BMSi) values were lower in HIV infected individuals independent of BMD [131].

2.3.2 Bone Healing

Although the risk for fracture and the incidence of fracture are significantly greater in the HIV positive population [132], it is unclear whether fracture healing is negatively impacted in this group. Richardson et al. posited that there may be several pathways to impaired healing in HIV patients including low bone mass, effects on the immune system, and other comorbidity effects [133]. In the context of osteoporosis, animal studies looking at both postmenopausal estrogen-deficient and senile osteoporosis have shown delayed healing and impairment of healing outcomes including early mesenchymal stem cell recruitment and differentiation and callus formation and remodelling [37, 134]. Given the

critical inflammatory phase of fracture healing, it is not surprising that immune cells play an important role in fracture healing [135]. Specifically, depletion of T and B lymphocytes expedites bone healing [136] but at the expense of the quality of callus formation and mineralization [137], and they have been shown to be present in the fracture callus at all phases of healing except during soft callus formation and in cartilaginous regions [138]. Indeed, both systemic and local chronic inflammation can impair fracture healing but the underlying mechanisms have yet to be fully elucidated [37, 139].

Clinically, successful fracture healing is assessed radiographically and by clinical observation [140]. Impaired bone healing is subsequently categorized as delayed union, nonunion, or malunion [141]. Several clinical investigations have included this question of impaired bone healing in their studies with HIV infected individuals but the findings are inconclusive [13]. The predominant concern for orthopaedic surgeons has been infection given the possible immune-compromised status of HIV positive individuals. Sufficient research has been put forth showing low risk of infection with closed fractures but there is an increased risk for infection in open fractures. With regards to impaired healing across multiples studies, the rates of nonunion ranged from 0% to 33%. However it is difficult to draw conclusions from these studies because of the many limitations inherent with them including small sample sizes, poor experimental design, poor or no criteria for assessing fracture union, and large variation in follow-up duration [13].

2.4 HIV and Animal Models

The search for an animal model that can be used as a surrogate for HIV-1 infection in humans began soon after the term AIDS was used to describe the disease. The closest

animal to humans is the chimpanzee which can be infected with the simian immunodeficiency virus (SIVcpz), the origin of HIV-1; however, it is an endangered species, rarely develops disease in captivity, and requires significant time, expense, and expertise to conduct research [15]. Other non-human primates have been found to host SIV and even chimeric viruses that are a combination of SIV and HIV genomes (SHIVs) have been created in the effort to find a model that can mimic the human condition. However, SIV, while similar to HIV, is genetically different and use of these large animal models are again limited by cost and technical expertise as well as small sample sizes [15, 142]. Other animals have a naturally occurring immunodeficiency virus including sheep, goats, cows, horses, and cats, but they are limited in their relevance to humans and in the practicality of their use [15, 143]. In the search for a small animal model, humanized mouse models were developed [142]. Considerable understanding in HIV/AIDS biology and therapy has been gained from the use of these mouse models, but they are challenging to use because of the technical expertise needed to produce and the inability to be bred to maintain phenotype [14, 23].

HIV-1 transgenic (tg) animals bypass the considerable complications and barriers to research that the aforementioned models have [144]. Transgenic animals are non-infectious, easily maintained as colonies, and have been shown to mimic elements of the human condition with HIV infection, specifically HIV-associated comorbidities. In the HIV-1 tg mouse model, cardiovascular disease [18, 19], renal dysfunction [16, 20], lipodystrophy [145], and B cell lymphoma [146, 147] have been studied. The HIV-1 tg rat model has been used extensively to study a variety of HIV-associated conditions including immune dysfunction [17, 148-150], cardiovascular disease [21, 151, 152], pulmonary

disease [153, 154], neurocognitive disorders [144, 155], liver disease [156, 157], and nephropathy [22, 158]. Despite the inability of rodents to be infected with HIV-1, the HIV-1 transgenic rodent models have proven useful for studying the effects of viral products especially in the context of a long-term chronic condition, and they have the added benefit of being more easily genetically modified than other models of HIV/AIDS to study specific viral and host factors [6, 159].

However, little bone-related research has been conducted in the HIV-1 tg mouse and rat models. In one study using the HIV-1 tg mouse, the findings suggested dysfunctional bone-derived mesenchymal stromal cells [109], and in a different HIV transgenic mouse, the researchers observed that the ribs in HIV tg mice were "thin and friable" compared to normal mice [160]. Most recently, Raynaud-Messina et al. utilized both humanized and transgenic mouse models to show that osteoclasts can be infected by HIV-1 and that this can lead to Nef-mediated bone fragility, decreased bone density, and increased osteoclast number and activity [103]. Interestingly, in tibias from a humanized mouse model, Springer et al. reported lower hardness, ultimate load, and stiffness values for HIV positive animals compared to controls [161]. Studies using the HIV-1 tg male rat showed that this model recapitulates an osteoporotic bone phenotype via heightened osteoclast activity [24, 162]. Therefore, there is an opportunity to investigate *in vivo* effects of HIV on the skeleton using HIV-1 tg rodent models.

CHAPTER 3. SKELETAL PHENOTYPE AND FRACTURE HEALING IN AN HIV-1 TRANSGENIC MOUSE

3.1 Introduction

HIV/AIDS continues to be a worldwide epidemic with over 36 million people in the world living with HIV [1]. Although the advent of antiretroviral therapy (ART) has dramatically extended the life expectancy those infected with HIV [3], this population is now faced with comorbidities traditionally associated with aging including osteoporosis and the risk for fragility fractures [4, 163]. In their work reporting the significance of osteoporosis in the HIV infected population, Brown and colleagues found that HIV infected patients were 6.4 times more likely to have reduced bone mineral density (BMD) and 3.7 times more likely to have osteoporosis [66]. Later studies have confirmed this increased prevalence at varying rates [67] and consequently, there is a greater risk for fracture [164]. Bone quality measures including bone microarchitecture and bone mechanical properties are known to be critical factors in skeletal fragility especially in osteoporotic patients [28, 165, 166]. However, considerable variability exists between clinical studies due to challenges with clinical studies in the HIV infected population including traditional risk factors for osteoporosis and the complicated interplay between HIV infection itself and ART on bone loss [113].

The rates for fracture in the HIV positive population are likewise increased compared to the HIV negative population [9, 132]. Whether this patient population subsequently experiences complications with recovery after fracture is controversial. Some

speculation has been made regarding an association between HIV and bone healing [133], but the limited number of studies including fracture nonunion in their reports have found significantly variable results with some studies reporting no prevalence of nonunion and others reporting up to 33% prevalence of nonunion within their HIV positive cohorts [13]. Additionally, many of these studies suffer from poor experimental design, low sample sizes, and a lack of clear definitions for assessing fracture union and nonunion. It is therefore unclear whether there is an effect of HIV on fracture healing.

Animal models thus provide an opportunity to study the effects of HIV on bone that would prove too difficult to isolate in the clinical setting. Current animal models of HIV infection (i.e., nonhuman primates and humanized mouse models) can be technically challenging and resource prohibitive and have been traditionally used in cure research [14, 15]. The development of noninfectious transgenic animals for HIV research has provided the opportunity to study the effects of HIV without the risk or cost of studying active HIV infection. As previously stated, HIV-1 tg mice have been used to study multiple HIV-associated comorbidities [16, 18-20, 145-147]. Less work has presented bone-relevant research with the few studies suggesting abnormal bone cell function and bone integrity that may result in compromised bone function [16, 103, 109, 160].

In this study, our objective was to characterize the skeletal phenotype of the HIV-1 tg mouse to determine if the constitutive HIV-1 gene expression in these animals negatively impacts their bone structure and function. Specifically, we first examined the bone structural and mechanical properties in order to show that HIV-1 tg mice exhibit a skeletal phenotype consistent with changes in bone microarchitecture seen with clinical osteoporosis. We hypothesized that HIV-1 tg mice will have deleterious alterations to bone

microarchitecture accompanied by decreased bone mechanics. Secondly, we investigated the bone healing process in the HIV-1 tg mice using a closed femoral fracture model with intramedullary stabilization. We further hypothesized that bone healing would be impaired in HIV-1 tg mice.

3.2 Materials and Methods

3.2.1 HIV-1 Transgenic Mouse Model

For the bone structure and mechanics investigation, male hemizygous NL4-3Δ *gag/pol* HIV-1 transgenic (tg) (n=10, HIV) and wild-type littermate (n=10, WT) mice in the FVB/N background were obtained from Dr. Roy Sutliff (Atlanta Veterans Affairs Medical Center, Decatur, GA) and Dr. Rudy Gleason (Georgia Institute of Technology, Atlanta, GA). All mice were euthanized at approximately 10-12 weeks of age. Hemizygous mice appear normal at birth but present with progressive renal dysfunction and glomerulopathy similar to that of HIV-associated nephropathy seen in humans [16, 20]. Compared to wild-type mice, homozygous HIV-1 Tg mice are born smaller, have decreased food intake, and typically die within 40 days after birth [16]. Only hemizygous mice were used in this study.

For the long bone fracture healing investigation, male HIV-1 tg (HIV) and wild-type littermate (WT) mice in the C57BL/6 background were used. Briefly, HIV-1 Tg mice that were backcrossed eight generations from the FVB/N background to a C57BL/6 background were obtained from Dr. Roy Sutliff (Veterans Affairs Medical Center, Atlanta, GA) [167]. A total of 24 animals per group approximately 12 to 14 weeks of age were used in this study. Animals were housed in a quarantined room on a 12:12 hour light/dark

schedule and provided food ad libitum. Procedure for closed fracture was previously reported and adapted for this study [168]. Briefly, mice were anesthetized via isoflurane inhalation, and the right hind limb was cleaned of hair by shaving and using depilatory cream (Nair). The surgical site was cleaned before an incision was made to then expose the femur via gross dissection. An intramedullary pin using K-Wire (Key Surgical) approximately 0.7 mm in diameter was inserted into the intramedullary canal through the distal end of the femur. Using a gigli wire saw (RISystem) approximately 0.22 mm thick, a mid-diaphyseal osteotomy was created, contact between bone ends was ensured, and stability of the pin was checked. The contralateral leg was left intact. Mice were allowed to recover on a heating pad, and after ambulation was confirmed, returned in their cages to the housing room. Any animals with evidence of intramedullary pin instability or displacement were removed from the study.

Two different mouse strains were utilized in this study due to restrictions on availability of samples and animal health and welfare concerns. HIV-1 tg mice on the FVB/N background presented with a more severe disease-like state resulting in death by 4 months. In contrast, HIV mice on the C57BL/6 background do not present with early cataracts like the FVB/N background HIV-1 tg mice and need to be genotyped by tail snip. All procedures were approved by the Georgia Institute of Technology and the Atlanta Veterans Affairs Medical Center Institutional Animal Care and Use Committee (IACUC).

3.2.2 X-Ray Radiographs and MicroCT

For the bone structure and mechanics investigation, the left femur and lumbar spines were harvested from each animal, wrapped in saline soaked gauze and stored at -20ºC until needed. Femurs and vertebrae were cleaned of soft tissue and scanned using micro-computed tomography (microCT, µCT 40 system, Scanco Medical) at a medium resolution with a voxel size of 12 µm, a voltage of 55 kVp, and a current of 145 µA. Using built-in software, a 1 mm section of the femur mid-diaphysis was evaluated for cortical bone morphology (bone area, BA; bone marrow area, MA; total area, TA; cortical thickness, Ct.Th; moment of inertia, MOI; polar moment of inertia, pMOI; and mineral density). The distal femur was evaluated at the metaphysis and epiphysis using a 0.6 mm section measured from the growth plate for trabecular microarchitecture (trabecular number, Tb.N; trabecular thickness, Tb.Th; trabecular spacing, Tb.Sp; structure model index, SMI; bone volume fraction, BV/TV; connectivity density, Conn.D; and mineral density). L6 vertebrae were isolated from the lumbar spine and cleaned of soft tissue. The central 2.4 mm section of the L6 vertebrae was also measured for trabecular measures. Cortical bone was excluded from trabecular analysis using an automated segmentation algorithm [169]. Contours were visually inspected for accuracy and manually adjusted as necessary.

For the fracture healing study, animals were x-rayed *in vivo* (Bruker Xtreme Imaging System) every week after fracture surgery to qualitatively assess fracture stability and progression of healing. Mice were euthanized at Week 2 (n = 10 WT, n = 10 HIV) and Week 4 (n = 10 WT, n = 8 HIV) using CO_2 inhalation following standard protocols. Both hind limbs were harvested, wrapped in saline soaked gauze, and stored at -20ºC until

needed. Prior to scanning, hindlimbs were allowed to thaw in PBS at room temperature. Femurs were isolated and cleaned of soft tissue before the intramedullary pin was carefully removed. Fracture calluses were scanned in a humid chamber at a resolution of 20 μm, a voltage of 55 kVp, and a current of 145 μA (μCT 40 system, Scanco Medical). Four WT and three HIV samples were excluded from microCT analysis due to errors in scanning that were not able to be resolved because biomechanical testing was performed immediately after the scans. The entire fracture callus was included by manually contouring the outer boundary, and the native cortical bone was contoured for exclusion from analysis. Following a procedure previously used [168, 170], new mineral formation was defined as 50% of the native cortical bone density. Using this threshold and built-in software, the fracture callus was segmented and analyzed for total callus volume, mineralized callus volume, mineral density, and polar moment of inertia.

3.2.3 Mechanical Testing

Femurs and L6 vertebrae intended for skeletal phenotype evaluation were mechanically tested to failure under displacement control. Femurs were allowed to thaw to room temperature prior to 3-point bending at a rate of 1 mm/min with a span of 6.2 mm between lower supports (ELF 3200, Bose EnduraTEC). Femurs were tested posterior side down and were loaded at the mid-diaphysis. Vertebrae were allowed to thaw to room temperature, then transverse and posterior processes were removed. Cranial and caudal growth plates were removed using a cutting slab to ensure parallel surfaces and a constant height of 2 mm. The L6 vertebrae were glued to the bottom compression plate before testing to failure using compression testing at a rate of 1 mm/min. During mechanical testing, all samples were kept moist with PBS. Structural properties (ultimate load,

stiffness, yield load, post-yield displacement, energy to ultimate load, and energy to failure load) were calculated directly from the load-displacement curve where appropriate. Derived material properties (Ultimate stress, elastic modulus, and toughness to ultimate stress) were calculated from the load-displacement data using standard equations [171].

Fracture callus samples and intact contralateral control femurs were mechanically tested to failure under torsion following previously reported methods [168]. Briefly, samples were cleaned of any remaining soft tissue from bone ends and potted in Wood's metal (Alfa Aesar) in custom fixtures with a gauge length of 6.5 mm. Samples were tested at a rate of 3 degrees per second until failure or until 60 degrees of rotation using an ELF 3220 testing system (Bose EnduraTEC). Samples were kept moist using PBS during mechanical testing. Mechanical properties were calculated from the torque-rotation data (maximum torque, torsional stiffness, rotation at maximum torque, and energy to maximum torque).

3.2.4 Vascular Perfusion and Analysis

Following previously reported methods [168], we analysed fracture callus vascularization in animals from the fracture healing study (n = 4 WT, n = 4 HIV). Mice were euthanized via CO_2 inhalation at Week 1 post fracture and immediately perfused sequentially with physiological saline, 10% neutral buffered formalin, and again with saline. A yellow-colored, radiopaque, lead chromate compound (Flow Tech Inc.) was then injected with steady pressure into the vasculature until yellowing was apparent on the internal organs and pads of the feet. Animals were stored at 4°C overnight to allow for polymerization of the contrast agent. Fractured femurs were isolated and intramedullary

pins carefully removed before storing in 10% neutral buffered formalin for 48 hours at 4°C. Samples were then soaked in a formic acid solution with citrate buffer (Newcomer Supply) under gentle agitation until decalcification was confirmed via soft x-ray imaging. Samples were then scanned at a voxel size of 10.5 μm and the callus was isolated via manual contours of 2-D images. 3-D reconstructions were evaluated for vessel volume, vessel volume fraction, vessel diameter, and vessel connectivity.

3.2.5 Statistics

All data are presented as mean ± SEM. Statistical analyses were performed using SPSS Statistics 24. Bone microarchitecture, bone mechanics, and microCT vascularization data were analysed using unpaired two-sample Student's t-tests or Mann-Whitney U tests. Fracture callus microCT data and biomechanics were analysed using two-way ANOVA as performed by the univariate general linear model in SPSS. Pairwise comparisons were adjusted using the Bonferroni correction. A significance level of 0.05 was set for all analyses.

3.3 Results

3.3.1 Bone Microarchitecture

In order to evaluate bone structural differences in cortical and trabecular bone, we scanned the femoral mid-diaphysis, distal femur, and L6 vertebra of each animal. The femoral mid-diaphysis was evaluated for cortical bone architecture measures. Compared to WT animals, HIV animals had severely compromised cortical bone structure with thinner cortices (-38.2%, $p < 0.001$, Ct.Th) and less bone measured by average cross-

sectional cortical bone area (-27.9%, $p < 0.01$, BA) (Figure 3-1). Interestingly, the total cross-sectional area ($p = 0.638$, TA) did not differ between WT and HIV animals suggesting that while HIV mice may weigh less and have slightly shorter femurs (Table B-1), the transverse growth of the bone is similar. Accordingly, the larger cross-sectional marrow area (12.6%, $p < 0.01$, MA) in HIV mice may be a consequence of greater endosteal bone resorption. Additional data are presented in Table B-1.

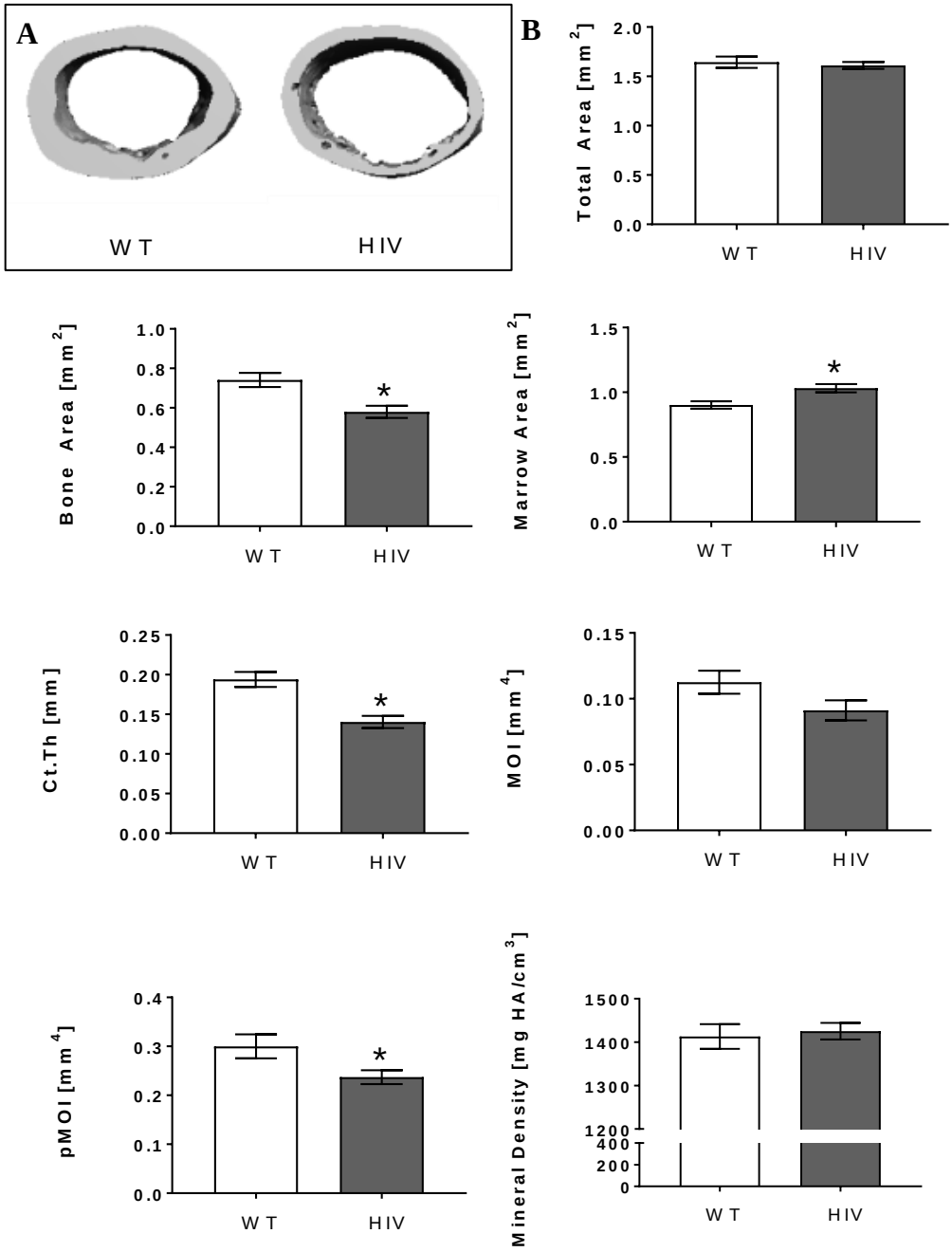

Figure 3-1: (A) Representative microCT 3D reconstructions of femur mid-diaphysis. (B) MicroCT evaluation of femur mid-diaphysis. n = 10 per group. Error bars indicate SEM. * indicates significant difference between groups ($p < 0.05$). Ct.Th = cortical thickness; MOI = moment of inertia; pMOI = polar moment of inertia.

We scanned the distal femur to examine two different regions of trabecular bone: the epiphyseal area and the metaphyseal area. At both sites of trabecular bone, HIV mice had less bone as measured by bone volume fraction (epiphysis: -33.0%, $p = 0.011$; metaphysis: -41.1%, $p = 0.014$; BV/TV) and thinner trabeculae (epiphysis: -19.2%, $p < 0.01$; metaphysis: -13.3%, $p = 0.035$; Tb.Th) when compared to WT mice (Figure 3-2 and Figure 3-3). No other differences were found at the epiphysis but significant alterations to trabecular architecture were found at the metaphysis including greater average structure model index (SMI) values ($p = 0.018$) and decreased connectivity density (-49.5%, $p = 0.049$, Conn.D) in HIV femurs (Figure 3-3). SMI values are an estimation of the average plate-like (SMI = 0) or rod-like (SMI = 3) characteristic of the trabecular bone analyzed. For example, trabecular bone in the epiphyseal compartment is more plate-like in nature (Figure 3-2) while in the metaphyseal region, the trabeculae are more rod-like (Figure 3-3). These site-specific differences within the same bone may be reflective of the different mechanical and biological environment each region experiences. Additional data are presented in Table B-1.

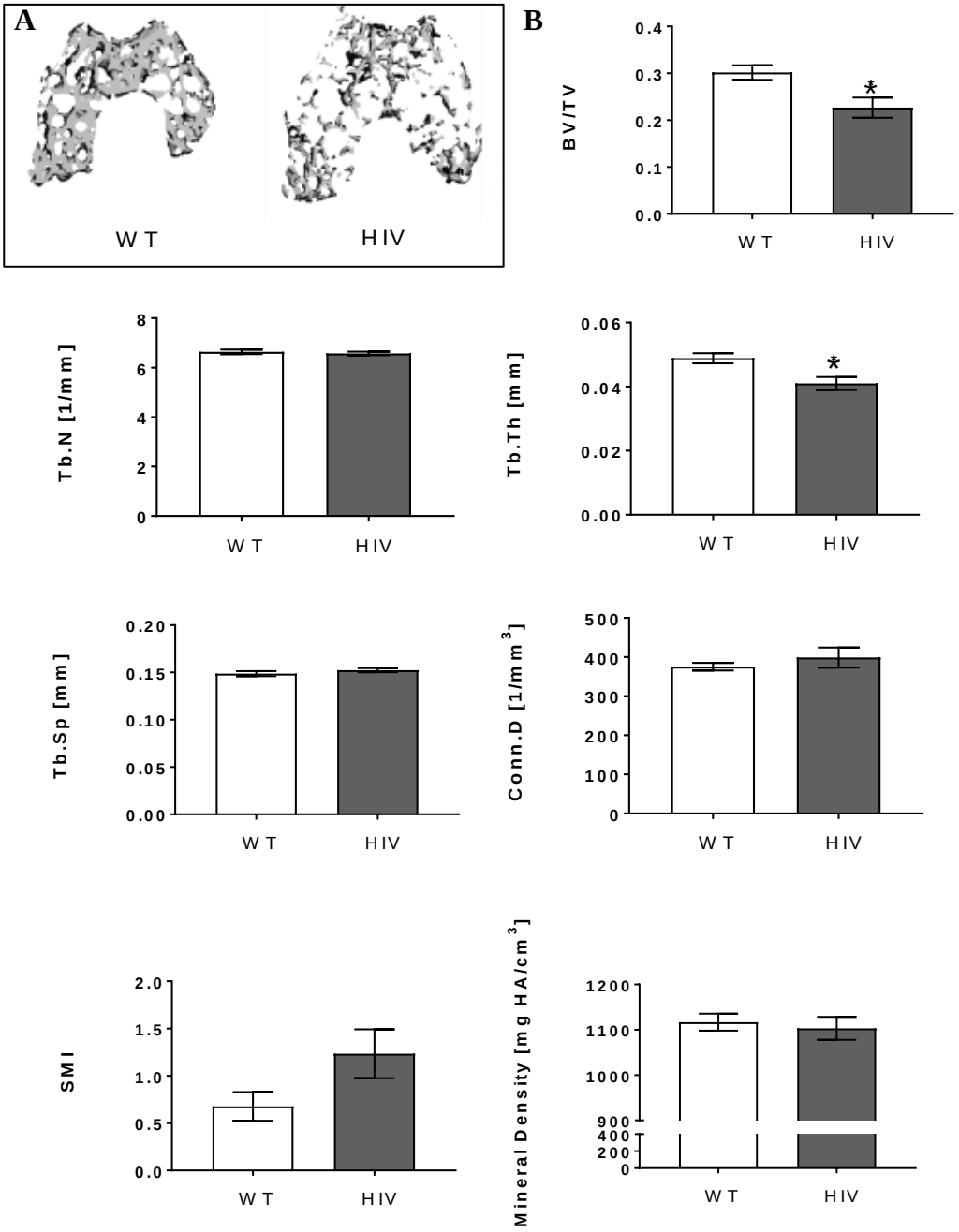

Figure 3-2: (A) Representative microCT 3D reconstructions of distal femur epiphysis. (B) MicroCT evaluation of trabecular bone at distal femur epiphysis. n = 10 per group. Error bars indicate SEM. * indicates significant difference between groups ($p < 0.05$). BV/TV = bone volume / total volume, i.e. bone volume fraction; Tb.N = trabecular number; Tb.Th = trabecular thickness; Tb.Sp = trabecular spacing; Conn.D = connectivity density; SMI = structure model index.

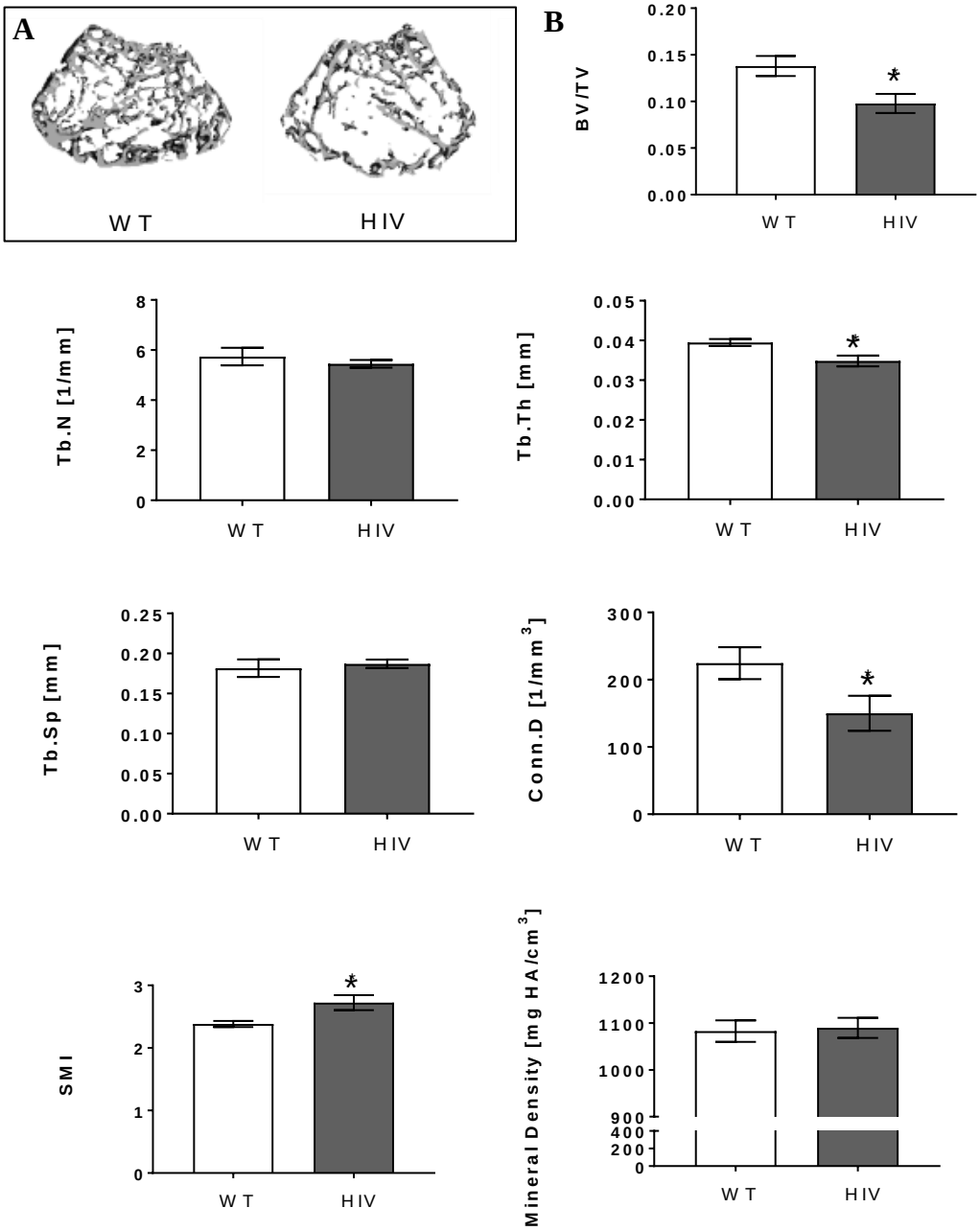

Figure 3-3: (A) Representative microCT 3D reconstructions of distal femur metaphysis. (B) MicroCT evaluation of trabecular bone at distal femur metaphysis. n = 10 per group. Error bars indicate SEM. * indicates significant difference between groups ($p < 0.05$). BV/TV = bone volume / total volume, i.e. bone volume fraction; Tb.N = trabecular number; Tb.Th = trabecular thickness; Tb.Sp = trabecular spacing; Conn.D = connectivity density; SMI = structure model index.

We further investigated effects on trabecular bone by scanning the trabecular compartment of L6 vertebra in the lumbar spine (Figure 3-4). Similar to the results found in the distal femur metaphysis, the BV/TV in HIV mice was lower (-24.8%, $p < 0.01$), trabeculae were significantly thinner (-27.1%, $p < 0.001$, Tb.Th), and SMI values were greater ($p < 0.001$) when compared to WT mice (Figure 3-4). In contrast to the metaphysis, we found HIV vertebrae had lower mineral density values (-6.9%, $p < 0.001$) and greater trabecular connectivity (40.3%, $p < 0.01$, Conn.D) which may be a consequence of greater resorption of plate-like trabeculae leading to an increased number of more rod-like trabeculae and less mature mineralized tissue. Although not statistically significant, comparison of the HIV vertebrae average trabecular number (15.7%, $p = 0.245$, Tb.N) and trabecular spacing (-10.9%, $p = 0.156$, Tb.Sp) values with WT vertebrae appears to support this observation. Additional data are presented in Table B-1.

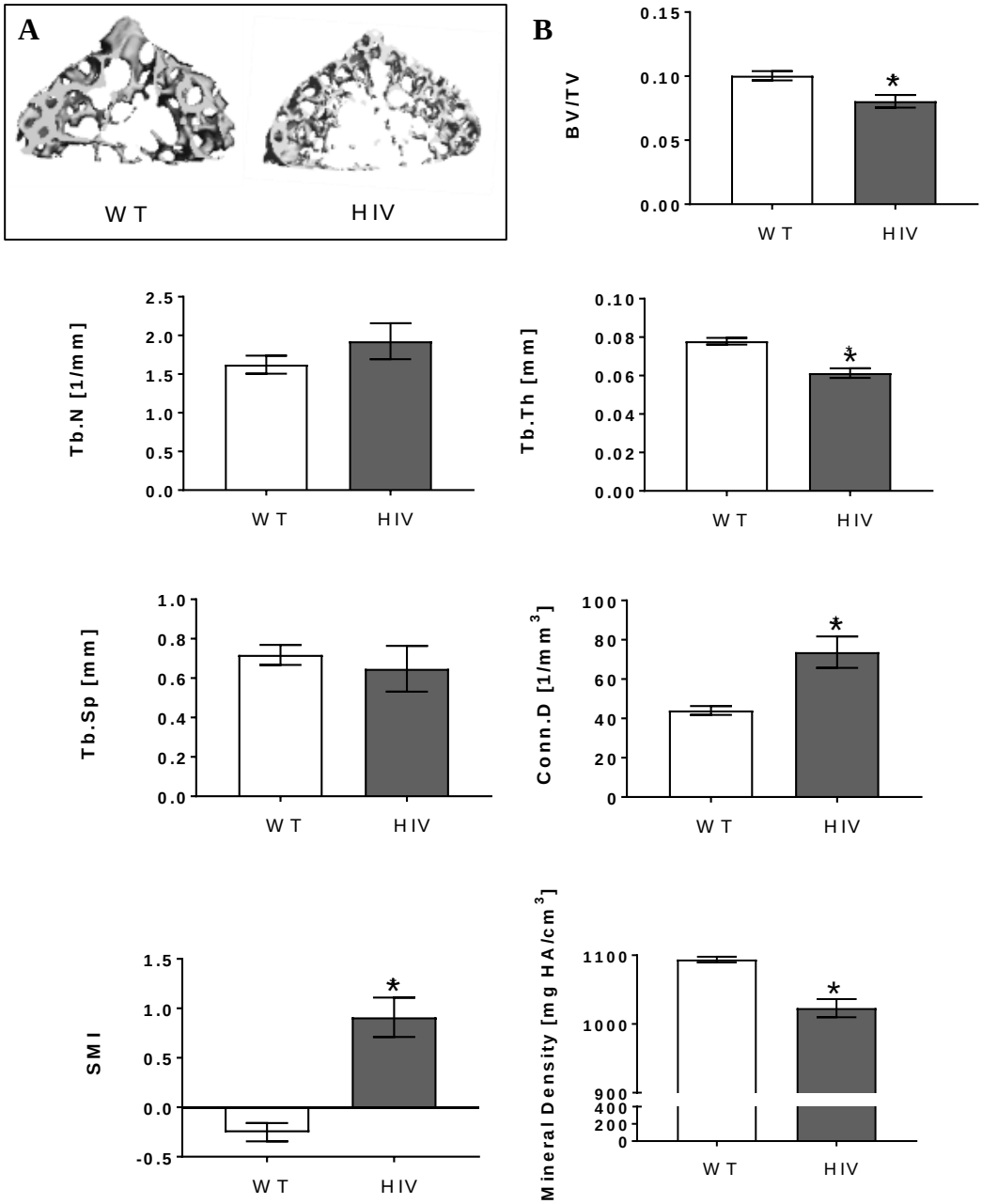

Figure 3-4: (A) Representative microCT 3D reconstructions of L6 vertebra. (B) MicroCT evaluation of trabecular bone at L6 vertebra. n = 10 WT; n = 9 HIV. Error bars indicate SEM. * indicates significant difference between groups ($p < 0.05$). BV/TV = bone volume / total volume, i.e. bone volume fraction; Tb.N = trabecular number; Tb.Th = trabecular thickness; Tb.Sp = trabecular spacing; Conn.D = connectivity density; SMI = structure model index.

Supplemental data for this section can be found in Table B-1.

3.3.2 Bone Biomechanical Phenotype

Through whole bone biomechanical testing, we sought to determine if bone mechanical properties were altered in HIV mice. Femurs were tested in three-point bending to assess cortical bone strength. Compared to WT mice, HIV mouse femurs were structurally weaker with lower ultimate load values (-19.8%, $p = 0.023$) and a 14.9% average lower stiffness value ($p = 0.165$) (Figure 3-5). Additionally, femurs from HIV animals absorbed less energy prior to failure (-28.8%, $p = 0.014$). However, we were unable to detect differences in derived material properties, suggesting that the diminished cortical bone mechanical properties in HIV femurs are due to the changes found in cortical bone morphology. Additional data are presented in Table B-1.

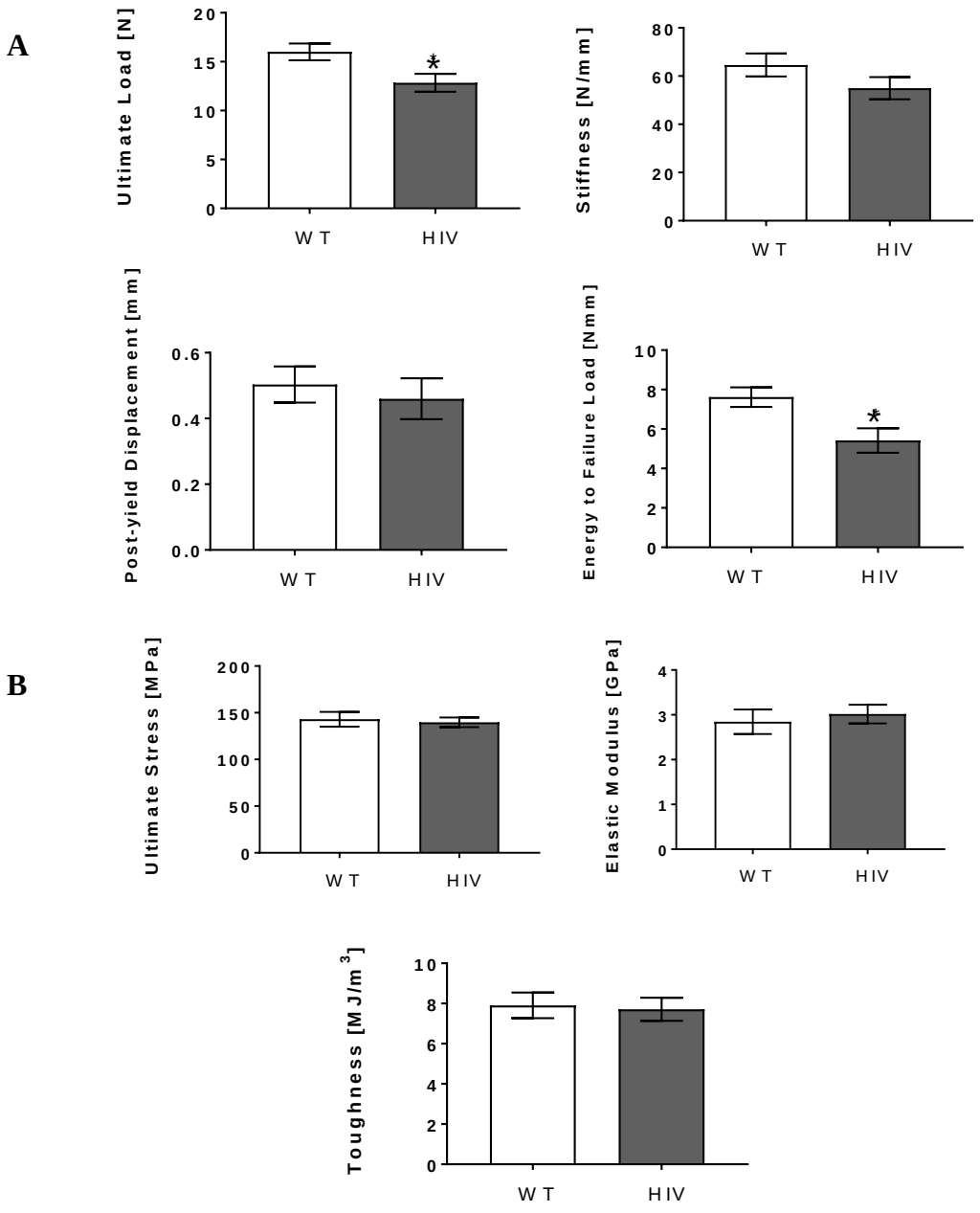

Figure 3-5. Biomechanical properties of whole femurs tested in three-point bending. (A) Measured structural properties. (B) Estimated derived material properties. n = 9 WT; n = 10 HIV. Error bars indicate SEM. * indicates significant difference between groups ($p < 0.05$).

In order to assess composite cortical and trabecular bone strength, we tested isolated whole vertebrae in displacement controlled compression. We found significantly weaker vertebrae in HIV mice with lower ultimate load (-39.8%, $p = 0.021$) and lower yield load

(-51.8%, p = 0.012) values (Figure 3-6). While not statistically significant, HIV vertebrae also had an average 29.9% reduction in stiffness (p = 0.089) and 43.7% decreased energy to ultimate load (p = 0.189). Similar to the femur, no significant differences were found when comparing derived material properties, again suggesting bone mass and microarchitectural changes are driving changes in mechanics. Additional data are presented in Table B-1.

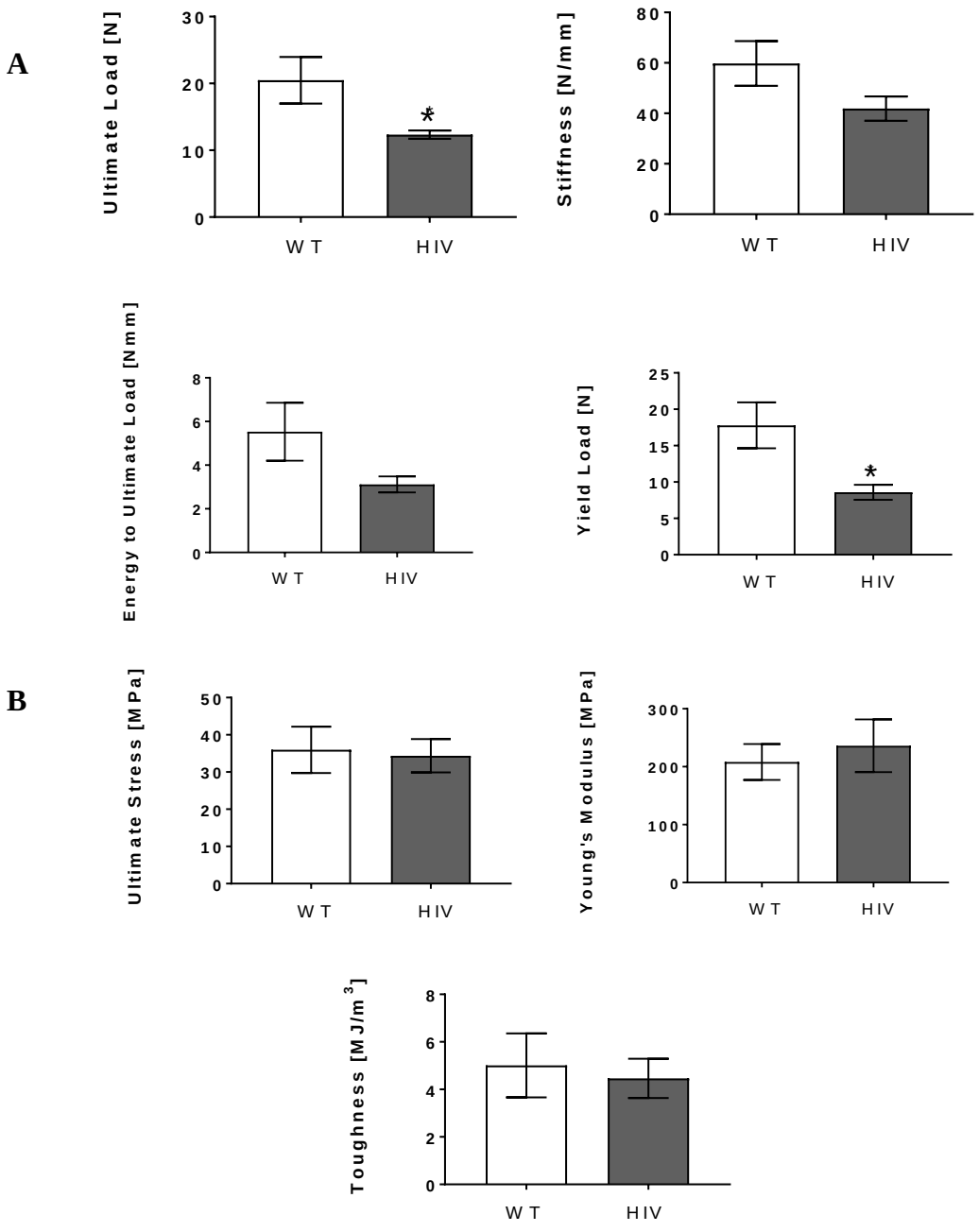

Figure 3-6. Biomechanical properties of L6 vertebrae tested in compression. (A) Measured structural properties. (B) Estimated derived material properties. n = 7 WT; n = 8 HIV. Error bars indicate SEM. * indicates significant difference between groups ($p < 0.05$).

3.3.3 Radiographic and MicroCT Evaluation of Fracture Healing

Digital 2-D radiographs were used to qualitatively assess pin stability and *in vivo* bone healing. No visual differences in the healing process were observed between WT and HIV animals (Figure 3-7). In contrast, analysis of microCT scans revealed significant differences in fracture healing between groups. At two weeks post fracture, although on average decreased in HIV animals, no differences were found in callus volume (WT: 44.91 ± 5.32 mm^3; HIV: 34.95 ± 4.39 mm^3; $p = 0.082$) or in mineralized callus volume (WT: 2.94 ± 0.33 mm^3; HIV: 2.16 ± 0.25 mm^3; $p = 0.355$) (Figure 3-8). At four weeks post fracture, callus volume for both groups was expectedly diminished from two weeks, but mineralized callus volume was found to be significantly lower in HIV mice (WT: 4.97 ± 0.68 mm^3; HIV: 3.6 ± 0.42 mm^3; $p = 0.041$). This difference was maintained even when comparing the percentage of mineralized tissue present in the callus between groups (WT: 22.84 ± 3.87 %; HIV: 14.93 ± 1.91 %; $p = 0.039$). The cross-sectional distribution of mineralized tissue within the callus as measured by polar moment of inertia (pMOI) was also significantly different between WT and HIV animals at Week 4 (WT: 1.07 ± 0.18 mm^4; HIV: 0.6 ± 0.08 mm^4; $p < 0.01$). No differences in average mineral density were found at any time point.

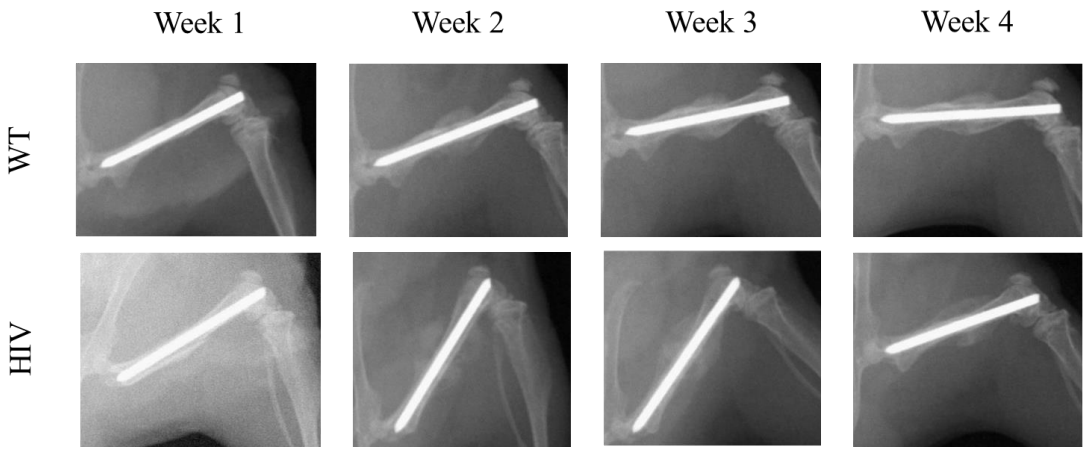

Figure 3-7. Representative 2-D radiographs of fracture healing

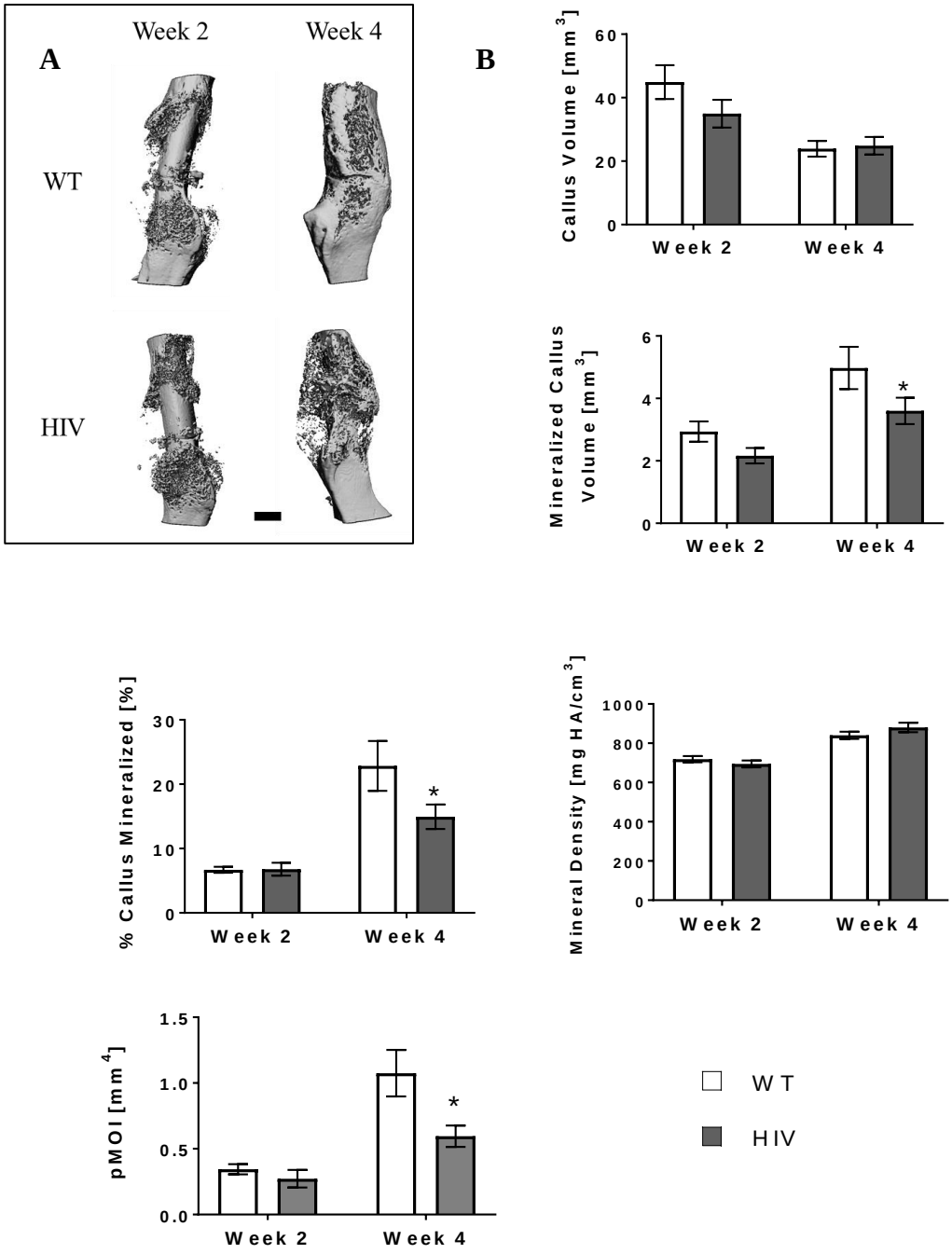

Figure 3-8. MicroCT evaluation of fracture healing. Week 2: n = 6 WT, n = 7 HIV; Week 4: n = 10 WT, n = 8 HIV. Error bars indicate SEM. Scale = 1 mm. * indicates significant difference between groups ($p < 0.05$).

3.3.4 Fracture Callus Biomechanical Properties

We performed torsional mechanical tests on fractured femurs to assess restoration of functional mechanics. Comparison of fractured femurs revealed an overall effect of HIV status for maximum torque ($p = 0.025$), energy to maximum torque ($p = 0.029$), and polar moment of inertia ($p < 0.01$, pMOI). Torsional stiffness data likewise warranted further analysis ($p = 0.051$), but the rotation to maximum torque did not ($p = 0.380$). As expected, no differences were found at Week 2 after fracture surgery (Figure 3-9). However, HIV fractured femurs were found to be mechanically weaker by Week 4 with lower maximum torque, torsional stiffness, and work to maximum torque. Neither HIV nor WT fractures at 4 weeks healed to the level of intact femur rotational mechanical properties (Table B-1).

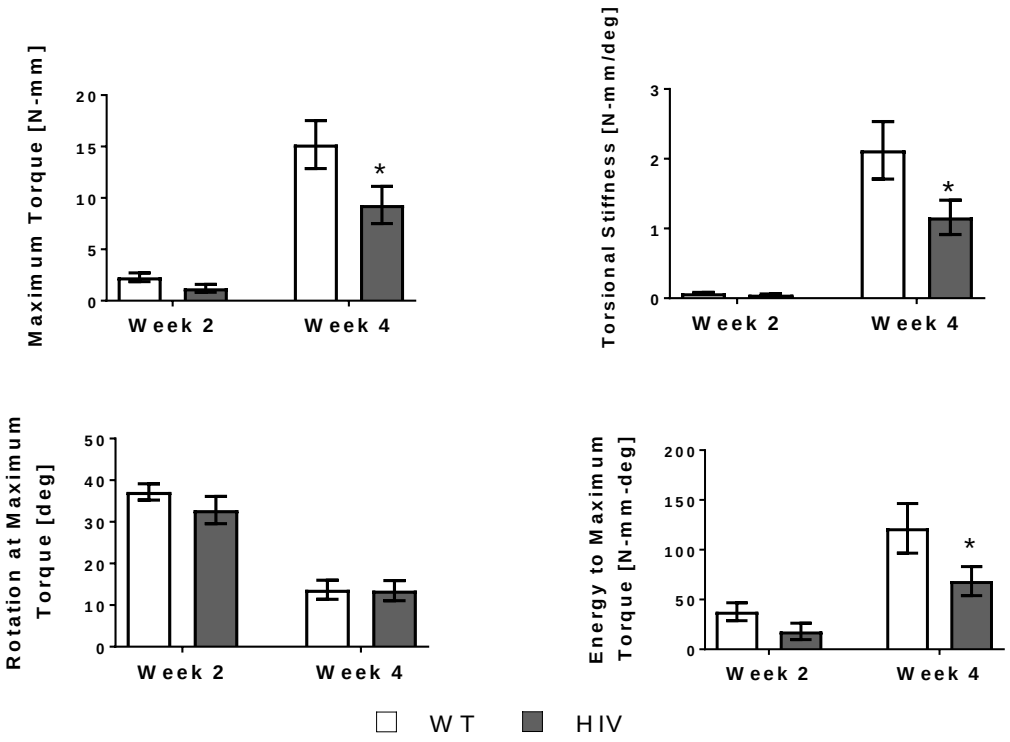

Figure 3-9. Biomechanical properties of fractured femurs. Week 2: n = 10 WT, n = 10 HIV; Week 4: n = 10 WT, n = 8 HIV. Error bars indicate SEM. * indicates significant difference between groups ($p < 0.05$).

3.3.5 Early Vascularization of Fracture Callus Analysis

Our microCT findings suggested that HIV animals may have deficiencies in early fracture callus formation and overall decreased mineralization resulting in compromised mechanical properties at four weeks post fracture. Taking these results together, we asked whether early vascularization in the fracture healing process could explain these later effects. Thus, utilizing contrast-agent enhanced microCT angiography, we quantitatively evaluated the vascular volume and morphology within the entire fracture callus at one week post fracture. No differences were found between groups for any measures (Figure 3-10). However, given the small sample size, it is not possible to draw any conclusions from these results.

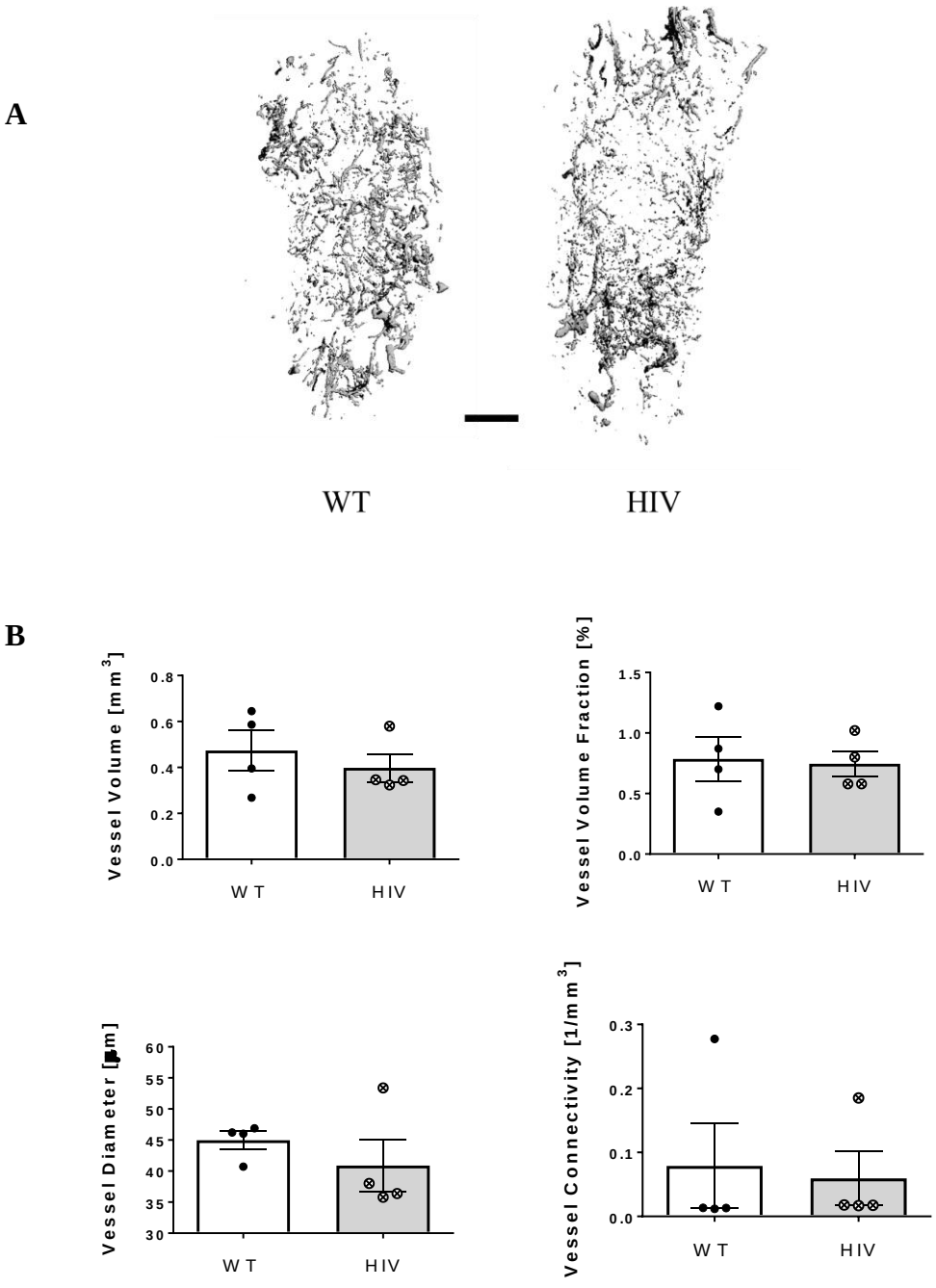

Figure 3-10. MicroCT analysis of Week 1 fracture callus vascularization. (A) Representative 3-D microCT reconstruction. (B) Quantitative evaluation of callus vasculature. n = 4 WT; n = 4 HIV. Error bars indicate SEM.

3.4 Discussion

Skeletal health in the HIV infected population is challenged by an increased risk for osteoporosis and fracture. Whether fractures in this group are at greater risk for impaired healing is unknown. We investigated whether an HIV-1 tg mouse with a *gag-pol* deleted HIV-1 provirus would present with similar decrements to bone microarchitecture and biomechanics as seen in humans, and we further sought to determine if bone healing is altered in this mouse model of HIV. We showed that HIV-1 tg mice had lower bone mass as reflected in measures of cortical bone area and trabecular bone volume fraction. HIV animals were also found to have thinner cortical bone and lower moment of inertia leading to reduced long bone structural mechanical properties. Additionally, trabecular bone in the distal femur was found to be altered with significant differences in the metaphysis. The trabecular compartment of the L6 vertebra likewise had thinner trabeculae with greater SMI values. Biomechanical testing of the vertebra revealed significant reductions in structural mechanical properties. We further showed a significant impairment of bone healing in the HIV animals that resulted in lower fracture callus mechanics by 4 weeks post injury.

Bone microarchitecture contributes to bone quality and is a key determinant of fracture risk [28, 64]. In the HIV-1 tg mouse, we found a reduction in cortical thickness and cortical area with a corresponding increase in marrow area. Interestingly, the average total cross-sectional area did not differ between groups. This may suggest similar periosteal growth characteristics between WT and HIV mice but a significantly greater level of endosteal resorption in the HIV mice. To study alterations in trabecular bone, we focused on the distal femur epiphysis and metaphysis and the L6 vertebra. At all sites, we found

decreased bone volume fraction and trabecular thickness in HIV mice and no differences in trabecular number or spacing. Differences in connectivity density and SMI were reflective of the unique physiologic environment seen by each skeletal site. HIV mice tended to have higher SMI values suggestive of a more rod-like characteristic although the epiphysis and L6 vertebra had a clear plate-like average morphology and the metaphysis had a clear rod-like average morphology. This is suggestive of a greater level of remodeling in the metaphysis with less direct mechanical loading. Changes in connectivity density that accompany decreased BV/TV may be a consequence of perforations of trabeculae which leads to an increase in connectivity or loss of trabecular struts leading to a decrease in connectivity. HIV animals had less connections in the metaphysis possibly reflecting the latter situation and more connections in the L6 vertebra reflecting the former scenario. There was no difference in connectivity density in the epiphysis suggesting that the reduction in BV/TV was mediated mainly by trabecular thinning in HIV mice. Together, these findings show an overall decrease in bone mass primarily as a consequence of thinning of both cortical and trabecular bone with site-specific negative changes to trabecular microarchitecture.

Unlike humans, mice continue to experience longitudinal bone growth after sexual maturity at 6-8 weeks and reach peak bone mass between 4 and 6 months of age [172]. The mice used to investigate bone structure and mechanics were 10-12 weeks of age, falling just short of the reported peak bone mass seen in other mice. However, local attainment of peak bone mass depends on the anatomical site and the differing ratios of cortical to trabecular bone [173]. Trabecular bone compartments tend to reach peak bone mass earlier in life and slowly decrease with age while adapting to loads by adjusting geometry and

orientation [173]. Thus, our findings suggest either an early deficit in bone mass accrual or accelerated loss of bone with age in HIV-1 tg mice. Longitudinal studies to investigate changes in bone microarchitecture with age are needed to determine how and when the deficits in bone microarchitecture occur and if there is an interplay between age and expression of HIV-1 proteins in the HIV-1 tg mouse.

It is possible that bone remodeling is altered as a consequence of HIV-1 gene expression in the HIV-1 tg mouse used in this study. This model expresses HIV-1 genes in skin, muscle, tail, and less abundantly in kidneys, intestine, and thymus [174]. Cheng et al. showed that mesenchymal stromal cells isolated from compact bone from HIV-1 tg mice expressed HIV-1 genes and subsequently had impaired proliferation and differentiation [109]. In a different transgenic mouse expressing HIV-1 Nef, osteoclast resorption was enhanced resulting in reduced bone density and increased bone fragility [103]. Multiple studies have shown *in vitro* HIV-1 protein effects on osteoclastogenesis [99-101], osteoclast activity [102], osteoblast activity [104-107], and mesenchymal stem cells [105, 108, 110-112] that suggest imbalanced bone turnover processes through increased bone resorption and impaired bone formation. Bone remodeling can also be influenced by immune cells through the immuno-skeletal interface [113]. Specifically, T and B cells are involved in modulation of osteoclastogenesis and bone resorption by secretion of OPG and RANKL to influence the RANKL/OPG ratio in the local bone environment. In both HIV-1 transgenic mice expressing either *nef* or *tat*, alterations to T cell development occur along with dysfunctional T cell activity and loss of peripheral CD4+ T cells [175-177]. Alterations to B cell development may also occur in HIV-1 tg mice used in this study, however the severity of this effect may be highly variable from animal to animal [146].

Additionally, a pair of studies in the HIV-1 tg rat and in HIV infected humans have uncovered a severe imbalance in the B cell RANKL/OPG ratio that correlates with low BMD in humans [24, 114]. HIV-1 proteins can therefore influence normal bone remodeling in the HIV-1 tg mice through various avenues resulting in the bone microarchitectural deficits seen in our study.

Although it is known that bone microarchitecture is critical in determining bone strength and ultimately fracture risk, few studies have investigated bone mechanical properties in HIV patients. In this study, changes in bone microarchitecture led to deficits in bone biomechanics in both the femur and the L6 vertebra of HIV mice. Derived material properties were not different between groups suggesting that structural differences in bone microarchitecture and not tissue level alterations contribute to the loss of mechanical strength in HIV bone. Our findings are supported by the few studies found in the literature. One study used micro finite element analysis using HR-pQCT scans of human distal radius and distal tibia and showed a reduction in stiffness in HIV positive young men [87]. In a humanized mouse model infected with HIV and treated with tenofovir disoproxil fumarate (TDF), femurs were tested using microindentation using the Vickers hardness test and tibiae were tested under three-point bending [161]. The HIV and TDF mice had the lowest average hardness value followed by HIV mice, but HIV mice had the lowest ultimate load and stiffness values. Contrary to our findings, Guerri-Fernandez and colleagues used microindentation at the midpoint of the midshaft anterior tibial plateau and found decreased bone material properties in HIV patients, especially women, that was independent of BMD and ART [131]. Whether bone from HIV individuals or HIV-1 tg mice have diminished

bone material properties leading to vulnerability to formation of microdamage and thus fractures warrants further study.

Clinical studies have shown an increased risk and incidence of fractures in the HIV-infected population [9, 132]. Spontaneous fractures do not occur in mice, but methods have been developed to create controlled fractures in order to investigate bone healing under varying conditions [26, 178]. We utilized a small long bone osteotomy with intramedullary pin model to create a closed fracture in HIV-1 tg mice in order to investigate bone healing. Early callus size and amount of mineralization at 2 weeks post fracture, although not significant, were 22.2% and 26.4% greater, respectively, in the WT mice, but the percent mineralized callus volume was not different. This suggests a similar early fracture healing process between WT and HIV that is attenuated in the HIV mouse. However, 4 weeks after bone injury showed distinctly greater mineralized callus volume in the WT mice that conferred sufficient structural integrity for differences in mechanical properties to be apparent.

Early soft callus formation is initiated by the inflammatory phase which recruits osteochondroprogenitors necessary for deposition of cartilage and subsequent woven bone [37, 135]. It may be in the HIV-1 tg mice potentially having dysfunctional T and B cells that early bone healing is attenuated as reflected in the microCT data. Interestingly, although complete depletion of T and B cells results in faster bone healing and recovery of callus mechanical properties, this is because of a quicker progression of callus formation and mineralization that ultimately compromises the quality of the subsequent bone [136, 137]. We did not see this accelerated healing in the HIV-1 tg mice because the adaptive immune system is not depleted in this model, but that does not preclude any negative

impact on bone healing due to dysfunctional T cells [179] or direct HIV-1 protein effects in this model. Studies of systemic and local chronic inflammation in mice have shown decreased bone healing [180] and delayed bone healing [181], respectively, suggesting an effect of systemic inflammation and not local chronic inflammation on bone healing in the HIV-1 tg mouse. Based on the findings presented here, it appeared bone healing may have been impaired at an earlier stage possibly due to impaired vascularization of the fracture region. A brief investigation of early vascularization did not show differences between groups, but this may be due in part to the small sample size. However, there may be an effect of HIV on vascularization in fracture healing and on angiogenesis in general [182-185] that has yet to be fully investigated.

This study has several limitations. The HIV-1 tg mouse is not a model of direct HIV infection and therefore does not model the human situation. However, multiple studies have investigated HIV associated conditions using this animal model, validating it as a useful model of HIV-1 infection under effective ART. Although HIV-1 gene expression varies by degree and anatomical location in the HIV-1 tg mouse, the localization of proteins in lymphoid tissues reflects that seen in HIV-infected persons [62]. The use of two different mouse strains was necessary due to availability of samples and animal health and welfare concerns. HIV-1 tg mice on the FVB/N background presented with a more severe disease-like state resulting in death by 4 months. In contrast, HIV mice on the C57BL/6 background do not present with early cataracts and need to be genotyped by tail snip. However, C57BL/6 mice have low bone mass compared to other strains [186] and compared to FVB/N may have reduced bone microarchitecture measures [187] and decreased bone healing [188]. It would be valuable to compare the severity of disease symptoms between

the two strains and determine if differences in skeletal phenotype and bone healing exist, potentially providing insight into the genetic differences in the effects of HIV on bone development and healing.

The relationship between HIV and skeletal health is complex and requires further study to fully elucidate. The HIV-1 tg mouse provides an attractive vehicle for this exploration. This small animal model is noninfectious, easily bred and maintained, and recapitulates conditions seen in the human condition. Our work further shows that this model additionally recapitulates an osteoporotic bone phenotype with altered microarchitecture and decreased mechanics. Notably, the HIV-1 tg mouse also presents with impaired fracture healing characterized by decreased callus mineralization and mechanics.

CHAPTER 4. SKELETAL PHENOTYPE OF GROWING HIV-1 TRANSGENIC RAT

4.1 Introduction

With effective antiretroviral therapy (ART), the HIV infected population has a life expectancy near that of the uninfected population [2, 3]. However, an increase in life span has brought with it comorbidities not seen before the era of ART including cardiovascular disease, renal disease, neurocognitive impairment and osteoporosis [4, 117, 163]. As the rate of new infections remains significant and adherence to treatment improves [189], this population continues to grow and age bringing with it risks to skeletal health, specifically osteoporosis and fracture risk, associated not just with HIV and ART but also with aging [117, 190]. In a trend analysis between 2003 and 2013 of US patients receiving healthcare coverage commercially, from Medicaid, or from Medicare, prevalence of osteoporosis and fractures was 7.8%, 13.3%, and 24.4% with a significant increase over time in the Medicare and Medicaid groups but not the commercial group [4]. Gallant et al. also found a significantly greater prevalence of osteoporosis and fractures in the commercial and Medicaid payers but not the Medicare payers when compared to uninfected controls. Given the proportion of patients 50 years or older in the commercial (24.7%), Medicaid (21.5%), and Medicare (97.4%) groups, it is apparent that the HIV population is at risk of osteoporosis and fractures at all ages with greater risks at older age. With an estimated 4.2 million HIV infected individuals over the age of 50, a number that will continue to increase [54], there is substantial concern for an increased burden on healthcare systems [51, 191].

In addition, there are over 2 million children under 15 years of age living with HIV globally [1]. Whether infected perinatally or early in life, this population sees the greatest negative impact over their lifetime on their bone health from HIV infection and ART [192]. Bone mass accrual occurs rapidly from birth to about the mid-20s at which point peak bone mass is achieved [88, 89]. Peak bone mass in turn is a critical predictor of osteoporosis and fracture risk [193, 194]. In a study of HIV infected males in their early 20s, Yin et al. showed that early infection results in a subnormal peak bone mass [87]. Several studies have also shown that HIV infected children and adolescents have lower bone mass compared to their uninfected counterparts [84-86]. Additionally, given the sex differences in skeletal growth [89, 195], HIV infected females may be at a greater risk of detrimental impacts on later life skeletal health [86, 196].

The laboratory rat has been used extensively to study osteoporosis [197]. Although rats do not naturally experience age-related bone loss, models have been developed that approximate closely the human condition. Reid et al published the first work establishing an HIV-1 rat model that was transgenic for an HIV provirus lacking the *gag-pol* region [17]. This provirus was adapted from the one used to establish the HIV-1 tg mouse utilized in Chapter 3 of this work [16, 20]. In contrast with the mouse, the HIV-1 tg rat exhibits more efficient viral gene expression especially in the lymph nodes, spleen, thymus, and blood [17, 144]. This model has since been used in studies on many HIV-associated comorbidities including cardiovascular disease [21, 151, 152], pulmonary disease [153, 154], neurocognitive disorders [144, 155], liver disease [156, 157], and nephropathy [22, 158]. Additionally, Peng et al. showed that the HIV-1 tg rat model could be used as a model for patients on effective ART [198]. Interestingly, they found that the distribution of HIV

gene expression varied with age changing from high expression of proteins in the spleen at 2-3 months of age to high expression in the spinal cord and cerebellum at 10-11 months. Recently, Vikulina and colleagues showed that the HIV-1 tg male rat recapitulates the osteoporotic phenotype seen in humans [24]. They found decreased BMD and altered microarchitecture in male rats at 8-9 months of age but no skeletal growth or mechanics data were reported.

The main objective of this study was to investigate the longitudinal skeletal changes of the growing HIV-1 tg female rat in order to determine if there are age-dependent changes in bone structure. Since the rat develops AIDS-like symptoms between the ages of five and nine months [17], we hypothesized that the HIV-1 tg rat would exhibit significant changes to bone microarchitecture between five and nine months of age that would lead to long term changes in bone structure and biomechanics.

4.2 Materials and Methods

4.2.1 HIV-1 Transgenic Rat Model

Female HIV-1 transgenic (tg) rats (n = 10, HIV) and control F344/NHsd rats (n = 11, WT) were purchased from Harlan Laboratories at approximately 9 to 10 weeks of age. Animals were used for this study beginning at four months of age and ending at twelve months of age. Rats were pair-housed in sterile caging under a 12 hour light/dark cycle and provided food (Teklad Global Diet 2918) and water *ad libitum*. All procedures were approved by the Georgia Institute of Technology Institutional Animal Care and Use Committee (IACUC).

4.2.2 Microcomputed Tomography

Each month from 4 to 12 months of age, animals were anesthetized using isoflurane inhalation and scanned *in vivo* using microCT (vivaCT40, Scanco Medical) at a resolution of 21 μm, energy of 55 kVp, and current of 145 μA. A total of three skeletal sites were scanned each month in the left femur (mid-diaphysis, distal femur) and the L6 vertebra. The approximately central 1 mm region of the femoral mid-diaphysis was analyzed for cortical bone morphometric parameters (bone area, BA; bone marrow area, MA; total area, TA; cortical thickness, Ct.Th; moment of inertia, MOI; polar moment of inertia, pMOI; and mineral density). The distal femur at two regions of approximately 1 mm – epiphysis and metaphysis – and a 2.1 mm region in the L6 vertebra were analyzed for trabecular bone parameters (trabecular number, Tb.N; trabecular thickness, Tb.Th; trabecular spacing, Tb.Sp; structure model index, SMI; bone volume fraction, BV/TV; connectivity density, Conn.D; and mineral density). Regions of interest were identified relative to the distal growth plate for the distal femur and the cranial growth plate for the L6 vertebra.

At twelve months of age, animals were euthanized via CO_2 inhalation and femurs and lumbar spine were harvested. Samples were wrapped in saline soaked gauze and stored at -20°C. Samples were placed in PBS to thaw to room temperature prior to preparation for microCT scanning. Femurs were cleaned of all soft tissue and scanned at a 16 μm resolution (55 kVp, 145 μA, μCT40 system, Scanco Medical). Approximately a 1 mm region at the mid-femur was analyzed for cortical bone morphometric parameters. Vertebral bodies of L6 vertebrae were isolated and scanned at a voxel size of 12 μm. A 2.1 mm region below the cranial growth plate was analyzed for total bone volume fraction.

4.2.3 Blood Collection and Serological Analysis

Blood was collected at 4, 5, 7, 9, and 11 months of age. Observations of rats after the first two consecutive months of microCT scanning and blood collection suggested slow recovery of animal weight and vitality. In addition, one WT rat was found dead in its cage the following day after blood collection. Therefore, blood collection frequency was reduced to once every two months. No more than 10% of the total circulating blood volume up to 1 mL of blood was collected from the tail ventral artery of each animal [199]. Briefly, animals were anesthetized on a heating pad and acepromazine maleate – a vasodilator and mild sedative – was administered at a concentration of 1.5 mg/kg. After waiting 7 minutes, blood was collected into a blood collection tube and allowed to sit undisturbed for at least 1 hour to allow for clotting. Blood samples were centrifuged at 15,000g RCF for 5 min, divided into aliquots, and stored at -20°C. Any serum samples that were not clear and had any signs of pink coloration were excluded from analysis. To assess global bone turnover differences, serum levels of osteocalcin and C-terminal telopeptides of type I collagen (CTx) were measured using commercially available ELISA kits (Rat-MID and RatLaps, respectively; Immunodiagnostic Systems).

4.2.4 Mechanical Testing

Femurs were tested to failure displacement controlled 3-point bending at a rate of 0.6 mm/min with a span of 19 mm using a servo-hydraulic mechanical testing system (858 Mini Bionix II, MTS Corp). Femurs were centrally loaded in the anterior to posterior direction. Vertebrae were tested under displacement controlled compression to failure at a rate of 0.5 mm/min. Structural properties were calculated directly from the load-

displacement curve (ultimate load, stiffness, and energy to ultimate load or failure load). Derived material properties were calculated from the load-displacement data using standard equations (Ultimate stress, elastic modulus, and toughness to ultimate stress or failure stress) [171]. All samples were kept moist with PBS throughout testing.

4.2.5 Statistics

All data are presented as mean ± SEM. Data from *in vivo* microCT and serum analysis were analyzed using a mixed ANOVA following the general linear model (GLM) repeated measures procedure in SPSS (SPSS Statistics 24). Pairwise comparisons were adjusted using the Bonferroni correction. Biomechanical properties between WT and HIV rats were analyzed using unpaired two-sample Student's t-test. A significance level of 0.05 was set for all analyses.

4.3 Results

4.3.1 General Observations

Body weight was significantly different between WT and HIV animals at all ages in this study (Figure 4-1). Linear regression analysis revealed that the rate of weight gain – defined as the slope (m) of the regression equation ($y = b + m*x$) – for WT rats was significantly greater than HIV rats (WT: $m = 7.10 \pm 0.66$, $b = 163.2 \pm 5.56$, $R^2 = 0.5431$; HIV: $m = 5.12 \pm 0.50$, $b = 139.5 \pm 4.17$, $R^2 = 0.5474$; $p = 0.019$).

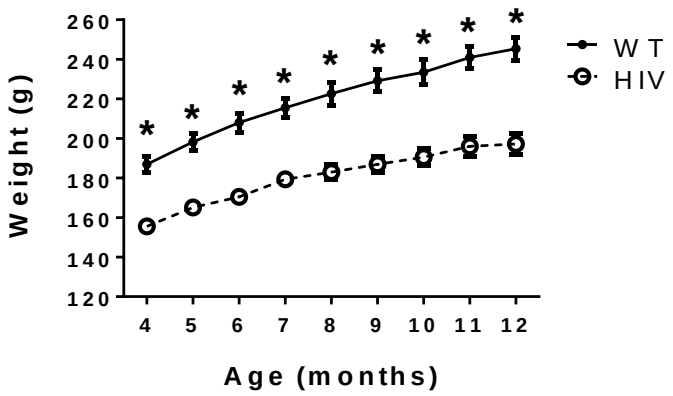

Figure 4-1. Body mass of WT and HIV rats. n = 11 WT, n = 10 HIV. Error bars indicate SEM. * indicates significant difference between groups ($p < 0.05$).

4.3.2 Longitudinal Bone Microarchitecture

In order to evaluate bone microarchitecture changes, microCT scans were performed over a period of nine months at three different skeletal sites: femur mid-diaphysis, distal femur, and L6 vertebra. Femurs were significantly longer in WT animals compared to HIV at every time point (Figure 4-2). Evaluations of the cortical bone at the femoral mid-diaphysis also showed significantly smaller bones in HIV animals at every time point (Figure 4-3). Differences in bone average mineral density were not found. For measures with significant differences, linear regression analysis showed no differences in the slopes between WT and HIV rats. Despite the greater rate of weight gain in WT animals, we do not see a corresponding difference in the rates of cortical bone growth.

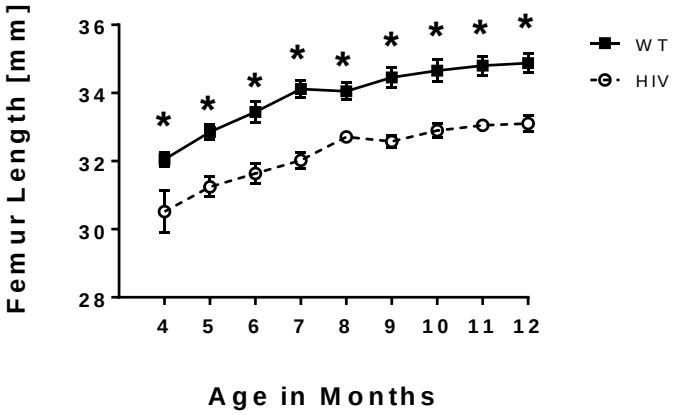

Figure 4-2. Femur lengths of WT and HIV animals. n = 11 WT, n = 10 HIV. Error bars indicate SEM. * indicates significant difference between groups ($p < 0.05$).

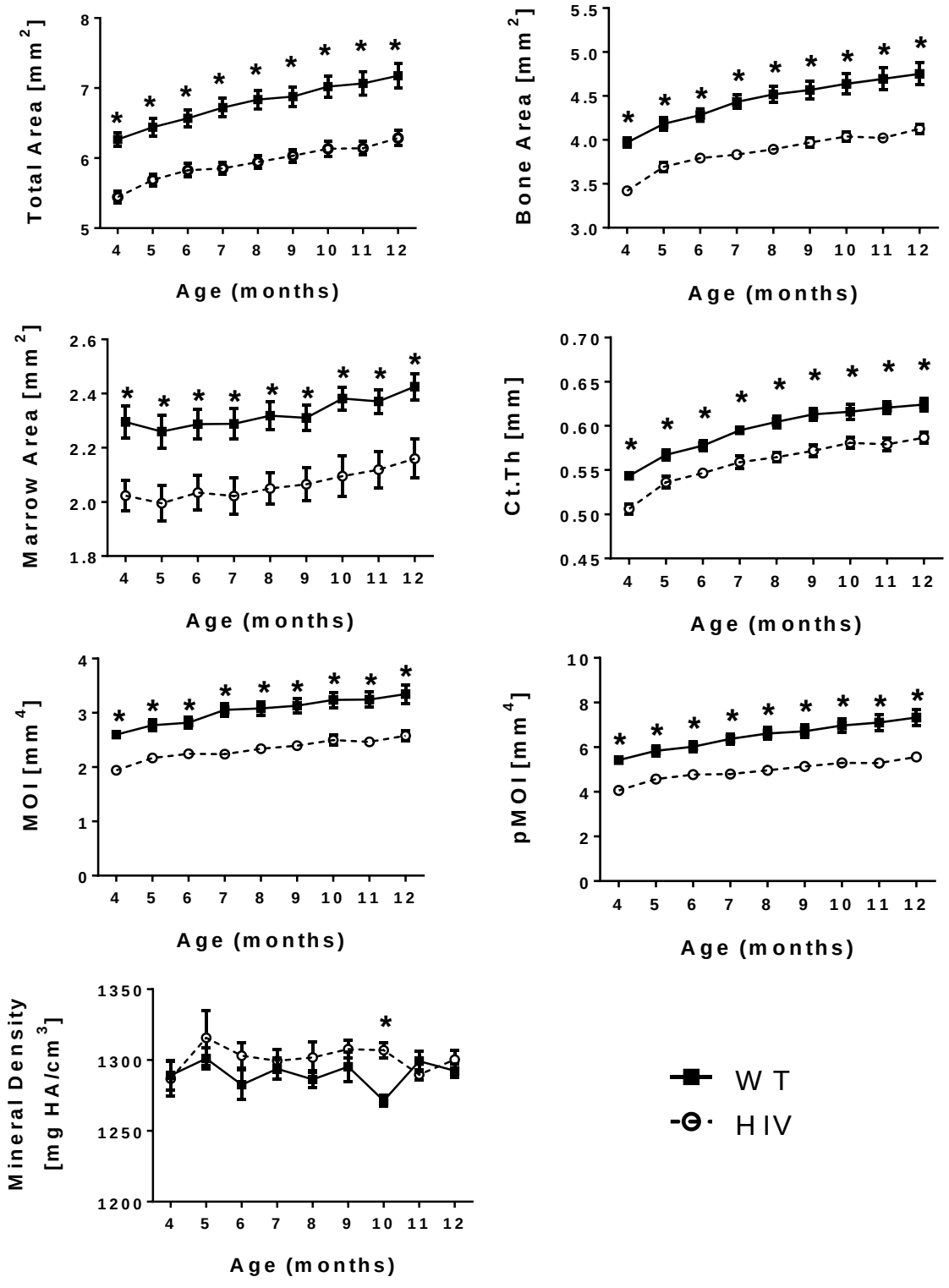

Figure 4-3. MicroCT evaluation of cortical bone morphology at the femur mid-diaphysis. n = 11 WT, n = 10 HIV. Error bars indicate SEM. * indicates significant difference between groups ($p < 0.05$). Ct.Th = cortical thickness; MOI = moment of inertia; pMOI = polar moment of inertia.

The distal femur epiphysis and metaphysis were analyzed separately for trabecular bone architecture. Overall evaluation of the data showed that for both groups, the bone volume fraction in the femoral epiphysis increased with age from four months to twelve months (Figure 4-4). This increase in bone mass is mediated by increases in trabecular thickness (Tb.Th) as trabecular number (Tb.N) and spacing (Tb.Sp) appear to remain at a constant level. Connectivity density (Conn.D) decreased with age as did SMI values suggesting loss of more rod-like trabecular struts in favor of more plate-like trabeculae. At the femoral epiphysis, no overall differences between WT and HIV animals in bone mass were detected ($p = 0.667$, BV/TV), but early time point evaluation at four ($p = 0.083$) and five ($p = 0.044$) months of age suggest there may be differences at earlier ages. While there were no differences in trabecular morphology between groups especially with Tb.Th ($p = 0.838$), further analysis of Tb.N ($p = 0.090$), Tb.Sp ($p = 0.054$), and Conn.D ($p = 0.054$) suggested that HIV animals may have fewer trabeculae (4 months: $p =0.044$; 6 months: $p = 0.078$; 8 months: $p = 0.079$; 9 months: $p = 0.084$) with greater spacing (4 months: $p =0.029$; 5 months: $p = 0.083$; 6 months: $p = 0.027$; 8 months: $p = 0.041$; 9 months: $p = 0.032$) and lesser degree of connectivity (4 months: $p = 0.056$) at earlier ages.

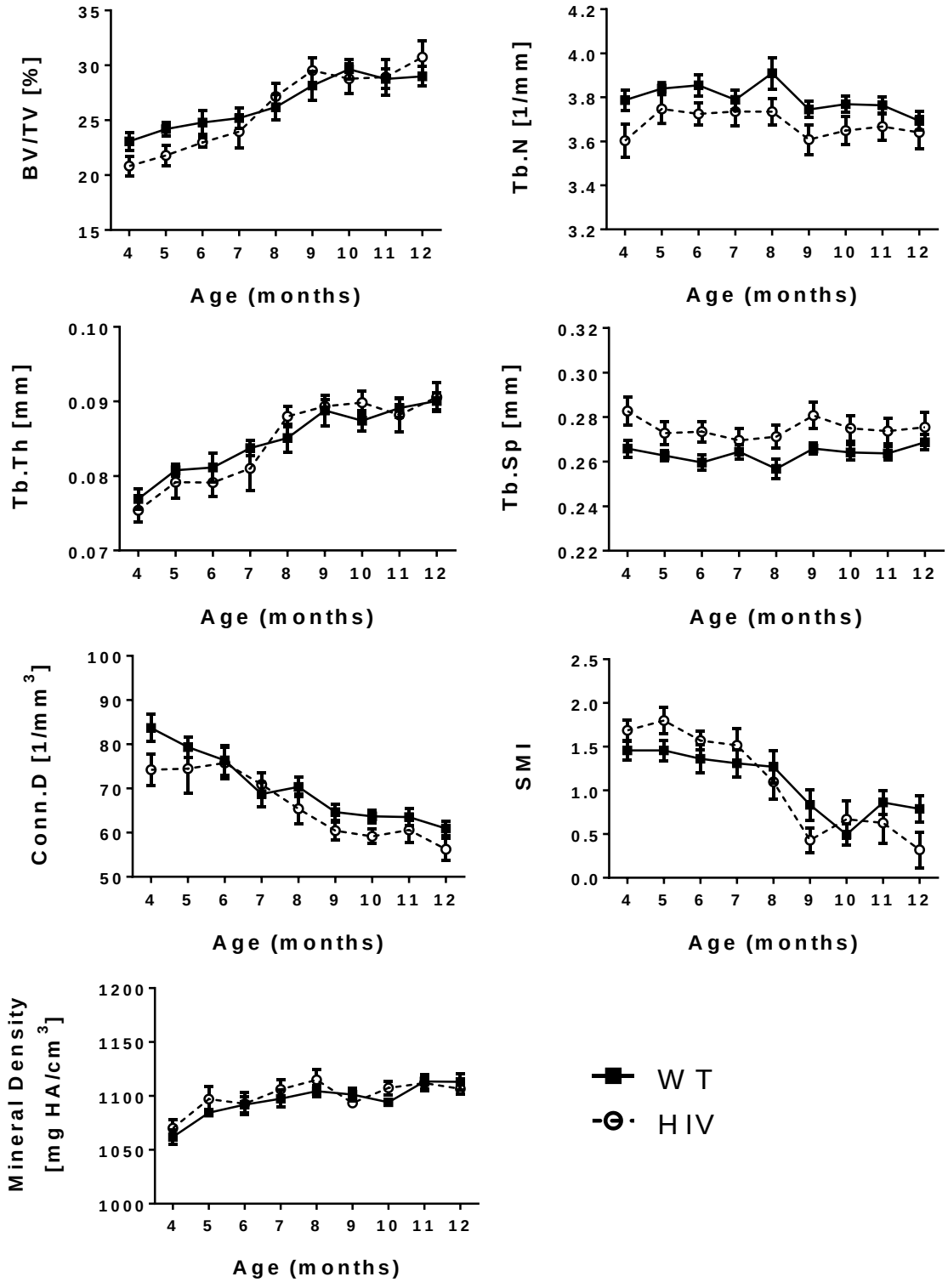

Figure 4-4. MicroCT evaluation of trabecular bone architecture at the distal femur epiphysis. n = 11 WT, n = 10 HIV. Error bars indicate SEM. * indicates significant difference between groups ($p < 0.05$). BV/TV = bone volume / total volume, i.e. bone volume fraction; Tb.N = trabecular number; Tb.Th = trabecular thickness; Tb.Sp = trabecular spacing; Conn.D = connectivity density; SMI = structure model index.

As in the femur epiphysis, general changes in bone for both WT and HIV animals in the femur metaphysis consisted of increasing BV/TV, Tb.Th, and mineral density with unchanging values for Tb.N and Tb.Sp between four and twelve months of age (Figure 4-5). An increase in Conn.D was also seen with increasing age for both groups. In contrast to the epiphysis, analysis of the distal femur metaphysis revealed significant alterations to the morphology of trabeculae in HIV animals. Overall, HIV animals had less bone in the metaphysis ($p < 0.01$, BV/TV) with specific differences at 4, 6, 8, 9, and 10 months of age. Similarly, Tb.Th was lower in HIV rats overall ($p = 0.004$) with significant differences at nearly all time points except 7, 11, and 12 months of age. No differences were found in Tb.N, Tb.Sp, or bone mineral density, but the trabecular network in HIV animals was characterized by less connectivity ($p = 0.011$) and more rod-like architecture ($p < 0.01$).

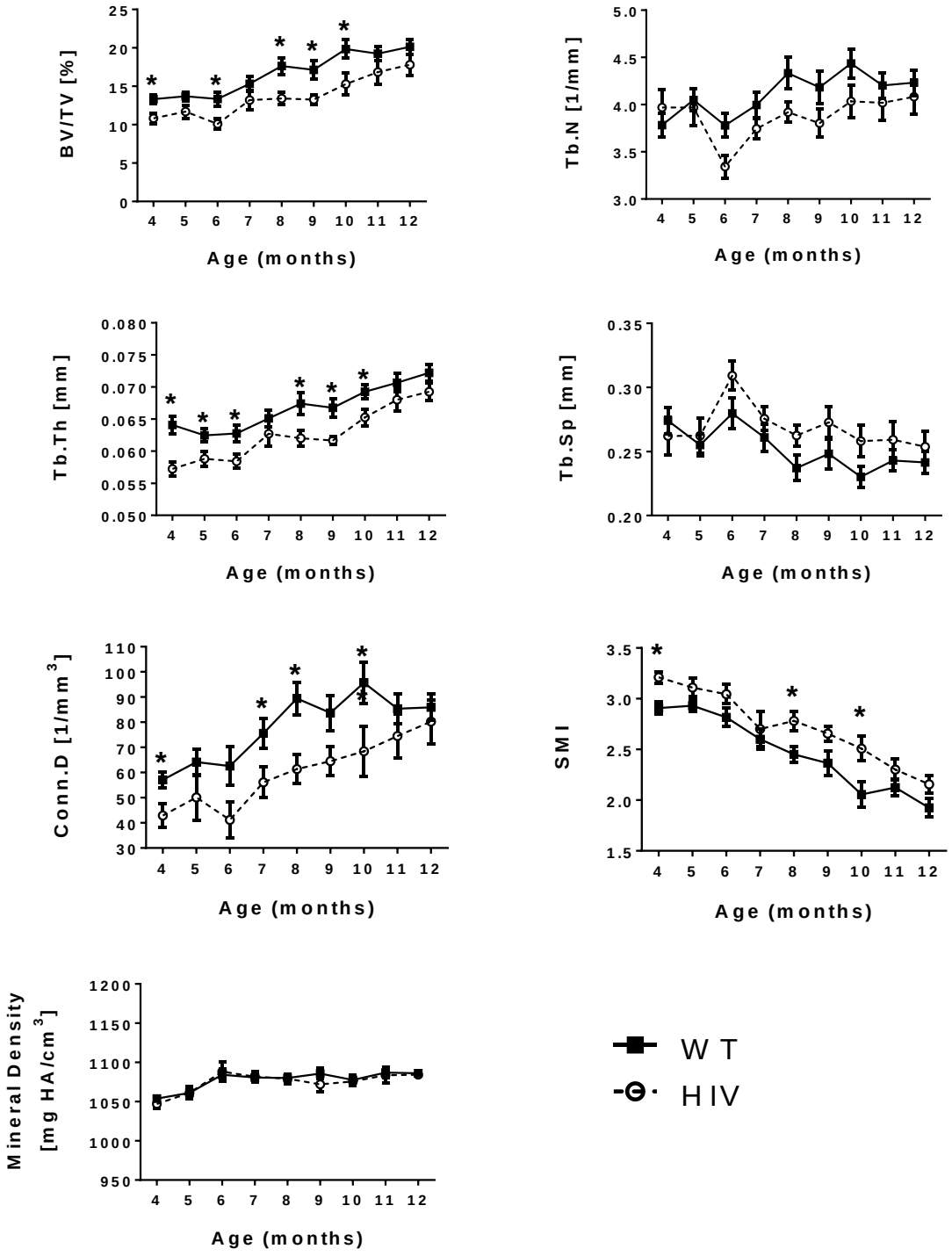

Figure 4-5. MicroCT evaluation of trabecular bone architecture at the distal femur metaphysis. n = 11 WT, n = 10 HIV. Error bars indicate SEM. * indicates significant difference between groups ($p < 0.05$). BV/TV = bone volume / total volume, i.e. bone volume fraction; Tb.N = trabecular number; Tb.Th = trabecular thickness; Tb.Sp = trabecular spacing; Conn.D = connectivity density; SMI = structure model index.

Unlike the changes in the femur, the vertebral trabecular bone structure appears to be more stable during this period of growth in the female rat. Both groups had initial increases in BV/TV, Tb.N, and Tb.Th and decreases in Tb.Sp and SMI values from four to six months of age (Figure 4-6). With the exception of Conn.D, which appears to increase then decrease with age, all other measures remain relatively stable from six to twelve months of age. When comparing between groups, BV/TV was significantly lower in the HIV group ($p < 0.001$) for all time points except at six ($p = 0.056$) and seven ($p = 0.058$) months of age. Similarly, Tb.Th values were lower in the HIV group ($p < 0.001$) for all time points except seven ($p = 0.209$) and eight ($p = 0.087$) months of age, and SMI values were larger in the HIV group ($p = 0.001$) for all time points except six ($p = 0.086$) and twelve ($p = 0.093$) months of age. No differences were detected for Tb.N, Tb.Sp, Conn.D or mineral density.

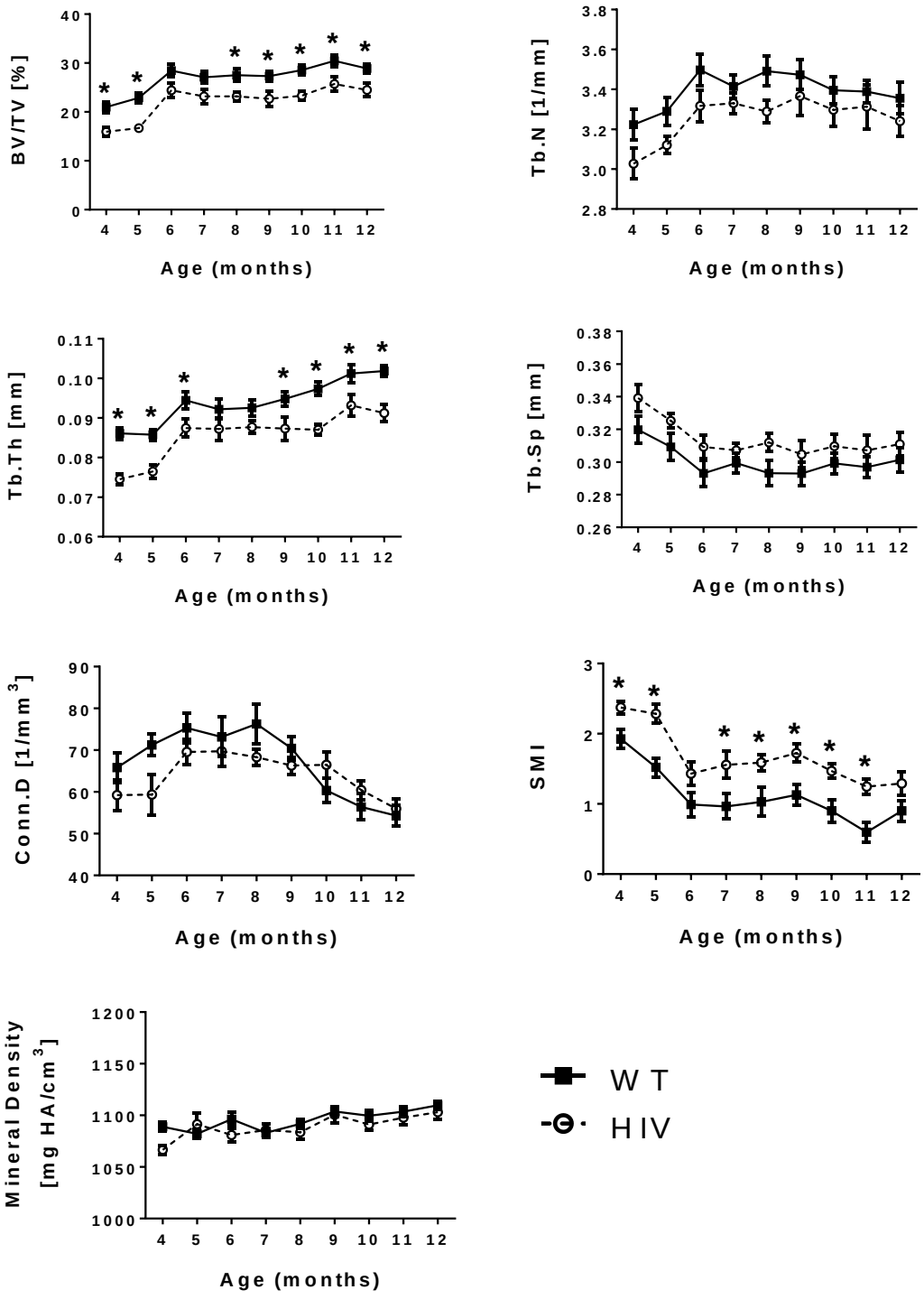

Figure 4-6. MicroCT evaluation of trabecular bone architecture at the L6 vertebra. n = 11 WT, n = 10 HIV. Error bars indicate SEM. * indicates significant difference between groups ($p < 0.05$). BV/TV = bone volume / total volume, i.e. bone volume fraction; Tb.N = trabecular number; Tb.Th = trabecular thickness; Tb.Sp = trabecular spacing; Conn.D = connectivity density; SMI = structure model index.

4.3.3 Bone Turnover Markers

Blood was collected from rats at 4, 5, 7, 9, and 11 months of age to evaluate serum levels of C-terminal telopeptide (CTx) and osteocalcin, biochemical markers of bone resorption and formation, respectively. At five months of age, serum CTx levels in HIV animals were on average 13.6% greater than in WT animals ($p = 0.07$) with a significant difference detected at seven months of age ($p < 0.01$) suggesting a sustained state of bone resorption during this time that is not seen in WT animals (Figure 4-7). While no differences were found in levels of bone formation between groups, HIV animals had an 18.9% greater level of osteocalcin on average at 5 months of age. Additionally, both groups showed a decrease in bone formation levels from five to seven months of age.

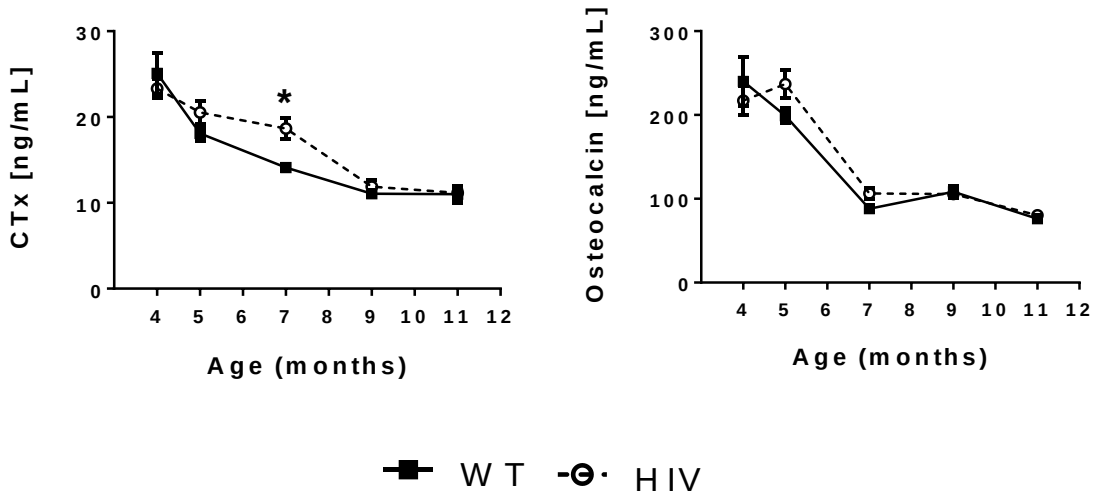

Figure 4-7. Bone turnover markers in HIV and WT rats. C-terminal telopeptide (CTx) is a marker for bone resorption. Osteocalcin is a marker for bone formation. n = 5-11 WT, n = 7-10 HIV. Error bars indicate SEM. * indicates significant difference between groups ($p < 0.05$).

4.3.4 Bone Biomechanical Phenotype

Given the significant differences in bone microarchitecture, mechanical testing was performed on femurs and L6 vertebrae to assess differences in mechanical strength. HIV femurs were found to be mechanically weaker than WT animals (Figure 4-8). Ultimate load and stiffness values were lower in HIV femurs but no differences in energy to ultimate load were found. Values for derived material properties showed no differences between groups suggesting that effects on femur mechanics are driven mainly by structural differences. However, in the L6 vertebra, no differences were detected in either measured structural properties or estimated derived material properties (Figure 4-9).

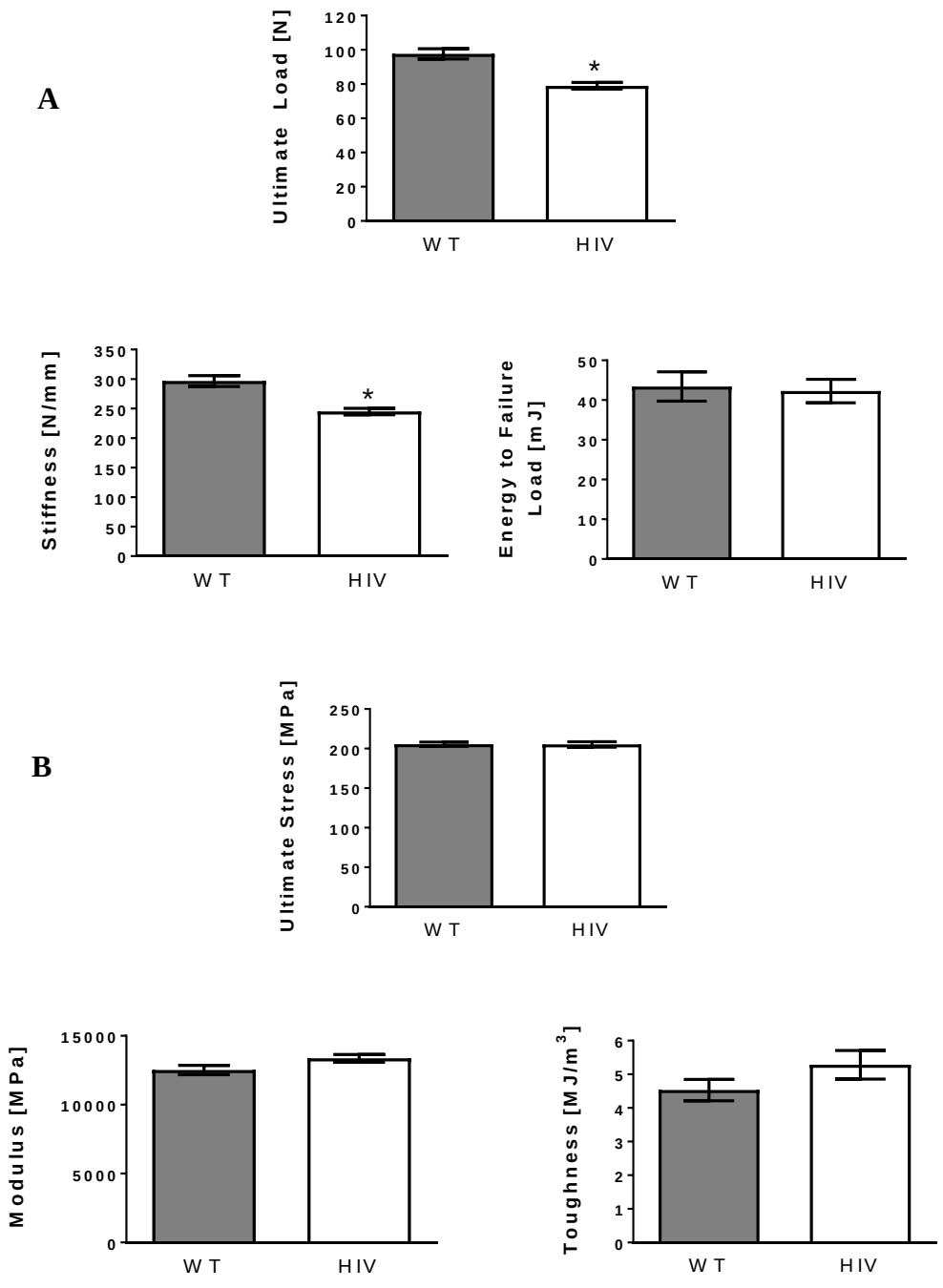

Figure 4-8. Mechanical properties of the femur. (A) Measured structural properties. (B) Estimated derived material properties. Error bars indicate SEM. * indicates significant difference between groups ($p < 0.001$).

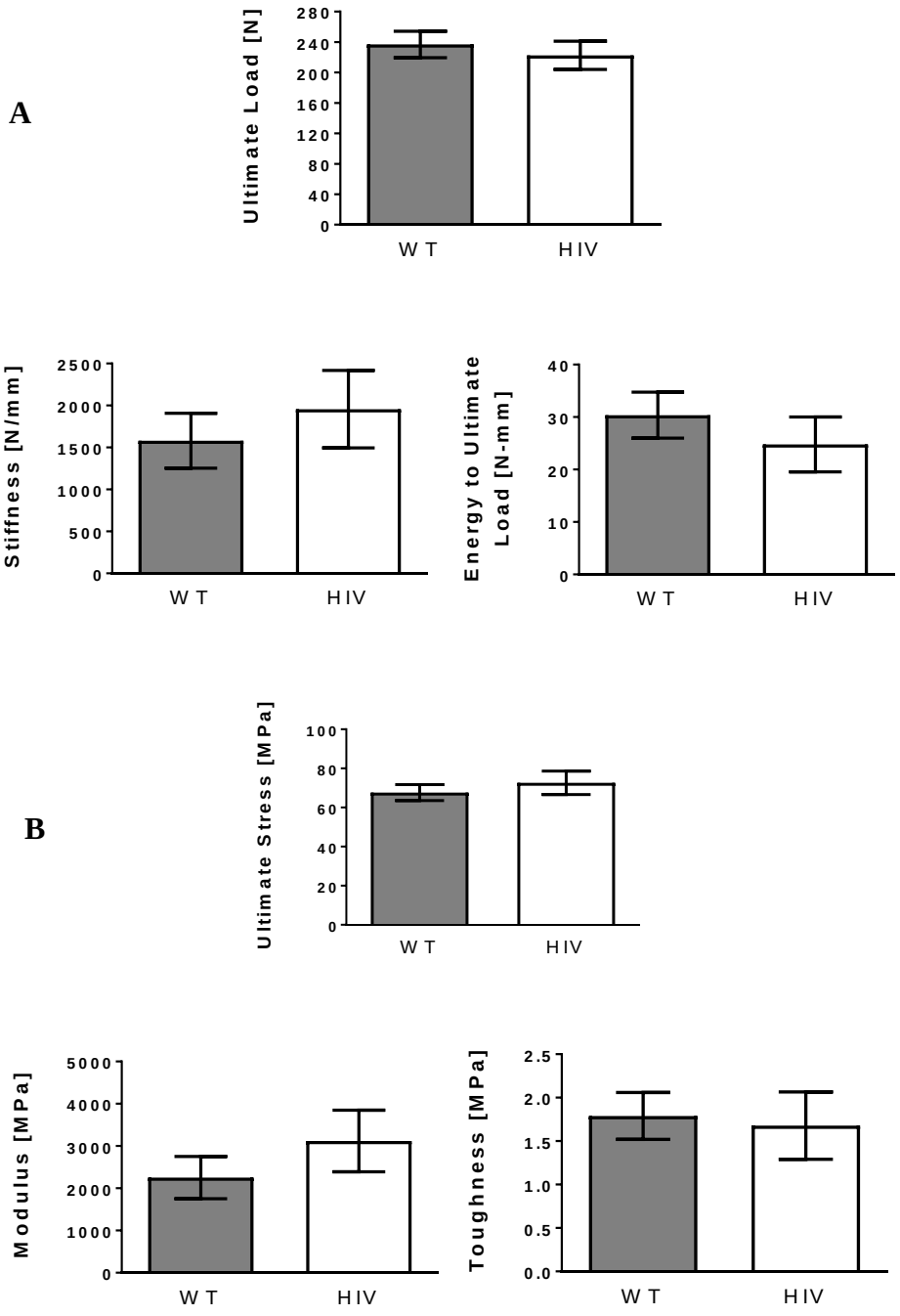

Figure 4-9. Mechanical properties of the L6 vertebra. (A) Measured structural properties. (B) Estimated derived material properties. Error bars indicate SEM.

4.4 Discussion

Low bone mass and risk for fracture are of critical concern in the HIV-infected population that afflicts people of all ages. In this study, we characterized the longitudinal skeletal changes in the growing HIV-1 tg rat and assessed alterations to bone microarchitecture, bone turnover, and bone biomechanics. Contrary to our initial hypothesis, we did not find significant changes in microarchitecture between five and nine months of age in the HIV-1 tg rat. In fact, the general growth pattern in the HIV-1 tg rat for all bone morphology patterns seemed to follow that of the WT rat with no notable exceptions. Even normalizing for differences in body mass maintained significant differences in bone mass in the femur mid-diaphysis and L6 vertebra. However, if changes in bone morphology were driven by changes in body mass alone, we would expect diverging growth rates in various bone microarchitecture measures – especially in cortical bone – that follow the differences in weight gain between WT and HIV animals. Although we saw significantly sustained serum levels of bone resorption at seven months of age in the HIV animals, we did not observe any notable changes in microarchitecture around that age compared to WT animals.

Cortical bone grew with age for all animals and was significantly reduced in HIV animals throughout the study supporting the idea that cortical bone of long bones is heavily dependent on early life growth and HIV status [87]. However, trabecular bone in the distal femur appeared to have more age-dependent changes, increasing in mass via trabecular thickness with increasing age. In the epiphyseal region, overall differences were marginal for trabecular number and spacing and did not reach statistical significance, but differences were found to be significant in the metaphysis for multiple measures of trabecular bone

structure. Additionally, trabecular number and spacing were more stable in the epiphysis but fluctuated considerably in the metaphysis suggesting active long bone growth accentuates the effects on trabecular bone in HIV animals. In contrast, the L6 vertebra was markedly more stable in trabecular characteristics over time except for early changes from 4 to 6 months with more consistent decrements in HIV animals compared to WT animals. Interestingly, bone volume fraction did not increase with age after 6 months of age supporting the understanding that vertebral growth stabilizes earlier than in long bones [197, 200]. Taken together, we have shown that the HIV-1 tg rat presents with age- and skeletal-site-dependent differences in bone microarchitecture that may in part be determined by early life alterations in bone development.

Overall, our microarchitecture and bone turnover findings are consistent with findings from Vikulina et al. [24]. Interestingly, contrary to our findings, they found no differences in cortical thickness between WT and HIV male rats at 8 to 9 months of age, and comparison with our study revealed similar average values but less variability in female rats. We would expect the male rats to have greater bone size both in terms of HIV status but also in comparison to our female rats at the same age [201]. Femurs obtained from the Weitzmann group harvested from 14 month old male HIV-1 tg rats were qualitatively compared to the 12 month old females from this study. Average cortical thickness values were similar as in 8-9 month old rats; however, all cross-sectional area measures (i.e., bone area, marrow area, and total area) were greater in the male rats (Table B-5). Consequently, MOI and pMOI values were greater in male rats resulting in considerably greater mechanical strength of femurs compared to female rats (Figure B-3). There were also striking differences in trabecular microarchitecture in male rats at 8-9

months old in the distal femur metaphysis that were also found in the female rats but to a lesser degree. This suggests that the effects of HIV status on cortical bone may be greater in male rats than in female rats. Alternatively, this may be due in part to differences in the resolution of scans or may be physiologically due to sex differences in baseline levels of bone mass and microarchitecture characteristics. Clinical investigations have shown that BMD in HIV positive women decline faster than in men [202], but similar or higher fracture rates have been found in HIV-infected men compared with women [132, 203]. In addition, men are less likely to be provided proper care for osteoporosis and have greater mortality following osteoporotic fracture highlighting the need to consider sex differences [204, 205]. Although additional studies are needed to determine if the sex differences in the HIV-1 tg rat translate to the clinical setting [121, 126], use of the HIV-1 tg rat may prove useful in investigating differential approaches to care based on sex.

The rat skeleton continues to grow throughout its lifetime, however peak bone mass is considered to be achieved at 10 months of age [197]. The findings here suggest that HIV status results in a lower peak bone mass; however, the finding that there were significant differences in body mass especially at the earliest age investigated raises the question of whether these differences are present at even younger ages. In a separate study, we found that HIV-1 tg rats and littermates have similar weights at 3-4 weeks of age with significant differences at approximately 4-5 weeks of age (Figure B-4). This is in agreement with other studies that showed similar weights between WT and HIV animals at early ages [206] that soon diverge as the animals age [21, 198, 207, 208]. Although we provided food *ad libitum* to our animals, another study saw significant differences in weight regardless of pair-feeding [21]. As stated earlier, WT rats gain weight at a faster

rate than HIV rats, a difference that is not reflected in the rate of change in bone microarchitecture. We may therefore offer a hypothesis that early skeletal effects of HIV prior to the age studied here in the HIV-1 tg rat lead to a reduced peak bone mass as seen in this study. In support of this, results from Yin and colleagues would suggest that perinatal and early life HIV infection leads to a below normal peak bone mass [87]. Further studies are warranted on prenatal and neonatal animals to determine when significant differences in body mass and skeletal development occur and whether these changes are what lead to the results presented here.

Skeletal site-specific changes are also dependent on age in the rat. Growth plates in the tibia of female rats close at 14 months of age while in the vertebra, growth plates close at 20 months of age [197]. Skeletal growth is also influenced by the transition from modeling to remodeling which is associated with very low rates of longitudinal growth. This transition occurs in trabecular bone between 6 to 9 months of age at the proximal tibia metaphysis and at 3 months of age in the vertebra. The human skeleton however stops growing after sexual maturity [32] which occurs in rats at approximately 2.5 months of age. This may partially explain the age- and site-related differences seen here that are similar to that seen in ovariectomized rats, although the changes due to ovariectomy are considerably more pronounced [200]. With osteoporosis in humans, fractures commonly occur at the spine, hip, or wrist making these important skeletal sites for investigation of bone quality [209]. Clinical studies have assessed bone microarchitecture using HR-pQCT and some even implement ITS-based morphological analyses, but this is limited to the distal radius and distal tibia [210]. In order to assess trabecular quality at the spine, DXA based TBS has been used but this technique does not offer the same granularity that HR-

pQCT provides [211]. The HIV-1 tg rat model provides an appropriate surrogate with which to study age-related and skeletal site-specific changes in bone microarchitecture that are challenging in the clinical setting.

Despite not being directly infected by HIV or hosting active viral replication, the HIV-1 tg rat exhibits significant changes to bone microarchitecture and bone turnover markers. This suggests there is also an effect of the HIV-1 protein expression that occurs constitutively in this model that may be occurring in HIV positive humans on effective ART as a consequence of viral reservoirs and low level HIV-1 activity [52, 58, 62]. Numerous studies have utilized the HIV-1 tg rat to study HIV associated disorders, and this has led to the establishment of this model as effectively reflecting HIV positive individuals on effective ART [23, 198]. These rats show localization of HIV-1 proteins that are similar to that seen in humans [59, 60, 62]. Additionally, studies of the HIV-1 tg rat immune response show differential immune cell responses and cytokine profiles with age as well as dysfunctional T cell development and function that are similar to the human condition [17, 148, 150, 212, 213]. Most notably, the findings in the HIV-1 tg rat by Vikulina et al. were translated to the clinical setting where HIV positive individuals were found to have increased bone resorption, low BMD, increased B cell expression of RANKL, and decreased B cell expression of OPG [114].

As the HIV population continues to grow and age, skeletal health will continue to be an area of concern and needed research. Furthermore, understanding how HIV can impact achievement of peak bone mass will help inform clinical management of bone care in child and adolescent patients infected with HIV. We reported here work towards

establishing the HIV-1 tg rat as an appropriate model to study skeletal disorders with interest towards HIV associated effects on peak bone mass.

CHAPTER 5. BONE HEALING IN HIV-1 TRANSGENIC RAT

5.1 Introduction

Bone defects can result from traumatic injury, infection, tumor resection, or fracture nonunion [27, 214]. Effective reconstruction of segmental bone defects is an elective procedure that continues to be a significant clinical challenge for orthopedic surgeons [214]. Clinical management of these defects still results in 5 to 10% progressing to delayed union or nonunion [27, 215]. There is concern that the HIV infected population may be more susceptible to impaired bone healing [133]. This may be due to low bone mass, a dysfunctional immune system, or an imbalance in the remodeling process. However, currently there is no consensus in the research literature on whether HIV positive patients have greater rates of nonunion [13]. In a prospective study including 36 HIV-positive and 141 HIV-negative individuals requiring implant surgery, Harrison et al. reported a greater proportion of reconstruction for nonunion in the HIV infected group with 14 patients identified to have delayed or nonunion [216, 217]. Bahebeck and colleagues reported 12.3% of HIV infected versus 8.6% of uninfected individuals had mal- or non-union as indications for implant surgery [218]. Xu et al. reported a 5.6% prevalence of nonunion in their HIV infected cohort compared to 2% in the uninfected controls [219]. In contrast, multiple studies reported no cases of nonunion in their HIV infected cohorts [13]. Additionally, while closed fractures in the HIV infected population appear to only require conventional care, it is not clear whether more complex fractures such as open fractures or segmental bone defects require additional interventions and management [13].

Current clinical studies addressing bone healing in the HIV infected population are challenged by poor study designs, widely variable demographics, and a greater focus on rates of infection [13]. Additionally, clinical assessment of adequate healing of fractures is still not standardized, complicating comparisons between studies [13, 140, 220]. Animal models thus provide an opportunity to study healing of segmental bone defects with significant controls over the variables confounding clinical studies of healing in HIV positive patients. There have also been no pre-clinical studies investigating bone healing, specifically segmental bone defect healing, utilizing the HIV-1 transgenic rat.

The HIV-1 tg rat has proven to be useful in the study of HIV associated comorbidities [21, 22, 148, 153, 155, 156] including osteoporosis [24, 162]. It has also been shown to express HIV-1 viral proteins throughout its life and is considered a model for HIV-1 infected individuals on effective suppressive ART [23, 198]. The effects of this chronic HIV-1 protein expression on the immune system of the transgenic rat include dysregulation of T cells [17, 150, 212, 221], changes to B cell activity [24, 148], and alterations to inflammatory response [148, 213]. Given the critical role that the inflammatory response plays in repairing bone [37], bone healing in the HIV-1 tg rat may therefore be impaired.

The objective of this work was to investigate the bone healing response in the HIV-1 tg rat. In order to mimic the clinical situation of a bone segmental defect receiving reconstructive care, we utilized a well-established model of a critically-sized long-bone segmental defect [222, 223]. To promote healing of the defect, we used a reliable hybrid growth factor delivery system consisting of a nanofiber mesh and injectable alginate hydrogel loaded with rhBMP-2 that our group has found leads to consistent healing [224,

225]. Thus, we sought to determine the bone healing response in the HIV-1 tg rat using a segmental bone defect model. We hypothesized that healing in the HIV-1 tg rat would be impaired despite the use of a therapeutic intervention.

5.2 Materials and Methods

5.2.1 Surgical Procedure

Female HIV-1 transgenic (tg) (HIV, n = 10) and littermate controls (WT, n = 10) were purchased from Harlan Laboratories at 3-4 weeks of age. Animals were maintained in sterile caging on a regular light/dark schedule. Food (Teklad Global Diet 2918) and water were provided *ad libitum.* At approximately 9 months of age, all animals underwent surgery to create a unilateral critically-sized 8 mm femoral segmental defect as previously described [222, 223]. Based on work done in our group showing consistent defect healing, defects in this study were treated with 2.5 μg of recombinant human BMP-2 (rhBMP-2; Pfizer, Inc.) loaded into a hybrid growth factor delivery system consisting of a nanofiber mesh and injectable alginate hydrogel [223].

Prior to surgery, one WT animal was found dead at approximately 6 months of age with cause of death unknown. Two animals from the HIV group were lost during the study due to complications during or after surgery. Three more WT animals were removed from the study due to post-surgery complications or they were determined to be statistical outliers. A total of 6 WT and 8 HIV animals remained for inclusion in this study.

5.2.2 Radiography and Microcomputed Tomography

In vivo radiographs (Faxitron MX-20, Digital, Faxitron X-ray Corp) were taken to assess qualitative bone regeneration and defect bridging at 2, 4, 8, and 12 weeks post-surgery. Bridging of the defect area was defined as continuous bone spanning the region and was evaluated by two blinded investigators. A third blinded investigator decided any instances of disagreement.

Post-operative *in vivo* microcomputed tomography (microCT, vivaCT 40, Scanco Medical) scans were performed at 4, 8, and 12 weeks to quantitatively assess bone regeneration. Animals were anesthetized via isoflurane inhalation for the duration of the scan. The scans were performed at a voxel size of 21 μm, energy of 55 kVp, and current of 145 μA. A consistent volume of interest (VOI) of approximately 5 mm (242 slices) encompassing the central region of each defect was analyzed. A threshold corresponding to approximately 50% of native cortical bone threshold was applied to segment newly formed bone tissue.

5.2.3 Biomechanical Testing

Animals were euthanized at 12 weeks post-surgery via CO_2 inhalation and femurs were harvested, wrapped in saline soaked gauze, and stored at -20°C. Femurs with defects were cleaned of all soft tissue and the fixation plate was removed in preparation for biomechanical testing. Torsional testing followed previously reported procedures [222]. Briefly, femurs were potted into custom made blocks with Wood's metal (Alfa Aesar) and mounted into torsion fixtures on a Bose system (ELF 3220, Bose EnduraTEC). Samples were tested to failure under rotation control at 3 degrees per second and rotation and torque

data were recorded. Torque-rotation data were analyzed for maximum torque, torsional stiffness, and rotation at maximum torque.

5.2.4 Statistics

All data are presented as mean ± SEM. MicroCT data were analyzed using a mixed ANOVA following the general linear model (GLM) repeated measures procedure in SPSS (SPSS Statistics 24). Pairwise comparisons were adjusted using the Bonferroni correction. Biomechanical testing data was analyzed using unpaired two-sample Student's t-test. A significance level of 0.05 was set for all analyses.

5.3 Results

5.3.1 Segmental Defect Surgery

A total of 10 animals per group were assigned to undergo unilateral femur segmental defect surgery at 9 months of age. A total of four WT and two HIV animals were excluded from the study for the following reasons. One WT animal died at nearly 6 months of age; no cause of death could be determined by the animal facility veterinarian. Another WT animal's fixation plate was found to be exposed outside of the skin at 8 weeks after surgery. The final two WT rats showed no evidence of defect mineralization by 12 weeks post-surgery and were identified as statistical outliers. One HIV animal died approximately 2 days post-surgery possibly due to complications from surgery. An additional HIV animal was excluded from the study because it was not possible to properly suture the muscle tissue around the defect. The remaining animals (n = 6 WT; n = 8 HIV) were used for the remainder of this study.

5.3.2 Radiographic and MicroCT Evaluation of Bone Healing

Two-dimensional radiographs revealed a qualitatively similar bone healing response in WT and HIV animals (Figure 5-1). In the WT group, five out of six animals had bony bridging by Week 4 with the remaining defect bridged by Week 8. In the HIV group, five out of eight animals had evidence of bony bridging by Week 4. The remaining three samples were bridged by Week 8. In contrast, quantitative microCT evaluation of bone healing showed that HIV animals had impaired healing. At Week 4 post surgery, HIV defects had on average 43.1% less mineralized tissue per volume (BV/TV, $p = 0.051$) with significantly lower levels of bone at Week 8 ($p < 0.01$) and Week 12 ($p < 0.01$) (Figure 5-2). Absolute levels of defect bone volume followed a similar pattern of differences. As expected, we saw an increase in average mineral density as bone healing progressed, but we did not find differences between WT and HIV defects. We analyzed units of mineralization as trabeculae and found no differences in mineral number ($p = 0.121$) or mineral thickness ($p = 0.236$). However, when comparing HIV to WT, we found a decreasing difference in mineral number from Week 4 (-32.2%) to Week 8 (-12.9%) to Week 12 (-5.6%). In contrast, we found an increasing difference in mineral thickness from Week 4 (7.7%) to Week 8 (-11.7%) to Week 12 (-10.8%). Interestingly, we found differences between groups in mineral connectivity density (Conn.D) at Week 4 ($p = 0.048$) and Week 8 ($p = 0.029$) but not at Week 12.

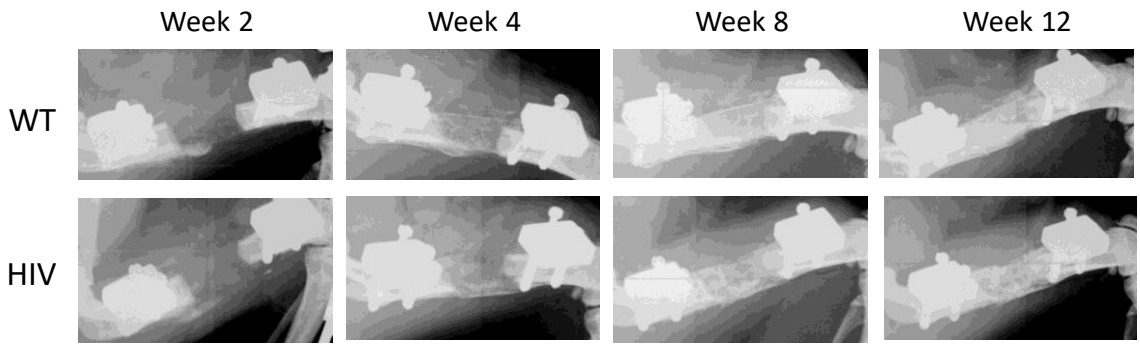

Figure 5-1. Representative longitudinal 2-D radiographs of bone healing in WT and HIV animals.

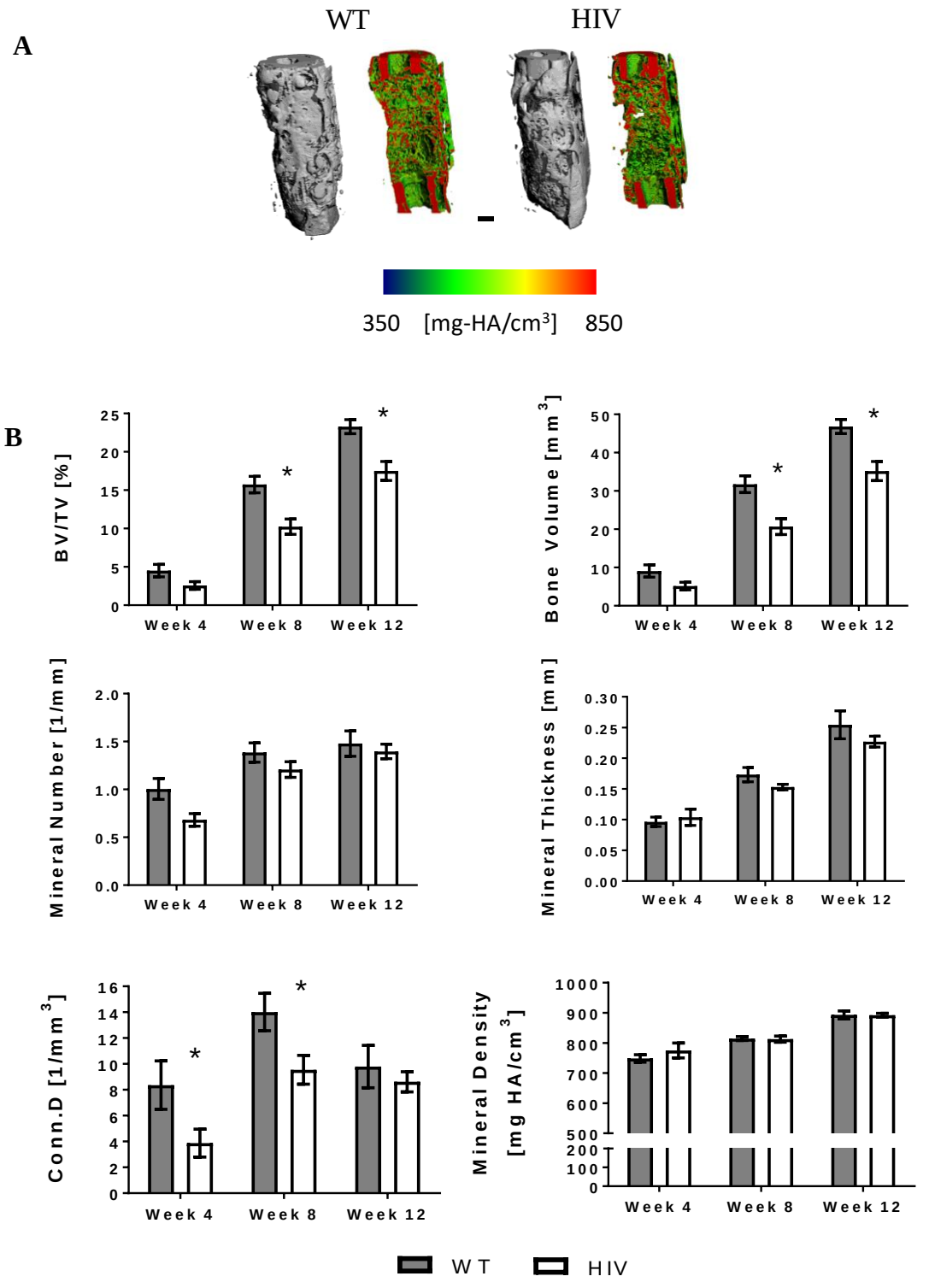

Figure 5-2. MicroCT analysis of bone healing response. (A) Representative Week 12 *ex vivo* 3-D reconstructions of defect area. Cortical bone ends have been included for orientation. (B) Longitudinal evaluation of new bone growth. n = 6 WT; n = 8 HIV. Error bars indicate SEM. Scale = 1 mm. * indicates significant difference between groups ($p < 0.05$).

5.3.3 Biomechanical Testing

We next performed biomechanical testing to assess the functional restoration of bone mechanical properties. No differences in maximum torque (-69.9%, $p = 0.18$) or torsional stiffness (-48.4%, $p = 0.059$) were found when comparing HIV to WT groups. We further asked if there was a relationship between the microCT measures and the observed biomechanical properties. *Ex vivo* Week 12 microCT values were compared with maximum torque and torsional stiffness (Table 5-1). Overall correlations showed a strong relationship between maximum torque and bone volume (BV), bone volume fraction (BV/TV), and mineral connectivity density (Conn.D). When the correlations were calculated for each group, no significance was found with the WT animals. However significant correlations between BV, BV/TV, and Conn.D with maximum torque were found in the HIV group with BV and Conn.D combined being the best predictors of maximum torque. Interestingly, a significant correlation between total volume (TV) and torsional stiffness was found which remained significant after subtracting out the bone volume. This suggests that the soft tissue within the defect contributes significantly to torsional stiffness in HIV animals.

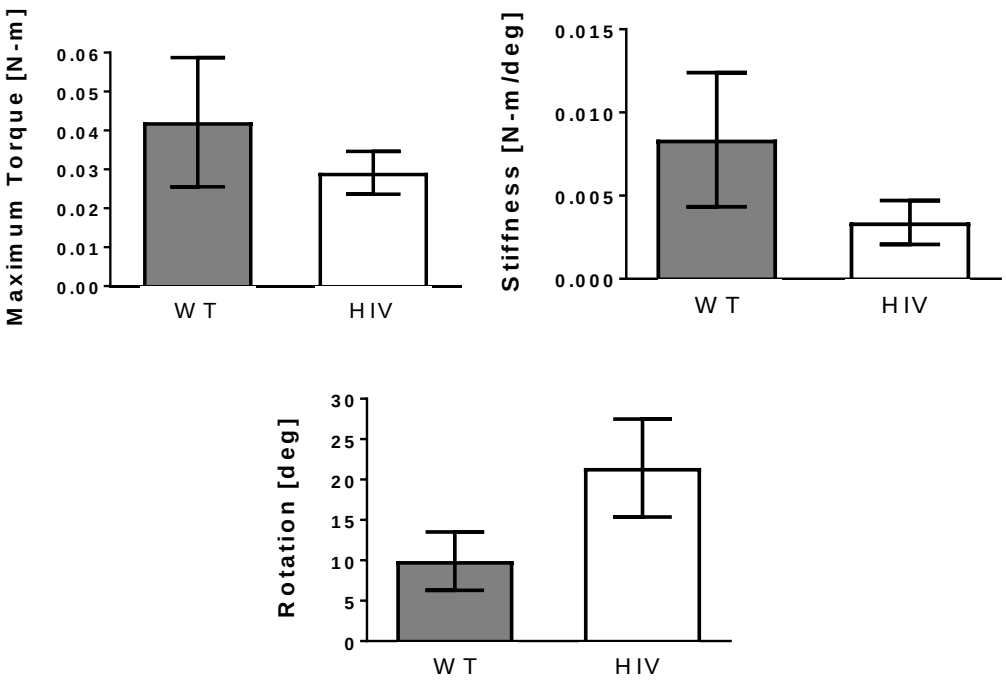

Figure 5-3. Biomechanical properties of bone defects. n = 6 WT; n = 8 HIV. Error bars indicate SEM. * indicates significant difference between groups ($p < 0.05$).

Table 5-1. Pearson's Correlation Coefficient (*r*) between biomechanical properties and microCT measures (n = 5 WT, n = 8 HIV).

Overall						
	TV	BV	(TV-BV)	BV/TV	Conn.D	Mineral Density
Maximum Torque	0.079	0.745**	-0.086	0.673*	0.644*	-0.163
Torsional Stiffness	0.432	0.395	0.352	0.150	0.325	-0.145
WT						
	TV	BV	(TV-BV)	BV/TV	Conn.D	Mineral Density
Maximum Torque	0.056	0.002	-0.159	-0.048	0.217	-0.030
Torsional Stiffness	0.028	-0.205	-0.078	-0.19	0.193	-0.164
HIV						
	TV	BV	(TV-BV)	BV/TV	Conn.D	Mineral Density
Maximum Torque	0.190	0.893**	0.057	0.813*	0.745*	-0.011
Torsional Stiffness	0.773*	0.451	0.754*	-0.188	-0.105	0.501

* $p < 0.05$

** $p < 0.01$

TV = Total Defect Volume; BV = Bone Volume; (TV-BV) = Soft tissue volume; BV/TV = Bone volume fraction; Conn.D = Connectivity Density

5.4 Discussion

In this study, we investigated the bone healing process in the HIV-1 tg rat using an established critically-sized long-bone segmental defect model. Confirming our hypothesis, the HIV-1 tg animals had less mineralized tissue at every time point after surgery. The characteristic of the mineral units provided more information, revealing that while the thickness increased over time and tended to be greater in the WT animals over time, the absolute difference between groups in number of mineral units decreased as the HIV group reached a similar number by Week 12. These findings combined with the initial greater connectivity in WT animals suggests that the bone healing response in HIV animals is impaired as early as Week 4, forming fewer, less connected but similarly thick mineral units that eventually increase in number and thicken but remodel to a network of newly formed bone. Contrary to the microCT findings, we were unable to detect differences in defect mechanical properties. These results are consistent with our pilot data utilizing bilateral segmental defects and present the first pre-clinical evidence for impaired bone healing in the HIV-1 transgenic rat despite therapeutic intervention. This impairment may be mediated by a decrease or a delay in mineralization but further studies are needed to investigate this.

Fracture healing in the HIV infected population has long been suspected to be negatively impacted due to the effects of HIV on bone mass, bone turnover, and the immune system [133]. In Chapter 4, we showed that the HIV-1 tg rat has decreased bone mass at 9 months as measured in cortical bone at the femur middiaphysis, and in trabecular bone at the femur distal metaphysis and L6 vertebra. However, the amount of bone present is more associated with the risk for fragility fractures – not a natural occurrence in rodents

[226] – and in terms of bone healing, risk for failure of fracture fixation [227]. Qualitatively, we did not find any loosening or loss of stability of our fixation plates in the HIV animals nor did we observe any differences in screw removal difficulty from WT or HIV bone when preparing for mechanical testing. This is further supported by the findings in Chapter 4 that no differences in bone mineral density were present between groups suggesting that, at least for the cortical bone of the femur, the decreased amount of bone does not impact implant stability in the HIV-1 tg rat. Whether this is the case in trabecular bone remains to be investigated. Current clinical findings would suggest that failure of fracture fixation is not a cause for concern [13], but given the inherent variability in studying fracture healing especially in the HIV population, further studies are needed to address this issue.

Based on results from Chapter 4, WT and HIV rats may have similar global levels of bone turnover markers by the time of surgery at 9 months of age. However, there may be local differences in bone formation and resorption. Multiple *in vitro* studies have suggested a detrimental effect of HIV on osteoblast precursors [105, 108-112] and osteoblast activity [104-107]. In line with these findings, our bone healing results in HIV animals are suggestive of impaired mineralization specifically reflected in the relative changes in mineral unit thickness. Although the HIV-1 tg rat has a more pro-osteoclastogenic bone marrow environment [24], this may not result in increased resorption in our model of bone healing. Looking at the changes over time in connectivity and number of mineral units suggests a similar healing process that is attenuated in the HIV animals. Additionally, the differences in new mineralized tissue are apparent as early as 4 weeks after bone injury. This would suggest that there is not a difference in resorption activity

between groups within the period of bone healing studied here but perhaps an early and continued suppression of bone formation. Since our segmental defect model is critically-sized and does not heal spontaneously without intervention, we utilized a hybrid growth factor delivery system consisting of a nanofiber mesh and injectable alginate hydrogel loaded with rhBMP-2 to induce bone healing. BMP-2 promotes chondrogenic and osteogenic differentiation early in the inflammatory phase of fracture healing [38, 228], and it was shown in our model that over 90% of the dose of BMP-2 delivered to the defect area is cleared by 21 days [229]. This suggests that the HIV animals in this study may have less sensitivity to BMP-2 osteoinductive effects and further supports the notion that the HIV-1 tg rat has an impairment of bone healing via attenuation of bone formation.

Fracture healing in the context of osteoporosis is generally characterized by a delayed healing response [134]. While an imbalance of bone resorption and formation seems to characterize bone loss in HIV patients as with primary osteoporosis, the mechanism behind this disruption with HIV appears to be driven by direct effects of HIV infection, HIV viral products, and ART on the immune system leading to an increase in bone resorption [113, 230]. Specifically, T and B lymphocytes have been found to be key mediators in the fracture healing process [135-138] and have been shown in the HIV-1 tg rat to be negatively impacted [17, 24, 148, 150, 212, 221] resulting in alterations to inflammatory response [148, 213]. Interestingly, pro-inflammatory cytokines are increased in HIV-1 tg rats suggestive of a systemic chronic inflammatory state that may have a negative impact on bone healing [37, 139]. The complex interplay between immune cells, inflammatory cytokines, HIV gene expression, and bone healing has been poorly studied and warrants further investigation.

There are notable differences between our study and previous studies from our group [223, 229]. The choice of a 2.5 µg dose of rhBMP-2 was motivated by the consistent bridging seen in 2-D radiographs from previous work. Although we likewise found complete bridging by 12 weeks post-surgery, the resulting amount of tissue mineralization (i.e., bone volume) seen via microCT analysis was noticeably lower, reflecting values seen at a BMP-2 dose of 1 and 2.5 µg at 8 weeks post-surgery [229]. Biomechanical properties of the healed defect were similar to results seen from defects treated with 0.5 and 1 µg BMP-2. While this work utilized rats on an F344/NHsd inbred background and the previous work was conducted in SASCO Sprague Dawley outbred rats, the greater cause for discrepancy may be in the age of animals at surgery. Owing to the reported onset of HIV/AIDS clinical symptoms between 5 and 9 months of age, surgeries in this study were performed on animals at 9 months of age whereas rats at 13 weeks of age underwent surgery in our previous studies. Aging is associated with a pro-inflammatory state and via multiple factors, may impair bone healing [231-233]. In particular, older rats have delayed healing [234-236] and have different gene expression in the fracture callus than younger rats with a notable decrease in BMP-2 expression [237, 238]. How bone healing varies with age in this model requires further study, especially to determine if this segmental defect model eventually heals to a mechanically competent level in both WT and HIV rats.

This study had several important limitations. Animals used in this study were age-matched but not weight-matched. However, given the considerable variability in age that would occur with weight-matching and the significant age-related effects on bone healing, animals were age-matched for this study. Other studies utilizing the HIV-1 tg rat have also seen weight differences between WT and HIV animals [21, 24, 198] but the mechanism

for this is unknown and may be a consequence of HIV effects on multiple organ systems. Our study also did not investigate healing time points prior to 4 weeks or beyond 12 weeks post-surgery. Although we found significant differences in healing between groups in our study, further investigation into the progression of bone healing, specifically early inflammation and functional recovery of bone tissue, are needed to fully understand bone healing in the HIV-1 tg rat model. Finally, previous work from our group has shown that the alginate gel in our delivery system remains in the defect area up to 30 weeks post-surgery and, although bone is remodeled to a lamellar structure and the regenerated tissue provides sufficient mechanical strength for ambulation, may interfere with secondary bone remodeling as the bone is not restored to a cortical bone architecture.

Effective care and management of segmental bone defects remain a significant challenge for orthopedic surgeons. As the HIV infected population grows and ages, presentation of a segmental bone defect in an HIV positive patient may become more common. Additionally, in the United States, HIV testing is not mandated, and 15% of those infected with HIV are not aware of their HIV status [49]. Increasing understanding of bone healing in the context of HIV may provide healthcare providers with additional criteria by which appropriate care can be provided. We reported here work towards furthering this understanding as well as establishing the HIV-1 tg rat as an appropriate model to study bone healing and more specifically critically-sized bone defects that require intervention to achieve functional restoration of bone. This work further emphasizes the need to investigate the negative impact HIV infection may have on bone healing outcomes.

CHAPTER 6. SUMMARY AND FUTURE DIRECTIONS

6.1 Overall Summary

The HIV infected population is a growing and aging demographic that requires unique healthcare considerations. Current understanding of the complex relationship between HIV and bone remains incomplete. Animal models allow for significant investigations into diseases and therapies that would be prohibitive with humans. Although there exist animal models of HIV/AIDS, they are primarily used for cure research and require significant resources for study. The HIV-1 tg rodent models provide decreased barriers to conducting research with specific regard to the study of skeletal disorders in HIV infected individuals on effective viral suppression treatment.

It is widely accepted in the literature that individuals infected with HIV – both with and without ART – are at a greater risk for osteoporosis and fracture. Aside from the study showing that the HIV-1 tg male rat mimics an osteoporotic phenotype [24], limited studies have addressed bone-relevant dysfunction in the HIV-1 tg rodent models with no studies addressing effects on bone biomechanical properties or bone healing. Additionally, there is no reported data on the HIV-1 tg female rat regarding skeletal defects nor has the skeleton of the HIV-1 tg mouse been characterized for bone microarchitecture or bone healing. Therefore, the *overall objective* of this work was to investigate the effects of HIV on skeletal growth and bone healing as exhibited by two noninfectious HIV-1 transgenic rodent models, specifically the mouse and the rat. The *central hypothesis* of this project was that HIV-1 transgenic animals will present with significant deficiencies in skeletal development and bone repair.

To test this hypothesis, we explored the skeletal phenotype, bone mechanics, and bone healing of the HIV-1 tg mouse and rat models. First, utilizing the HIV-1 tg mouse model, we studied bone microarchitecture and biomechanics for the femur and L6 vertebra at 10-12 weeks of age (Aim I, Chapter 3). This was followed by an investigation into the fracture healing process utilizing a closed femur fracture with intramedullary pin stabilization. HIV mice had significant decrements in bone microarchitecture at all skeletal sites studied accompanied by a reduction in structural mechanical properties in the femur and L6 vertebra. Fracture healing in the HIV-1 tg mouse was found to be significantly impaired by four weeks post injury resulting in a significant loss of mechanical properties. Second, we characterized the longitudinal skeletal growth of the HIV-1 tg rat and assessed whole bone mechanics at twelve months of age (Aim II, Chapter 4). Overall, HIV-1 tg rats did not show a significant characteristic change between five and nine months of age. However, we did find significant deficits in bone mass and microarchitecture in both cortical and trabecular bone in the HIV rats compared to WT rats throughout the study. This was accompanied by a reduction in femoral but not vertebral biomechanics. Finally, we investigated the bone healing process in the HIV-1 tg rat using a critically-sized bone segmental defect (Aim III, Chapter 5). The HIV group had an impaired healing response characterized by lower bone volume and decreased mineral characteristics that led to nonsignificant reductions in average biomechanical measures. Collectively, the findings from this thesis provide evidence for a potential negative effect on bone structure and function that may be independent of HIV infection or ART and directly or indirectly related to HIV-1 protein expression as presented by the HIV-1 tg rodent models. Notably, this

work presents the first pre-clinical evidence for impaired bone healing in HIV-1 transgenic rodents.

6.2 Skeletal Development and HIV

The results from the skeletal phenotype studies in both the mouse and rat showed significant decrements to cortical and trabecular morphology generally consistent with that reported in the HIV positive population. There were however differences between the two models and skeletal site-specific differences. Notably for cortical bone, cortical total area was not different in mice, but was different in rats while all other cortical morphology measures were different between WT and HIV groups in mice and rats, respectively. For trabecular bone, differences in the distal femur metaphysis and L6 vertebra were similar between mice and rats but measures at the distal femur epiphysis were not; in mice, we found significant differences between WT and HIV groups that were not mirrored in rats. The discrepancies between these models may be a consequence of differences in experimental design, species skeletal characteristics, and HIV gene expression.

Although we can estimate the age of rodents in terms of human years based on different growth periods [239, 240], this comparison is still an approximation of development and aging. However, it provides us with information to make general comparisons between pre-clinical rodent models that can then be translated to human studies. Bones from mice were studied *ex vivo* at 10-12 weeks of age, falling short of the average time of skeletal maturity of 4 months [172] while rat bones were studied *in vivo* across multiple ages including the time of skeletal maturity at 10 months of age [197]. We can roughly estimate that 10-12 weeks of age in the mouse is approximately 25-30 weeks

(or 6.25 to 7.5 months) of age in the rat by using the age of skeletal maturity as the reference. Comparing results at these ages suggests that more differences between WT and HIV may have been found in the rat, especially in the distal femur epiphysis. Nevertheless, in order to make adequate comparisons between HIV-1 tg mice and rats would require a similar longitudinal study in the mouse such that relative changes in bone microarchitecture can be compared.

Furthermore, skeletal growth and aging effects vary by species and sex at different skeletal sites. While both species continue to grow after sexual maturity, loss of both cortical and trabecular bone in mice is remarkably similar to that seen in humans, beginning after peak bone mass is attained and the majority of bone loss occurring by 6 months of age [172]. In rats, loss of bone does not occur with age but does slow appreciably and transitions from bone modeling to remodeling at different skeletal sites and at different ages [32]. To match more closely the loss of bone seen in humans, models of osteoporosis have been developed in both mice and rats. The various approaches to inducing loss of bone in rats have proven to closely mimic osteoporosis in humans and thus bypasses the challenge of a lack of age-related bone loss in these animals [197]. Sex differences between mice and rats are similar with females having smaller bones that undergo greater losses to bone mass or mechanics compared with males [173, 201]. In support of this, in Chapter 4 we discussed the differences between the microarchitecture and biomechanics in HIV-1 tg female and male rats. Our findings suggested that HIV effects may be more detrimental in males than in females or that baseline sex differences in bone highlight the negative effect in males more than in females. These sex differences are seen in humans as well with women generally having less bone and losing bone faster with age [202, 204] while

fractures at osteoporotic sites occur at similar or higher rates in men [132, 203]. Despite these species and sex differences, our work has shown that there is an overall similar loss of bone in both mouse and rat models that results in an HIV skeletal phenotype similar to that reported in the HIV positive population. Future work could use the HIV-1 tg rodent models to study site-specific and sex-dependent changes in bone microarchitecture with age and with an induced osteoporotic phenotype. Further work could then investigate the complex combination of HIV, osteoporosis, and various interventions for recovering bone such as antiresorptive drugs, diet and supplementation, sex steroids, and physical activity.

Importantly, the expression of HIV genes is variable with age and between HIV-1 tg mice and rats. Mice have high expression of HIV proteins in the skin, muscle, and tail but low expression in the thymus, a critical organ in the immune system especially for T cell development [174]. They have primarily been shown to present with renal disease [16, 20] and cardiovascular dysfunction [18, 19]. Rats have likewise been reported to present with HIV/AIDS symptoms including skin lesions, wasting, and muscle atrophy, but more importantly efficiently express proteins in the liver, kidney, and essential lymphoid tissues including the spleen, thymus, lymph nodes, and blood [17, 21, 144]. They have been used to investigate a multitude of disorders associated with HIV [21, 22, 24, 144, 151-158]. Each model offers its own unique advantages and disadvantages when it comes to studying HIV associated disorders. Mouse models in general offer greater opportunities for genetic modification. Our work here utilized mice on both the FVB/N and C57BL/6 backgrounds and given the differences in skeletal phenotypes [187, 188] and severity of disease presentation, there may be interesting genetic contributions to these differences. Additionally, gene specific transgenic HIV-1 mice have been created that have allowed for

study of specific protein effects [159, 175-177]. The HIV-1 tg rat model has been studied considerably more owing to the more efficient expression of HIV-1 genes and has thus been characterized more heavily especially in the study of neurocognitive disorders [23, 155]. Coupled with their added size, rats allow for more clinically relevant investigations especially of effects in HIV infected individuals on effective ART [144, 148, 198]. In spite of the differences between the mouse and rat, we found similar deficits in bone microarchitecture and biomechanics suggestive of an HIV phenotype that may be HIV-1 protein specific. Future work could investigate the localization of HIV-1 gene expression in different bones, in bone marrow, and in bone cells and how this might be related to differences in bone microarchitecture. Additionally, protein specific effects could be investigated via genetic modification or via direct injection of HIV viral products.

Interestingly, there may be a similar disruption to immune function specifically a dysfunction of T cells and B cells in both mice [146, 147, 177] and rats [17, 24, 148, 150] perhaps suggestive of a chronic immune activation state in both models [241, 242]. It has been suggested that in humans, HIV reservoirs – replication-competent, transcription-competent, and translation-competent – and so-called "defective" proviruses may in part be responsible for this chronic immune activation [62, 243, 244] and thus low bone mass and increased fracture risk in HIV infected individuals [230]. As researchers gain further understanding of the role of HIV reservoirs and viral products in the HIV infected population, the HIV-1 tg rodent models may prove useful in studying tissue- and age-specific effects of HIV proteins especially as it relates to skeletal disorders.

Peak bone mass is of critical concern for perinatally HIV infected individuals or those infected at a young age [85, 87, 192]. Both mice and rats can be used to study effects

on peak bone mass as alluded to earlier, and in our work, we studied mice and rats near their respective age of skeletal maturity. We found that HIV animals had lower bone mass and significant decrements to bone microarchitecture. Based on the longitudinal data in the rats, these differences may be a consequence of early developmental effects of HIV. In a study looking at early development of chronic neurological impairment, HIV-1 tg rats had similar weights but opened their eyes later – indicative of selective somatic growth – as measured before postnatal day 21 and were also found to have alterations in early locomotor activity [206]. Significant effects of HIV gene expression may similarly occur with skeletal development in both the HIV-1 tg mouse and rat either prenatally or postnatally. In fact, maternal HIV infection is associated with a higher risk of preterm birth, low birth weight, and small-for-gestational-age whether the mother is ART-naïve or not [80, 81] suggesting negative effects on skeletal health may begin *in utero*. Further investigation could study these early effects on the skeleton using the HIV-1 tg rodent models by looking at both genetic and mechanical effects on embryonic skeletal development [245].

Our work here presented that HIV bone biomechanics showed reductions to structural mechanical properties but not to derived material properties. This is in agreement with Yin et al. who used microFEA and found a reduction in stiffness in bone from the distal tibia and distal radius of young men infected with HIV [87] and with Springer et al. who, in a humanized mouse infected with HIV, determined that femurs had lower hardness and tibiae had lower ultimate load and stiffness values compared with controls [161]. However, contrary to our findings, Guerri-Fernandez and colleagues used microindentation at the midpoint of the midshaft anterior tibial plateau and found decreased

bone material properties in HIV patients, especially women, that was independent of BMD and ART [131]. It may be that there were differences in material properties that we were unable to detect in this study. Specifically, we did not investigate in depth the tissue level material properties of bone and relied on common equations derived from beam theory for estimating these values [171]. Further studies are needed to determine if there are differences beyond the structural mechanical property differences we found here.

6.3 Bone Healing and HIV

In both HIV-1 transgenic rodent models, we showed impairment of bone healing as reflected by reductions in bone formation and a failure to recover functional bone mechanics. We simulated a closed fracture in the mouse femur by creating a small osteotomy followed by fracture reduction and stabilization via an intramedullary pin. This model closely mimics the clinical use of intramedullary rods or nails to internally stabilize a long bone fracture [246]. In the rat, we simulated a challenging bone segmental defect under reconstructive care by creating a critically-sized 8 mm mid-femur defect with plate stabilization treated with a hybrid growth factor delivery system. The standard of care for bone defects continues to be the use of autologous bone grafts [214], and while our model uses a pre-clinically established therapeutic intervention, the challenge to bone healing remains relevant. The bone injuries and management in the mouse and rat were considerably different and yet the disparity in healing response between WT and HIV animals was remarkably similar. At early time points corresponding to late stage soft callus establishment and early mineralization, we found no statistical differences in the volume of newly mineralized tissue between WT and HIV groups. At later time points at which

most of the mineralized cartilage matrix has been replaced by woven bone and coupled remodeling is underway, we saw significantly lower amounts of bone in HIV animals. The association between HIV and increased osteoclastogenesis [99-101] and osteoclast activity [24, 102, 103] suggested that perhaps resorption would be increased in the HIV animals at the relevant phases of bone healing. Looking at the volume of bone formed, the absolute difference between WT and HIV animals increased with time suggesting attenuated bone formation or increased bone resorption or a combination of the two in the respective HIV groups. In the rats, however, we saw differences in mineralized tissue connectivity at 4 and 8 weeks after surgery but this difference was not seen at 12 weeks. In mice, we saw a reduction in absolute difference in total callus volume to similar values at 4 weeks post fracture. Both of these findings suggest a resorption response that is proportional to the callus and mineralized tissue formed that ultimately results in a similar nominal level of tissue size and characteristics. Thus, the resulting differences in newly formed bone and tissue mechanics may be a consequence of attenuated bone formation.

In support of this, several *in vitro* studies have been performed to study the effects of HIV-1 and its proteins on osteoblast precursors and osteoblasts. These effects on mesenchymal stem cells include early senescence, decreased proliferative capacity, decreased osteogenic potential, and increased adipogenic potential [105, 108-112] suggesting that even in the presence of the osteoinductive protein BMP-2, the level of bone formation will be decreased in HIV-1 tg rodents. Osteoblasts likewise have negative effects on their activity including decreased calcium deposition, decreased alkaline phosphatase (ALP) activity, reduced proliferation, and increased apoptosis [104, 105, 107]. Further work is needed in order to determine if the cells from the HIV-1 tg rodent models have a

similar dysfunction and to what extent they express HIV-1 proteins within these cells. Future work could look at specific protein effects on bone healing either by studying whether HIV proteins localize in the bone injury site or through genetic modification to isolate viral gene products. Additionally, direct injection of HIV-1 proteins into the bone injury site of normal non-HIV animals could provide an easier method for determining specific protein effects. This could also be accomplished by loading HIV-1 proteins into the nanofiber mesh and hydrogel growth factor delivery system.

As mentioned earlier, both HIV-1 tg mice and rats have differentially altered immune systems characterized partially by dysfunctional T and B lymphocytes. Both cell types have been shown to be intricately involved in the bone healing response mediating and coordinating both bone formation and resorption processes [37, 113, 135]. These cells are present at all stages of the bone healing process except during much of the soft callus stage of cartilage formation [138]. Interestingly, the absence of T and B cells results in enhanced fracture healing characterized by earlier mineralization and gain in mechanical strength [136]. However, this expedited mineralization is at the expense of building quality bone with adequate elastic properties for restoration of functional mechanics [137]. The HIV-1 tg rodent models have an intact adaptive immune system, so the apparent attenuation of bone formation in the healing process may be due in part to dysfunctional T and B cells. Future work in these models could investigate the spatiotemporal presence of T and B cells in and around the bone injury as well as the levels of different inflammatory cytokines to determine how the inflammatory response and more generally the immune system affect bone healing.

As previously discussed, we utilized two different models of bone healing. Additionally, the animal characteristics (i.e., species, age, and sex) were not similar across the healing studies. Regardless of these differences, we still found a significant detriment to bone healing mediated by either a decrease or delay in mineralization that was associated with the HIV status of the animal. There are a multitude of opportunities for studying bone healing utilizing the HIV-1 tg rodent models. In addition to the closed fracture and segmental defect models, there is also a need to study delayed union and nonunion in the context of HIV that may be met by small animal models [247]. In low-income countries, non-operative management is still widely used making delayed union and nonunion common indications for surgery [246]. Although clinical findings suggest no complications from reconstructive surgery in the HIV positive population, recovery may be delayed or the quality of healed bone tissue may be suboptimal. Given the significant impact and incidence of fractures in the young population in low- and middle-income countries [248, 249] and the growing population of aging HIV infected individuals, the HIV-1 tg rodent models provide avenues for addressing the possible age-related differences in bone healing. In particular, age-related loss of bone due to sex-specific osteoporosis can be studied using these HIV animals and either ovariectomy or orchidectomy.

6.4 Bone, ART, and HIV

Although it has been shown that HIV infection alone is associated with bone loss, the introduction of ART and subsequent improvement in life expectancy has created an increasingly complex situation for healthcare providers. Understanding the milieu of factors affecting the HIV positive patient will be critical for providing appropriate care. Investigating ART effects on bone in animals may not prove to be fruitful due to the fact

that these animals are not infected by HIV and the mechanisms by which ART influences bone mass and microstructure is indirectly through the immune system. Results from microCT analysis and biomechanical testing of bones obtained from FVB/N mice administered azidothymidine (AZT) via oral gavage at 100 mg/kg/day from a previous study [18, 250] showed no differences compared to mice administered water (Table B-4, Figure B-1, Figure B-2). This is in contrast to Pan and colleagues who showed that mice given AZT orally have decreased BMD compared to mice given water only [251]. Given that the effects of ART on bone may be driven by immune reconstitution and that rodents are not capable of being infected by HIV, the HIV-1 tg rodent models may not be useful for studying direct ART effects on bone. However, they may still prove useful for use in studies regarding ART toxicity or polypharmacy or for effects of immune reconstitution [116, 252].

Nevertheless, given that the HIV-1 transgenic mouse and rat models have been shown to mimic specific HIV-1 associated comorbid conditions seen in humans infected with HIV, these transgenic animals are considered to be appropriate models for studying the chronic conditions that present in HIV infected individuals on effective suppressive ART [23, 144, 198]. Additionally, as discussed earlier, these HIV-associated comorbidities may be partly a consequence of chronic immune activation stemming from various viral products from HIV reservoirs. The HIV-1 tg rodent models may thus be useful in understanding how the localization of viral products and HIV-1 protein toxicity affects bone tissue and bone cells.

6.5 Final Conclusions

The population living with HIV infection is growing and aging, a reality that will require significant research if this group is to be provided effective healthcare. It has been well established that HIV positive individuals are at an increased risk for osteoporosis and fragility fractures and alarmingly at a younger age. This thesis presents work towards supporting the utilizing of the HIV-1 transgenic mouse and rat models for studying skeletal disorders with specific attention to age-related changes to bone microarchitecture and biomechanics and bone healing. Our results show similar detriment to cortical and trabecular bone architecture seen in HIV patients with low bone mass. Additionally, we present whole bone mechanics that reflect a decrease in mechanical competency driven by changes in bone microarchitecture. Finally, we present for the first time pre-clinical evidence for impaired bone healing using two different models of bone injury. Further investigations using these models will help elucidate the complex relationship between HIV and bone dysfunction and promote continued use of animal models for the study of HIV associated diseases.

APPENDIX A. PROTOCOLS

A.1 Mouse Fracture Surgery Protocol

Protocol for the placement of the support pin and formation of a transverse femur fracture (*adapted from* Craig Duvall; Doctoral Thesis 2007; Georgia Tech)

Instrument and Materials List

1. Animal Prep:
    - Isoflurane
    - Ocular lubricant
    - 2x2 gauze
    - Alcohol
    - Chlorhexidine Solution
    - Scrub solution
    - Cotton tip applicator
    - Nair
    - 23g needles
    - 1 mL syringe
    - Buprenorphine
2. Surgery:
    - Sterile gloves (x2 pairs per animal)
    - Sterile drapes (at least 2 + 1 per animal)
    - Large scissors (x2)
    - Sterile 2x2 gauze
    - Pick-up Forceps with teeth (x3)
    - Forceps with teeth (x3)
    - Small scissors (x2)
    - Small curved tip forceps with teeth (x3)
    - #7 scalpel handle (x2)
    - #15 scalpel blades (at least 1x per animal)

- 25g needles (at least 1x per animal)
- K-wire cutters
- Needle drivers (x2)
- Gigli wire saw: ~8 in. lengths (1x per animal)
- Curve tip hemostats (x3)
- 5-0 sutures
- 7mm wound clips (at least 1x pack per 3 animals)
- 7mm wound clip applier
- Sterile stainless steel bowl
- Sterile saline for washing instruments

3. Bead sterilizer
    - Post-op:
    - Metronidazole
    - Newskin
    - Container to mix in

Procedure

1. Instruments will be autoclaved prior to surgery. In between surgeries, instruments will be sterilized with glass bead sterilizer. Only the tips of the instruments and not the handles will be sterilized.
2. Mouse will be anesthetized using isoflurane administered at 3% for induction and 1.5% for maintenance. Depth of anesthesia will be monitored via toe withdrawal response.
3. Lateral right side of animals will be shaved from knee up
4. Remainder of hair in this region will be removed with depilatory cream (Nair)
5. The skin will be cleaned with water to remove excess cream and hair and then the skin will be cleaned and prepared for surgery (scrub, alcohol rinse, and chlorhexaderm)
6. Longitudinal skin incision will be made along lateral side of leg from knee towards hip
7. A longitudinal cut along the lateral condyle of the femur will be made using a No.

15 scalpel

8. The biceps femoris and vastuslateralis muscles will be teased apart to expose the lateral side of the femur
9. The patella will be slid to the medial side of the condyle
10. The condyle will be exposed by flexing the knee and a 25-gauge needle will be inserted into the intramedullary canal to create a “pilot hole”
11. Using the trocar end of a K-wire (KI-71-100, Key Surgical) cut in half, the K-wire will be inserted into the intramedullary canal following the “pilot hole”
12. Then, using the 0.22 mm gigli wire saw cut to a length of approximately 8 inches, the gigli wire will be fed under the medial side of the femur and pulled up the anterior side of the femur
13. With an assistant stabilizing the pin and limb, the gigli wire will be used to saw a mid-diaphyseal transverse osteotomy
14. Any connected cortical bone on the lateral side of the femur will be cut using the No. 15 scalpel
15. The K-wire will be slid slightly back out of the intramedullary canal of the femur, and the needle will be cut to the appropriate length (so that the intramedullary support is flush with the surface of the condyle at the needle insertion point).
16. The patella will be slid back into its native position, covering the condyle.
17. Using 5-0 absorbable sutures, one suture will be placed to hold the biceps femoris and vastuslateralis muscles together.
18. One suture will be placed to connect the patellar ligament to the adjacent musculature on the lateral side (to keep the patella from sliding back out of place).
19. The skin incision will be closed using interrupted sutures and staples.
20. The animal will be allowed to awaken from anesthesia on a heating pad.
21. The animal will be allowed to ambulate freely upon awakening.
22. Staples will be removed after 7-9 days.
23. All animals will receive sustained released Buprenorphine (Bup SR) immediately prior to surgery at a dose of 1.0 mg/kg.
24. Postoperatively, animals will be observed for signs that are suggestive of distress (e.g., decreased activity levels, poor grooming, hunched posture, etc.).

A.2 Rat Tail Ventral Artery Blood Collection and Serum Isolation Protocol

I. Fasting

a. 6 hours MINIMUM before collecting blood (RatLaps EIA)

II. Room Preparation (record time in)

a. Set up anesthesia (2 separate stations)
    i. For multiple rats, use the multi-mask unit
        1. Check Iso and O_2 levels – refill if necessary
        2. Connect filter and O_2/Iso
        3. Check water pump level – refill if necessary
        4. Place heating pad over bed
        5. Hook up one warming bed to the water circuit and place it under the tail end of the heating pad
        6. Turn on the heating water pump
        7. Position heating lamp over bed and turn on
            a. **Note**: Be sure not to roast the rats (i.e. not too close)!
    ii. If single rat
        1. Same procedure as above except:
            a. Use a single mask
            b. Use two warming beds lined up end-to-end
    iii. For induction chamber
        1. Check Iso and O_2 levels – refill if necessary
        2. Make sure the induction chamber bottom is clean – replace if necessary
b. Gather materials for blood collection
    i. Heat Lamp
    ii. BD Microtainer SST REF365967
        1. For collecting blood and separating serum
    iii. Holder for collection tubes
    iv. Kendall Monoject Veterinary I.V. catheters 2419FEP
        1. To stick the ventral artery and guide blood to collection tube
    v. Terumo U-100 insulin syringe 3/10cc 29Gx1/2”
        1. To administer acepromazine
    vi. Acepromazine maleate
        1. Vasodilator
        2. Sedative

a. **Note**: This means the Iso can be turned down from normal levels since the drug will be assisting with sedation

vii. Calculator
viii. Clock
ix. Gauze pads
x. Alcohol and chlorhexiderm soaked gauze for sterilizing the tail

c. Gather materials for serum storage
    i. Note on centrifuge
    ii. 500uL tubes
    iii. 20uL pipette
    iv. Pipette tips
    v. Holder for tubes

III. Blood Collection

a. Transfer rats from rat holding room to procedure room (sign out animals)
b. Turn on Iso and O_2 and turn valve towards the induction chamber
c. Place rat into induction chamber and wait for it to go under
d. Turn on Iso and O_2 and turn valve towards the mask
e. Weigh the rat and record value
f. Move rat over to blood collection station
g. Ensure the rat is under anesthesia via toe pinch
h. Calculate amount of Acepromazine needed (weight (kg) X ~~2.0~~ 1.5 mg/kg X concentration of bottle (mL/mg))
i. Using insulin syringe, administer needed amount subcutaneously
    i. Record time of injection
    ii. Wait ~~10~~ 7 full minutes for drug to take effect before collecting blood
j. If necessary, tag the ear
    i. Be sure to decide which ear will be tagged (for multiple groups)
    ii. Tag with number on dorsal side
    iii. Record number
    iv. Write cage number if necessary on cage card and on record sheet
k. If multiple rats, follow e – j until time to collect blood
l. Sterilize the rat tail with three passes of alcohol and chlorhexiderm
m. Take catheter and remove bottom section, leaving the needle and catheter only
n. With non-dominant hand, hold the tail from under the base and trace down gently to midpoint
o. Visually track the artery from the base of the tail to the midpoint

p. With the dominant hand, stick the needle at that point at a shallow angle along the artery line and insert just over halfway
    i. With older rats, it may be necessary to push through the thicker skin at a steeper angle before changing to a shallow angle to penetrate the artery
q. Slowly withdraw the needle+catheter and watch for the flash of blood at the bottom
r. When flash occurs, STOP pulling
s. Quickly remove the needle, keeping the catheter in place
t. Grab a collection tube and collect the needed amount of blood
    i. Be sure to place the tube down in a secure place so that no shaking and potential hemolysis occurs
    ii. **Note**: If blood is collected off the tail and not directly into the collection tube, the resulting serum samples will be pink (bad) and not clear (good). Presumably this is due to hemolysis.
u. Using the non-dominant hand, immediately apply firm pressure at the insertion site and remove the catheter
v. Wait for adequate hemostasis
w. Record the time of blood collection
    i. Let blood sit in tubes for at least 1 hour at room temperature to allow for adequate clotting
    ii. Label collection tube
    iii. **Note**: No more than 3 hours from blood collection to serum separation (Rat-MID Osteocalcin EIA)
x. Move rat to recovery warming bed or in cage under heat lamp
y. When rat has regained consciousness, move it back to its cage and back to holding room when ready (sign in animals)
z. **Note**: Regularly check Iso and O_2 levels

IV. Serum Separation

a. Follow the directions provided with the serum separation tubes for proper centrifugation (at least 6000g RCF for 2 min. – BD Microtainer SST) → update to 15,000g RCF for 5 min.
b. Divide into 40uL aliquots
c. Be sure to properly label all samples (i.e. rat # and date)!!!
d. Place in freezer for storage (up to 18 months at -20°C – RatLaps EIA)

V. Clean up (record time out)

a. Turn off all Iso, O_2, and water pump units
b. Flush O_2
c. Clean all surfaces with sporacidin

d. Remove all induction chamber bottoms to dirty cagewash and replace with clean ones
e. Remove and clean all masks
f. Return any instruments and materials to original place
g. Record the use of any inventory on Supply Charge Sheet

APPENDIX B. SUPPLEMENTAL DATA

Table B-1. MicroCT Bone Microarchitecture - HIV-1 tg Male Mouse (FVB/N)

Skeletal Site	Measure	WT	HIV	p-value
	Body Mass (g)	28.44 ± 0.97	22.56 ± 0.90	**< 0.001**
Femur Mid-diaphysis	Femur Length (mm)	14.82 ± 0.22	14.19 ± 0.16	**0.035**
	Ct.Th (μm)	194 ± 9.4	140.4 ± 7.7	**< 0.001**
	Mineral Density (mg HA/cm^3)	1413 ± 28	1425 ± 19	0.727
	MOI (mm^4)	0.11 ± 0.01	0.09 ± 0.01	0.081
	pMOI (mm^4)	0.30 ± 0.02	0.24 ± 0.01	**0.040**
	BA (mm^2)	0.74 ± 0.04	0.58 ± 0.03	**0.003**
	TA (mm^2)	1.64 ± 0.06	1.61 ± 0.03	0.638
	MA (mm^2)	0.90 ± 0.03	1.03 ± 0.03	**0.007**
Distal Femur Epiphysis	BV/TV (%)	30.2 ± 1.5	22.7 ± 2.2	**0.011**
	Conn.D (1/mm^3)	375.5 ± 9.8	398.8 ± 25.6	0.405
	SMI	0.68 ± 0.15	1.23 ± 0.26	0.079
	Tb.N (1/mm)	6.64 ± 0.1	6.58 ± 0.07	0.585
	Tb.Th (μm)	48.90 ± 1.57	41.02 ± 2.02	**0.007**
	Tb.Sp (μm)	148.7 ± 2.7	152.4 ± 2.1	0.295
	Mineral Density (mg HA/cm^3)	1117 ± 19	1103 ± 25	0.669
Distal Femur Metaphysis	BV/TV (%)	13.8 ± 1.1	9.8 ± 1	**0.014**
	Conn.D (1/mm^3)	224.6 ± 23.8	150.2 ± 26	**0.049**
	SMI	2.38 ± 0.05	2.72 ± 0.12	**0.018**
	Tb.N (1/mm)	5.74 ± 0.35	5.45 ± 0.16	0.467
	Tb.Th (μm)	39.48 ± 0.86	34.85 ± 1.36	**0.035**
	Tb.Sp (μm)	181.7 ± 10.8	187 ± 5.3	0.664
	Mineral Density (mg HA/cm^3)	1083 ± 23	1090 ± 21	0.823
Lumbar Spine - L6 Vertebra	BV/TV (%)	10.0 ± 0.4	8.0 ± 0.5	**0.002**
	Conn.D (1/mm^3)	44.03 ± 2.27	73.72 ± 8.01	**0.006**
	SMI	-0.25 ± 0.09	0.91 ± 0.2	**< 0.001**
	Tb.N (1/mm)	1.62 ± 0.12	1.92 ± 0.23	0.245
	Tb.Th (μm)	77.9 ± 1.74	61.29 ± 2.52	**< 0.001**
	Tb.Sp (μm)	718.0 ± 50.9	647.3 ± 116.3	0.156
	Mineral Density (mg HA/cm^3)	1094 ± 4	1023 ± 13	**<0.001**

Data are presented as Mean ± SEM. Values in bold indicate significance met at $p < 0.05$.

Table B-2. Bone Biomechanical Properties - HIV-1 tg Male Mouse (FVB/N)

Bone	Measure	WT	HIV	p-value
Femur	Stiffness (N/mm)	64.58 ± 4.78	54.94 ± 4.61	0.165
	Ultimate Load (N)	16.00 ± 0.86	12.84 ± 0.91	**0.023**
	Displacement at Ultimate Load (mm)	0.42 ± 0.03	0.44 ± 0.03	0.565
	Energy to Ultimate Load (N-mm)	4.36 ± 0.44	3.60 ± 0.39	0.211
	Yield Load (N)	9.34 ± 0.87	7.23 ± 0.66	0.066
	Displacement at Yield Load (mm)	0.16 ± 0.01	0.16 ± 0.02	0.889
	Energy to Yield Load (N-mm)	0.75 ± 0.12	0.54 ± 0.07	0.152
	Failure Load (N)	13.00 ± 1.12	10.90 ± 0.93	0.164
	Displacement at Failure Load (N)	0.67 ± 0.05	0.62 ± 0.07	0.582
	Energy to Failure Load (N-mm)	7.62 ± 0.50	5.42 ± 0.62	**0.014**
	Postyield Displacement (mm)	0.50 ± 0.05	0.46 ± 0.06	0.61
	Ultimate Stress (MPa)	143.0 ± 7.9	139.7 ± 5.1	0.725
	Elastic Modulus (GPa)	2.84 ± 0.27	3.02 ± 0.21	0.619
	Toughness to Ultimate Stress (MJ/m^3)	7.91 ± 0.64	7.71 ± 0.58	0.822
L6 Vertebra	Stiffness (N/mm)	59.75 ± 8.86	41.87 ± 4.82	0.089
	Ultimate Load (N)	20.48 ± 3.49	12.33 ± 0.63	**0.021**
	Displacement at Ultimate Load (mm)	0.44 ± 0.06	0.39 ± 0.04	0.557
	Energy to Ultimate Load (N-mm)	5.53 ± 1.32	3.12 ± 0.37	0.189
	Yield Load (N)	17.79 ± 3.15	8.58 ± 1.03	**0.012**
	Ultimate Stress (MPa)	35.96 ± 6.22	34.36 ± 4.48	0.835
	Elastic Modulus (MPa)	208.1 ± 30.9	236.2 ± 45.5	0.629
	Toughness to Ultimate Stress (MJ/m^3)	5.01 ± 1.35	4.46 ± 0.83	0.729

Data are presented as Mean ± SEM. Values in bold indicate significance met at $p < 0.05$.

Table B-3. Mechanical Properties of Contralateral Intact Femurs - HIV-1 tg Male Mouse Fracture Study

Mechanical Property	Time Point (week)	WT			HIV			Overall p-value	p-value
		N	Mean	SEM	N	Mean	SEM		
Max Torque (N-mm)	2	10	23.96	0.88	8	21.67	1.64	0.060	0.314
	4	9	27.40	2.31	8	23.45	1.21		0.094
Rotation at Max Torque (deg)	2	10	10.98	0.75	8	12.38	1.50	0.030	0.227
	4	9	11.01	0.40	8	12.40	0.70		0.057
Torsional Stiffness (N-mm/deg)	2	10	2.69	0.21	8	2.34	0.23	0.128	0.270
	4	9	2.90	0.21	8	2.31	0.17		0.286
Energy to Max Torque (N-mm-deg)	2	10	151.60	13.68	8	164.26	27.36	0.890	0.622
	4	9	176.15	16.71	8	168.55	13.46		0.772

Data were analyzed using Two-way ANOVA followed by pairwise comparisons using the Bonferroni adjustment. (GLM-Univariate, SPSS 24).

Table B-4. MicroCT Bone Microarchitecture - FVB/N administered AZT or Water

Bone	Measure	AZT	Water	p-value
	Body Mass (g)	23.24 ± 0.67	25.39 ± 0.41	**0.014**
Femur Mid-diaphysis	Femur Length (mm)	14.94 ± 0.10	14.84 ± 0.11	0.542
	Ct.Th (μm)	187.4 ± 5.0	184.2 ± 3.1	1.000
	Mineral Density (mg HA/cm^3)	1444 ± 17	1443 ± 16	0.912
	MOI (mm^4)	0.106 ± 0.004	0.106 ± 0.003	0.945
	pMOI (mm^4)	0.302 ± 0.012	0.280 ± 0.008	0.148
	BA (mm^2)	0.73 ± 0.02	0.70 ± 0.01	0.184
	MA (mm^2)	0.93 ± 0.02	0.91 ± 0.02	0.296
	TA (mm^2)	1.67 ± 0.03	1.61 ± 0.02	0.103
Femur Distal Epiphysis	BV/TV (%)	29.04 ± 1.07	28.66 ± 1.02	0.739
	Conn.D (mm^{-3})	342.6 ± 13.9	355.7 ± 15.5	0.537
	SMI	0.69 ± 0.10	0.75 ± 0.09	0.673
	Tb.N (mm^{-1})	6.31 ± 0.11	6.40 ± 0.14	0.629
	Tb.Th (μm)	49.53 ± 0.47	49.14 ± 0.68	0.644
	Tb.Sp (μm)	155.0 ± 3.1	153.9 ± 4.4	0.848
	Mineral Density (mg HA/cm^3)	1150 ± 17	1132 ± 19	0.436
Femur Distal Metaphysis	BV/TV (%)	12.08 ± 0.84	11.63 ± 0.61	0.669
	Conn.D (mm^{-3})	186.2 ± 24.0	174.6 ± 15.0	0.686
	SMI	2.37 ± 0.08	2.43 ± 0.06	0.546
	Tb.N (mm^{-1})	5.28 ± 0.17	5.20 ± 0.11	0.695
	Tb.Th (μm)	40.02 ± 0.42	39.74 ± 0.47	0.661
	Tb.Sp (μm)	193.3 ± 6.9	196.5 ± 4.5	0.703
	Mineral Density (mg HA/cm^3)	1112 ± 17	1099 ± 17	0.606
Lumbar Spine - L6 Vertebra	BV/TV (%)	10.55 ± 0.35	10.00 ± 0.25	0.221
	Conn.D (mm^{-3})	42.12 ± 2.44	44.59 ± 1.50	0.399
	SMI	-0.14 ± 0.07	-0.05 ± 0.08	0.426
	Tb.N (mm^{-1})	1.85 ± 0.07	1.80 ± 0.09	0.669
	Tb.Th (μm)	78.09 ± 1.02	74.67 ± 0.65	**0.011**
	Tb.Sp (μm)	578.5 ± 21.3	586.4 ± 42.5	0.869
	Mineral Density (mg HA/cm^3)	1106 ± 5	1069 ± 14	**0.021**

Data are presented as Mean ± SEM. Values in bold indicate significance met at $p < 0.05$.

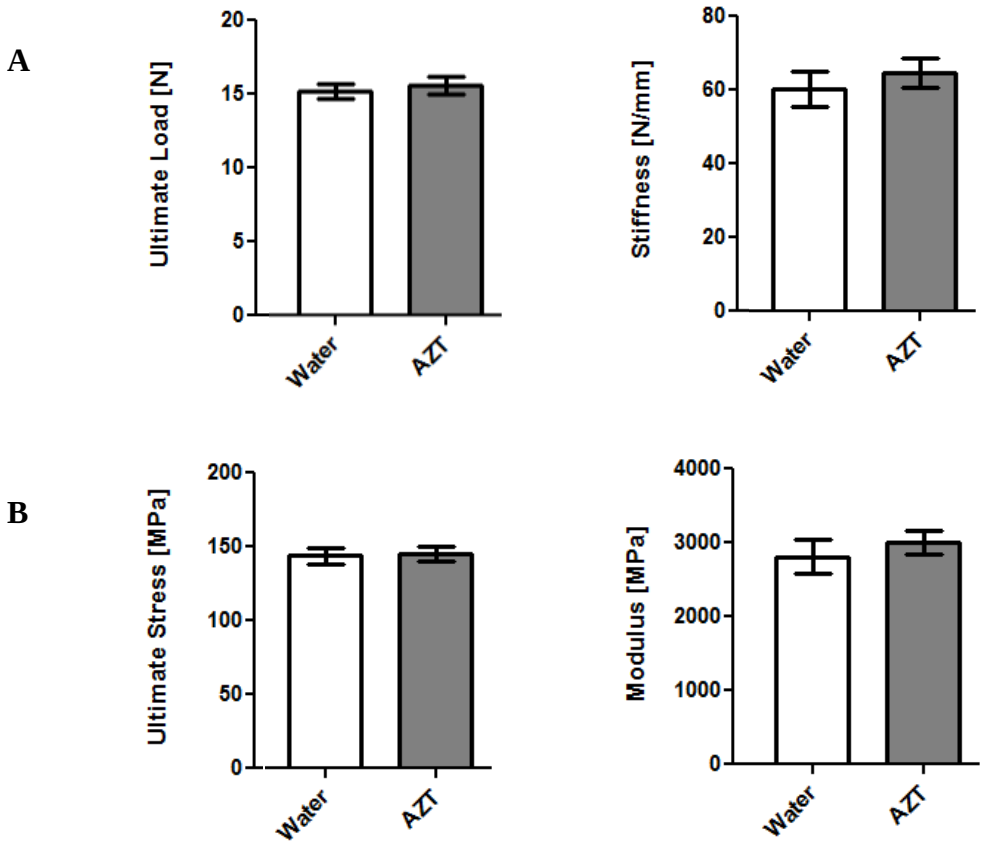

Figure B-1. Effect of AZT on biomechanical properties of whole femurs tested in three-point bending. (A) Measured structural properties. (B) Estimated derived material properties. n = 10 per group. Error bars indicate SEM.

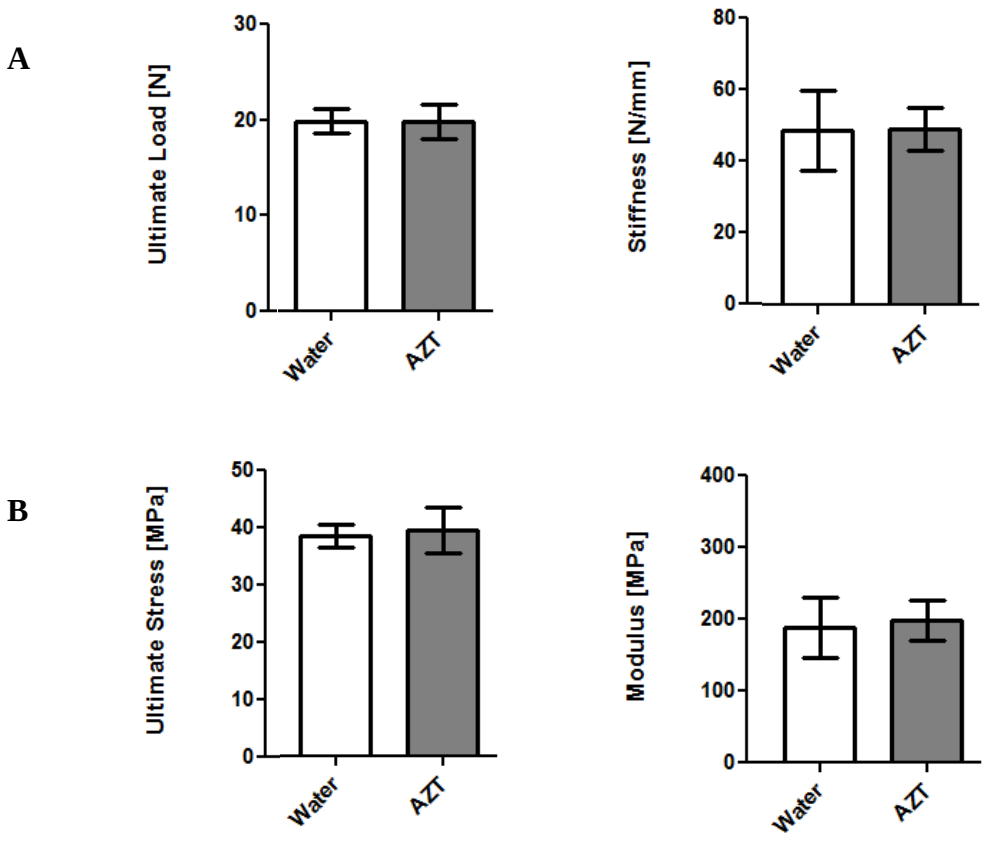

Figure B-2. Effect of AZT on biomechanical properties of L6 vertebrae tested in compression. (A) Measured structural properties. (B) Estimated derived material properties. n = 5 per group. Error bars indicate SEM.

Table B-5. MicroCT Bone Microarchitecture – HIV-1 tg Rat (Male, 14 months old)

	WT	HIV	P value
Femur Mid-diaphysis	n = 4	n = 6	
Femur Length (mm)	42.67 ± 0.29	40.73 ± 0.33	**0.033**
BV/TV (%)	63.55 ± 0.34	59.78 ± 0.89	**0.008**
Ct.Th (mm)	0.62 ± 0.02	0.54 ± 0.02	**0.025**
Mineral Density (mg HA/cm^3)	1285 ± 18	1326 ± 3	0.110
MOI (mm^4)	11.02 ± 0.80	6.63 ± 0.41	**0.008**
pMOI (mm^4)	23.82 ± 1.62	13.98 ± 0.86	**0.006**
BA (mm^2)	8.33 ± 0.32	6.15 ± 0.23	**0.003**
MA (mm^2)	4.77 ± 0.15	4.13 ± 0.12	**0.014**
TA (mm^2)	13.10 ± 0.46	10.27 ± 0.30	**0.004**
L6 Vertebra	n = 5	n = 6	
BV/TV (%)	37.28 ± 0.71	27.13 ± 0.93	**0.000**
Tb.N (mm^{-1})	4.32 ± 0.06	4.08 ± 0.20	0.290
Tb.Th (µm)	91.80 ± 1.71	74.00 ± 1.53	**0.000**
Tb.Sp (µm)	211.0 ± 3.7	238.5 ± 13.8	0.110
Conn.D (mm^{-3})	57.52 ± 1.59	82.00 ± 12.30	0.110
SMI	-0.73 ± 0.05	0.12 ± 0.08	**< 0.001**
Mineral Density (mg HA/cm^3)	1138 ± 12	1158 ± 12	0.280

Data are presented as Mean ± SEM. Values in bold indicate significance met at $p < 0.05$.

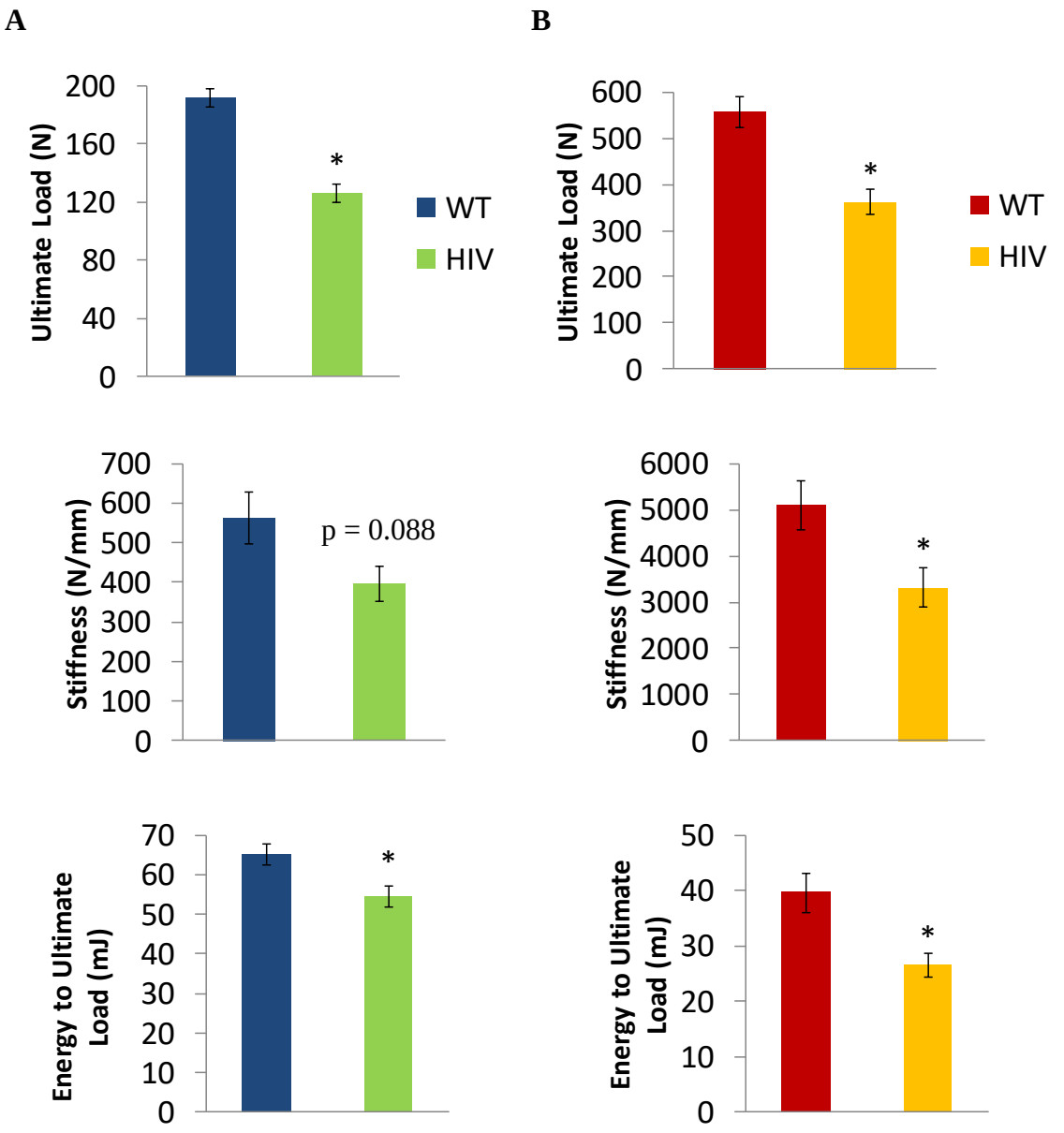

Figure B-3. Biomechanical properties of bones from HIV-1 tg male rats. (A) Measured structural properties of whole femurs tested in 3-point bending. n = 4 WT, n = 6 HIV (B) Measured structural properties of L6 vertebrae tested in compression. n = 5 WT, n = 6 HIV. Error bars indicate SEM. * indicates $p < 0.05$.

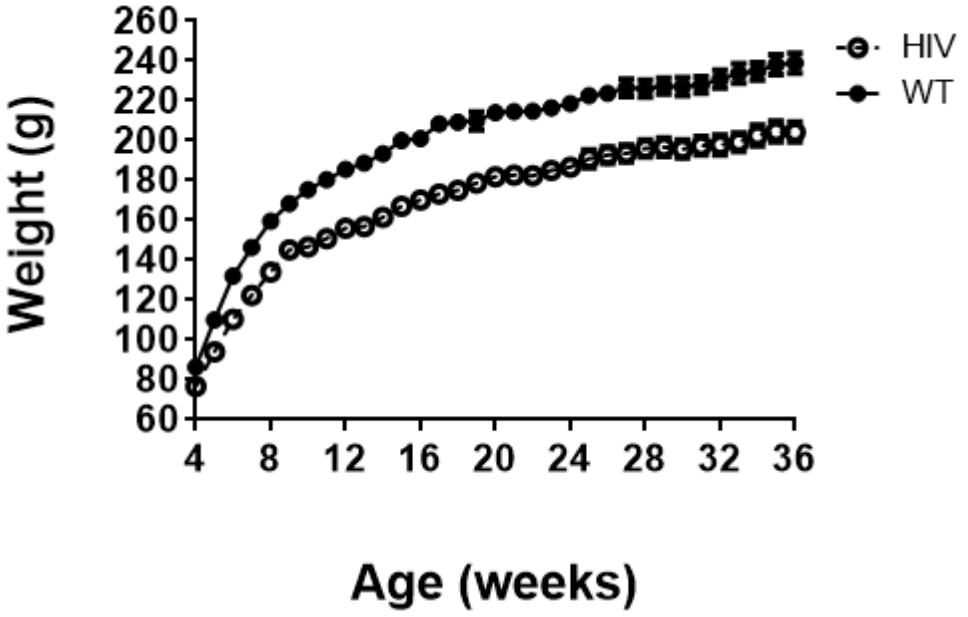

Figure B-4. Growth of HIV-1 tg female rats and littermates. Data are presented as Mean ± SEM.

REFERENCES

1. UNAIDS, *UNAIDS Data 2017*. 2017, Joint United Nations Programme on HIV/AIDS (UNAIDS).

2. Sabin, C.A., *Do people with HIV infection have a normal life expectancy in the era of combination antiretroviral therapy?* BMC Med, 2013. **11**: p. 251.

3. Teeraananchai, S., et al., *Life expectancy of HIV-positive people after starting combination antiretroviral therapy: a meta-analysis.* HIV Med, 2017. **18**(4): p. 256-266.

4. Gallant, J., et al., *Comorbidities Among US Patients With Prevalent HIV Infection-A Trend Analysis.* J Infect Dis, 2017. **216**(12): p. 1525-1533.

5. Hemkens, L.G. and H.C. Bucher, *HIV infection and cardiovascular disease.* Eur Heart J, 2014. **35**(21): p. 1373-81.

6. Saylor, D., et al., *HIV-associated neurocognitive disorder - pathogenesis and prospects for treatment.* Nat Rev Neurol, 2016. **12**(5): p. 309.

7. Ali, M.K., et al., *HIV and metabolic, body, and bone disorders: what we know from low- and middle-income countries.* J Acquir Immune Defic Syndr, 2014. **67 Suppl 1**: p. S27-39.

8. Mallon, P.W., *Aging with HIV: osteoporosis and fractures.* Curr Opin HIV AIDS, 2014. **9**(4): p. 428-35.

9. Shiau, S., et al., *Incident fractures in HIV-infected individuals: a systematic review and meta-analysis.* AIDS, 2013. **27**(12): p. 1949-57.

10. Borderi, M., et al., *Prevalence of sub-clinical vertebral fractures in HIV-infected patients.* New Microbiol, 2014. **37**(1): p. 25-32.

11. Compston, J., *HIV infection and osteoporosis.* Bonekey Rep, 2015. **4**: p. 636.

12. Madison, B.B.B., *HIV infection and its effects on fracture healing: a literature review.* South Sudan Medical Journal, 2014. **7**(4): p. 94-95.

13. Wijesekera, M.P., et al., *Fracture management in HIV positive individuals: a systematic review.* Int Orthop, 2016. **40**(12): p. 2429-2445.

14. Policicchio, B.B., I. Pandrea, and C. Apetrei, *Animal Models for HIV Cure Research.* Front Immunol, 2016. **7**: p. 12.

15. Hatziioannou, T. and D.T. Evans, *Animal models for HIV/AIDS research.* Nat Rev Microbiol, 2012. **10**(12): p. 852-67.

16. Kopp, J.B., et al., *Progressive glomerulosclerosis and enhanced renal accumulation of basement membrane components in mice transgenic for human immunodeficiency virus type 1 genes.* Proc Natl Acad Sci U S A, 1992. **89**(5): p. 1577-81.

17. Reid, W., et al., *An HIV-1 transgenic rat that develops HIV-related pathology and immunologic dysfunction.* Proc Natl Acad Sci U S A, 2001. **98**(16): p. 9271-6.

18. Hansen, L., et al., *Endothelial dysfunction, arterial stiffening, and intima-media thickening in large arteries from HIV-1 transgenic mice.* Ann Biomed Eng, 2013. **41**(4): p. 682-93.

19. Cheung, J.Y., et al., *Cardiac Dysfunction in HIV-1 Transgenic Mouse: Role of Stress and BAG3.* Clin Transl Sci, 2015. **8**(4): p. 305-10.

20. Dickie, P., et al., *HIV-associated nephropathy in transgenic mice expressing HIV-1 genes.* Virology, 1991. **185**(1): p. 109-19.

21. Pruznak, A.M., et al., *Skeletal and cardiac myopathy in HIV-1 transgenic rats.* Am J Physiol Endocrinol Metab, 2008. **295**(4): p. E964-73.

22. Ray, P.E., et al., *A novel HIV-1 transgenic rat model of childhood HIV-1-associated nephropathy.* Kidney Int, 2003. **63**(6): p. 2242-53.

23. Reid, W.C., et al., *Characterization of neuropathology in the HIV-1 transgenic rat at different ages.* J Neuroimmunol, 2016. **292**: p. 116-25.

24. Vikulina, T., et al., *Alterations in the immuno-skeletal interface drive bone destruction in HIV-1 transgenic rats.* Proc Natl Acad Sci U S A, 2010. **107**(31): p. 13848-53.

25. Komori, T., *Animal models for osteoporosis.* Eur J Pharmacol, 2015. **759**: p. 287-94.

26. Histing, T., et al., *Small animal bone healing models: standards, tips, and pitfalls results of a consensus meeting.* Bone, 2011. **49**(4): p. 591-9.

27. Ball, A.N., et al., *The challenges of promoting osteogenesis in segmental bone defects and osteoporosis.* J Orthop Res, 2017.

28. Seeman, E., *Bone quality: the material and structural basis of bone strength.* J Bone Miner Metab, 2008. **26**(1): p. 1-8.

29. Clarke, B., *Normal bone anatomy and physiology.* Clin J Am Soc Nephrol, 2008. **3 Suppl 3**: p. S131-9.

30. Oftadeh, R., et al., *Biomechanics and mechanobiology of trabecular bone: a review.* J Biomech Eng, 2015. **137**(1).

31. Osterhoff, G., et al., *Bone mechanical properties and changes with osteoporosis.* Injury, 2016. **47 Suppl 2**: p. S11-20.

32. Gasser, A.J.K., Michaela, *Bone Physiology and Biology*, in *Bone Toxicology*, S.V. Smith, Auorore; Samadfam, Rana, Editor. 2017, Springer International Publishing. p. 27-94.

33. Robling, A.G., A.B. Castillo, and C.H. Turner, *Biomechanical and molecular regulation of bone remodeling.* Annu Rev Biomed Eng, 2006. **8**: p. 455-98.

34. Lefebvre, V. and P. Bhattaram, *Vertebrate skeletogenesis.* Curr Top Dev Biol, 2010. **90**: p. 291-317.

35. Berendsen, A.D. and B.R. Olsen, *Bone development.* Bone, 2015. **80**: p. 14-18.

36. Marsell, R. and T.A. Einhorn, *The biology of fracture healing.* Injury, 2011. **42**(6): p. 551-5.

37. Loi, F., et al., *Inflammation, fracture and bone repair.* Bone, 2016. **86**: p. 119-30.

38. Einhorn, T.A. and L.C. Gerstenfeld, *Fracture healing: mechanisms and interventions.* Nat Rev Rheumatol, 2015. **11**(1): p. 45-54.

39. German Advisory Committee Blood, S.A.o.P.T.b.B., *Human Immunodeficiency Virus (HIV).* Transfus Med Hemother, 2016. **43**(3): p. 203-22.

40. Frankel, A.D. and J.A. Young, *HIV-1: fifteen proteins and an RNA.* Annu Rev Biochem, 1998. **67**: p. 1-25.

41. CDC. *About HIV/AIDS*. 2017 May 30, 2017 [cited 2018 April 25, 2018]; Available from: https://www.cdc.gov/actagainstaids/basics/whatishiv.html.

42. Kassutto, S. and E.S. Rosenberg, *Primary HIV type 1 infection.* Clin Infect Dis, 2004. **38**(10): p. 1447-53.

43. Fraser, C., et al., *Variation in HIV-1 set-point viral load: epidemiological analysis and an evolutionary hypothesis.* Proc Natl Acad Sci U S A, 2007. **104**(44): p. 17441-6.

44. Appay, V.L., Anya; Sauce, Delphine, *HIV-Associated Immune Exhaustion*, in *Encyclopedia of AIDS*. 2014, Springer Science.

45. Cummins, N.W. and A.D. Badley, *Making sense of how HIV kills infected CD4 T cells: implications for HIV cure.* Mol Cell Ther, 2014. **2**: p. 20.

46. Zhu, J. and W.E. Paul, *CD4 T cells: fates, functions, and faults.* Blood, 2008. **112**(5): p. 1557-69.

47. UNAIDS, *The Gap Report*. 2014, Joint United Nations Programme on HIV/AIDS (UNAIDS).

48. Moore, R.D., *Epidemiology of HIV infection in the United States: implications for linkage to care.* Clin Infect Dis, 2011. **52 Suppl 2**: p. S208-13.

49. CDC, *Estimated HIV incidence and prevalence in the United States, 2010–2015*, in *HIV Surveillance Supplemental Report*. 2018, Centers for Disease Control and Prevention.

50. CDC, *Diagnoses of HIV Infection in the United States and Dependent Areas, 2016*, in *HIV Surveillance Report*. 2016.

51. Wing, E.J., *HIV and aging.* Int J Infect Dis, 2016. **53**: p. 61-68.

52. Li, J.Z., et al., *The size of the expressed HIV reservoir predicts timing of viral rebound after treatment interruption.* AIDS, 2016. **30**(3): p. 343-53.

53. High, K.P., et al., *HIV and aging: state of knowledge and areas of critical need for research. A report to the NIH Office of AIDS Research by the HIV and Aging Working Group.* J Acquir Immune Defic Syndr, 2012. **60 Suppl 1**: p. S1-18.

54. McGettrick, P., E.A. Barco, and P.W.G. Mallon, *Ageing with HIV.* Healthcare (Basel), 2018. **6**(1).

55. Guaraldi, G., et al., *Morbidity in older HIV-infected patients: impact of long-term antiretroviral use.* AIDS Rev, 2014. **16**(2): p. 75-89.

56. Appay, V. and D. Sauce, *Assessing immune aging in HIV-infected patients.* Virulence, 2017. **8**(5): p. 529-538.

57. Klatt, N.R., et al., *Immune activation and HIV persistence: implications for curative approaches to HIV infection.* Immunol Rev, 2013. **254**(1): p. 326-42.

58. Massanella, M., R. Fromentin, and N. Chomont, *Residual inflammation and viral reservoirs: alliance against an HIV cure.* Curr Opin HIV AIDS, 2016. **11**(2): p. 234-41.

59. Popovic, M., et al., *Persistence of HIV-1 structural proteins and glycoproteins in lymph nodes of patients under highly active antiretroviral therapy.* Proc Natl Acad Sci U S A, 2005. **102**(41): p. 14807-12.

60. Santosuosso, M., et al., *HIV-1 envelope protein gp120 is present at high concentrations in secondary lymphoid organs of individuals with chronic HIV-1 infection.* J Infect Dis, 2009. **200**(7): p. 1050-3.

61. Imamichi, H., et al., *Defective HIV-1 proviruses produce novel protein-coding RNA species in HIV-infected patients on combination antiretroviral therapy.* Proc Natl Acad Sci U S A, 2016. **113**(31): p. 8783-8.

62. Baxter, A.E., U. O'Doherty, and D.E. Kaufmann, *Beyond the replication-competent HIV reservoir: transcription and translation-competent reservoirs.* Retrovirology, 2018. **15**(1): p. 18.

63. Nih Consensus Development Panel on Osteoporosis Prevention, D. and Therapy, *Osteoporosis prevention, diagnosis, and therapy.* JAMA, 2001. **285**(6): p. 785-95.

64. Pisani, P., et al., *Major osteoporotic fragility fractures: Risk factor updates and societal impact.* World J Orthop, 2016. **7**(3): p. 171-81.

65. (WHO), W.H.O., *WHO Scientific Group on the Assessment of Osteoporosis at Primary Health Care Level: Summary Meeting Report; May5–7, 2004 Brussels, Belgium*. 2007, World Health Organization: Geneva. p. 1-17.

66. Brown, T.T. and R.B. Qaqish, *Antiretroviral therapy and the prevalence of osteopenia and osteoporosis: a meta-analytic review.* AIDS, 2006. **20**(17): p. 2165-74.

67. Goh, S.S.L., et al., *Reduced bone mineral density in human immunodeficiency virus-infected individuals: a meta-analysis of its prevalence and risk factors.* Osteoporos Int, 2018. **29**(3): p. 595-613.

68. Amiel, C., et al., *BMD is reduced in HIV-infected men irrespective of treatment.* J Bone Miner Res, 2004. **19**(3): p. 402-9.

69. Arnsten, J.H., et al., *Decreased bone mineral density and increased fracture risk in aging men with or at risk for HIV infection.* AIDS, 2007. **21**(5): p. 617-23.

70. Grijsen, M.L., et al., *High prevalence of reduced bone mineral density in primary HIV-1-infected men.* AIDS, 2010. **24**(14): p. 2233-8.

71. Sharma, A., et al., *Prospective study of bone mineral density changes in aging men with or at risk for HIV infection.* AIDS, 2010. **24**(15): p. 2337-45.

72. Stephens, K.I., et al., *Dual-Energy X-Ray Absorptiometry and Calculated Frax Risk Scores May Underestimate Osteoporotic Fracture Risk in Vitamin D-Deficient Veterans with Hiv Infection.* Endocr Pract, 2016. **22**(4): p. 440-6.

73. Anastos, K., et al., *The association of bone mineral density with HIV infection and antiretroviral treatment in women.* Antivir Ther, 2007. **12**(7): p. 1049-58.

74. Arnsten, J.H., et al., *HIV infection and bone mineral density in middle-aged women.* Clin Infect Dis, 2006. **42**(7): p. 1014-20.

75. Dolan, S.E., et al., *Reduced bone density in HIV-infected women.* AIDS, 2004. **18**(3): p. 475-83.

76. Yin, M., et al., *Bone mass and mineral metabolism in HIV+ postmenopausal women.* Osteoporos Int, 2005. **16**(11): p. 1345-52.

77. Yin, M.T., et al., *Short-term bone loss in HIV-infected premenopausal women.* J Acquir Immune Defic Syndr, 2010. **53**(2): p. 202-8.

78. Yin, M.T., et al., *Low bone mass and high bone turnover in postmenopausal human immunodeficiency virus-infected women.* J Clin Endocrinol Metab, 2010. **95**(2): p. 620-9.

79. Matovu, F.K., et al., *Bone health and HIV in resource-limited settings: a scoping review.* Curr Opin HIV AIDS, 2016. **11**(3): p. 306-25.

80. Xiao, P.L., et al., *Association between maternal HIV infection and low birth weight and prematurity: a meta-analysis of cohort studies.* BMC Pregnancy Childbirth, 2015. **15**: p. 246.

81. Wedi, C.O., et al., *Perinatal outcomes associated with maternal HIV infection: a systematic review and meta-analysis.* Lancet HIV, 2016. **3**(1): p. e33-48.

82. Hovi, P., et al., *Decreased bone mineral density in adults born with very low birth weight: a cohort study.* PLoS Med, 2009. **6**(8): p. e1000135.

83. Oliver, H., et al., *Growth in early life predicts bone strength in late adulthood: the Hertfordshire Cohort Study.* Bone, 2007. **41**(3): p. 400-5.

84. Jacobson, D.L., et al., *Total body and spinal bone mineral density across Tanner stage in perinatally HIV-infected and uninfected children and youth in PACTG 1045.* AIDS, 2010. **24**(5): p. 687-96.

85. Arpadi, S.M., et al., *Bone health in HIV-infected children, adolescents and young adults: a systematic review.* J AIDS Clin Res, 2014. **5**(11).

86. Sudjaritruk, T., et al., *Adverse bone health and abnormal bone turnover among perinatally HIV-infected Asian adolescents with virological suppression.* HIV Med, 2017. **18**(4): p. 235-244.

87. Yin, M.T., et al., *Lower peak bone mass and abnormal trabecular and cortical microarchitecture in young men infected with HIV early in life.* AIDS, 2014. **28**(3): p. 345-53.

88. Heaney, R.P., et al., *Peak bone mass.* Osteoporos Int, 2000. **11**(12): p. 985-1009.

89. Lu, J., et al., *Peak Bone Mass and Patterns of Change in Total Bone Mineral Density and Bone Mineral Contents From Childhood Into Young Adulthood.* J Clin Densitom, 2016. **19**(2): p. 180-91.

90. Raisz, L.G., *Pathogenesis of osteoporosis: concepts, conflicts, and prospects.* J Clin Invest, 2005. **115**(12): p. 3318-25.

91. Bloch, M.G., Giovanni, *Bone Biomarkers in HIV*, in *Biomarkers in Bone Disease*, V.B.P. Patel, Victor R., Editor. 2017, Springer Netherlands. p. 755-781.

92. Haskelberg, H., A. Carr, and S. Emery, *Bone turnover markers in HIV disease.* AIDS Rev, 2011. **13**(4): p. 240-50.

93. Mulubwa, M., et al., *Bone turnover markers in HIV-infected women on tenofovir-based antiretroviral therapy.* Southern African Journal of HIV Medicine, 2017. **18**(1).

94. Vlot, M.C., et al., *Effect of antiretroviral therapy on bone turnover and bone mineral density in men with primary HIV-1 infection.* PLoS One, 2018. **13**(3): p. e0193679.

95. Hoy, J., et al., *Interruption or deferral of antiretroviral therapy reduces markers of bone turnover compared with continuous therapy: The SMART body composition substudy.* J Bone Miner Res, 2013. **28**(6): p. 1264-74.

96. Teichmann, J., et al., *Changes in calciotropic hormones and biochemical markers of bone metabolism in patients with human immunodeficiency virus infection.* Metabolism, 2000. **49**(9): p. 1134-9.

97. Shiau, S., et al., *Decreased bone turnover in HIV-infected children on antiretroviral therapy.* Arch Osteoporos, 2018. **13**(1): p. 40.

98. Tan, B.M., et al., *Bone metabolism in children with human immunodeficiency virus infection receiving highly active anti-retroviral therapy including a protease inhibitor.* J Pediatr, 2001. **139**(3): p. 447-51.

99. Fakruddin, J.M. and J. Laurence, *HIV envelope gp120-mediated regulation of osteoclastogenesis via receptor activator of nuclear factor kappa B ligand (RANKL) secretion and its modulation by certain HIV protease inhibitors through interferon-gamma/RANKL cross-talk.* J Biol Chem, 2003. **278**(48): p. 48251-8.

100. Gibellini, D., et al., *HIV-1 Tat protein enhances RANKL/M-CSF-mediated osteoclast differentiation.* Biochem Biophys Res Commun, 2010. **401**(3): p. 429-34.

101. Gohda, J., et al., *HIV-1 replicates in human osteoclasts and enhances their differentiation in vitro.* Retrovirology, 2015. **12**: p. 12.

102. Chew, N., et al., *HIV-1 tat and rev upregulates osteoclast bone resorption.* J Int AIDS Soc, 2014. **17**(4 Suppl 3): p. 19724.

103. Raynaud-Messina, B., et al., *Bone degradation machinery of osteoclasts: An HIV-1 target that contributes to bone loss.* Proc Natl Acad Sci U S A, 2018. **115**(11): p. E2556-E2565.

104. Butler, J.S., et al., *HIV-1 protein induced modulation of primary human osteoblast differentiation and function via a Wnt/beta-catenin-dependent mechanism.* J Orthop Res, 2013. **31**(2): p. 218-26.

105. Cotter, E.J., et al., *HIV proteins regulate bone marker secretion and transcription factor activity in cultured human osteoblasts with consequent potential implications for osteoblast function and development.* AIDS Res Hum Retroviruses, 2007. **23**(12): p. 1521-30.

106. Cummins, N.W., et al., *Human immunodeficiency virus envelope protein Gp120 induces proliferation but not apoptosis in osteoblasts at physiologic concentrations.* PLoS One, 2011. **6**(9): p. e24876.

107. Gibellini, D., et al., *HIV-1 triggers apoptosis in primary osteoblasts and HOBIT cells through TNFalpha activation.* J Med Virol, 2008. **80**(9): p. 1507-14.

108. Beaupere, C., et al., *The HIV proteins Tat and Nef promote human bone marrow mesenchymal stem cell senescence and alter osteoblastic differentiation.* Aging Cell, 2015. **14**(4): p. 534-46.

109. Cheng, K., et al., *Bone-derived mesenchymal stromal cells from HIV transgenic mice exhibit altered proliferation, differentiation capacity and paracrine functions along with impaired therapeutic potential in kidney injury.* Exp Cell Res, 2013. **319**(14): p. 2266-74.

110. Cotter, E.J., et al., *HIV type 1 alters mesenchymal stem cell differentiation potential and cell phenotype ex vivo.* AIDS Res Hum Retroviruses, 2011. **27**(2): p. 187-99.

111. Gibellini, D., et al., *HIV-1 and recombinant gp120 affect the survival and differentiation of human vessel wall-derived mesenchymal stem cells.* Retrovirology, 2011. **8**: p. 40.

112. Wang, L., et al., *Suppression of clonogenic potential of human bone marrow mesenchymal stem cells by HIV type 1: putative role of HIV type 1 tat protein and inflammatory cytokines.* AIDS Res Hum Retroviruses, 2002. **18**(13): p. 917-31.

113. Weitzmann, M.N. and I. Ofotokun, *Physiological and pathophysiological bone turnover - role of the immune system.* Nat Rev Endocrinol, 2016. **12**(9): p. 518-32.

114. Titanji, K., et al., *Dysregulated B cell expression of RANKL and OPG correlates with loss of bone mineral density in HIV infection.* PLoS Pathog, 2014. **10**(10): p. e1004497.

115. Brown, T.T., et al., *Body composition, soluble markers of inflammation, and bone mineral density in antiretroviral therapy-naive HIV-1-infected individuals.* J Acquir Immune Defic Syndr, 2013. **63**(3): p. 323-30.

116. Ofotokun, I., et al., *Antiretroviral therapy induces a rapid increase in bone resorption that is positively associated with the magnitude of immune reconstitution in HIV infection.* AIDS, 2016. **30**(3): p. 405-14.

117. Deeks, S.G., *HIV infection, inflammation, immunosenescence, and aging.* Annu Rev Med, 2011. **62**: p. 141-55.

118. Serrano, S., et al., *Bone remodelling in human immunodeficiency virus-1-infected patients. A histomorphometric study.* Bone, 1995. **16**(2): p. 185-91.

119. Silva, B.C., et al., *Trabecular bone score: a noninvasive analytical method based upon the DXA image.* J Bone Miner Res, 2014. **29**(3): p. 518-30.

120. Sharma, A., et al., *HIV Infection is Associated with Abnormal Bone Microarchitecture: Measurement of Trabecular Bone Score in the Women's Interagency HIV Study*. JAIDS Journal of Acquired Immune Deficiency Syndromes, 2018. **Publish Ahead of Print**.

121. Calmy, A., et al., *Long-term HIV infection and antiretroviral therapy are associated with bone microstructure alterations in premenopausal women.* Osteoporos Int, 2013. **24**(6): p. 1843-52.

122. Yin, M.T., et al., *Trabecular and cortical microarchitecture in postmenopausal HIV-infected women.* Calcif Tissue Int, 2013. **92**(6): p. 557-65.

123. Liu, X.S., et al., *Complete volumetric decomposition of individual trabecular plates and rods and its morphological correlations with anisotropic elastic moduli in human trabecular bone.* J Bone Miner Res, 2008. **23**(2): p. 223-35.

124. Liu, X.S., et al., *Individual trabecula segmentation (ITS)-based morphological analysis of microscale images of human tibial trabecular bone at limited spatial resolution.* J Bone Miner Res, 2011. **26**(9): p. 2184-93.

125. Liu, X.S., et al., *Individual trabecula segmentation (ITS)-based morphological analyses and microfinite element analysis of HR-pQCT images discriminate postmenopausal fragility fractures independent of DXA measurements.* J Bone Miner Res, 2012. **27**(2): p. 263-72.

126. Sellier, P., et al., *Disrupted trabecular bone micro-architecture in middle-aged male HIV-infected treated patients.* HIV Med, 2016. **17**(7): p. 550-6.

127. Biver, E., et al., *Microstructural alterations of trabecular and cortical bone in long-term HIV-infected elderly men on successful antiretroviral therapy.* AIDS, 2014. **28**(16): p. 2417-27.

128. Bedimo, R.J., et al., *The Differential Effects of Human Immunodeficiency Virus and Hepatitis C Virus on Bone Microarchitecture and Fracture Risk.* Clin Infect Dis, 2018. **66**(9): p. 1442-1447.

129. Lo Re, V., 3rd, et al., *Structural Bone Deficits in HIV/HCV-Coinfected, HCV-Monoinfected, and HIV-Monoinfected Women.* J Infect Dis, 2015. **212**(6): p. 924-33.

130. T. Yin, M., et al., *Bone density and microarchitecture in hepatitis C and HIV-coinfected postmenopausal minority women.* Osteoporosis International, 2018. **29**(4): p. 871-879.

131. Guerri-Fernandez, R.C., et al., *Microindentation for in vivo measurement of bone tissue material properties in atypical femoral fracture patients and controls.* J Bone Miner Res, 2013. **28**(1): p. 162-8.

132. Triant, V.A., et al., *Fracture prevalence among human immunodeficiency virus (HIV)-infected versus non-HIV-infected patients in a large U.S. healthcare system.* J Clin Endocrinol Metab, 2008. **93**(9): p. 3499-504.

133. Richardson, J., et al., *Fracture healing in HIV-positive populations.* J Bone Joint Surg Br, 2008. **90**(8): p. 988-94.

134. Cheung, W.H., et al., *Fracture healing in osteoporotic bone.* Injury, 2016. **47 Suppl 2**: p. S21-6.

135. Baht, G.S., L. Vi, and B.A. Alman, *The Role of the Immune Cells in Fracture Healing.* Curr Osteoporos Rep, 2018. **16**(2): p. 138-145.

136. Toben, D., et al., *Fracture healing is accelerated in the absence of the adaptive immune system.* J Bone Miner Res, 2011. **26**(1): p. 113-24.

137. El Khassawna, T., et al., *T Lymphocytes Influence the Mineralization Process of Bone.* Front Immunol, 2017. **8**: p. 562.

138. Konnecke, I., et al., *T and B cells participate in bone repair by infiltrating the fracture callus in a two-wave fashion.* Bone, 2014. **64**: p. 155-65.

139. Bastian, O., et al., *Systemic inflammation and fracture healing.* J Leukoc Biol, 2011. **89**(5): p. 669-73.

140. Azevedo Filho, F.A., et al., *Reliability of the radiographic union scale in tibial fractures (RUST).* Rev Bras Ortop, 2017. **52**(1): p. 35-39.

141. Nandra, R., L. Grover, and K. Porter, *Fracture non-union epidemiology and treatment.* Trauma, 2016. **18**(1): p. 3-11.

142. Marsden, M.D. and J.A. Zack, *Humanized Mouse Models for Human Immunodeficiency Virus Infection.* Annu Rev Virol, 2017. **4**(1): p. 393-412.

143. Anderson, E.R.X., Huangui; Gendelman, Howard E., *Animal Model Systems of HIV-Diseases*, in *In vivo Models of HIV Disease and Control*, H. Friedman, S. Specter, and M. Bendinelli, Editors. 2006, Springer US. p. 19-43.

144. Vigorito, M., K.P. Connaghan, and S.L. Chang, *The HIV-1 transgenic rat model of neuroHIV.* Brain Behav Immun, 2015. **48**: p. 336-49.

145. Villarroya, F., P. Domingo, and M. Giralt, *Drug-induced lipotoxicity: lipodystrophy associated with HIV-1 infection and antiretroviral treatment.* Biochim Biophys Acta, 2010. **1801**(3): p. 392-9.

146. Carroll, V.A., et al., *Expression of HIV-1 matrix protein p17 and association with B-cell lymphoma in HIV-1 transgenic mice.* Proc Natl Acad Sci U S A, 2016. **113**(46): p. 13168-13173.

147. Curreli, S., et al., *B cell lymphoma in HIV transgenic mice.* Retrovirology, 2013. **10**: p. 92.

148. Abbondanzo, S.J. and S.L. Chang, *HIV-1 transgenic rats display alterations in immunophenotype and cellular responses associated with aging.* PLoS One, 2014. **9**(8): p. e105256.

149. Davinelli, S., et al., *Altered expression pattern of Nrf2/HO-1 axis during accelerated-senescence in HIV-1 transgenic rat.* Biogerontology, 2014. **15**(5): p. 449-61.

150. Reid, W., et al., *HIV-1 transgenic rats develop T cell abnormalities.* Virology, 2004. **321**(1): p. 111-9.

151. Duan, M., et al., *HIV Tat induces expression of ICAM-1 in HUVECs: implications for miR-221/-222 in HIV-associated cardiomyopathy.* PLoS One, 2013. **8**(3): p. e60170.

152. Fiala, M., et al., *HIV-1 induces cardiomyopathyby cardiomyocyte invasion and gp120, Tat, and cytokine apoptotic signaling.* Cardiovasc Toxicol, 2004. **4**(2): p. 97-107.

153. Lund, A.K., et al., *Human immunodeficiency virus transgenic rats exhibit pulmonary hypertension.* Am J Physiol Lung Cell Mol Physiol, 2011. **301**(3): p. L315-26.

154. Porter, K.M., et al., *Human immunodeficiency virus-1 transgene expression increases pulmonary vascular resistance and exacerbates hypoxia-induced pulmonary hypertension development.* Pulm Circ, 2013. **3**(1): p. 58-67.

155. McLaurin, K.A., R.M. Booze, and C.F. Mactutus, *Evolution of the HIV-1 transgenic rat: utility in assessing the progression of HIV-1-associated neurocognitive disorders.* J Neurovirol, 2018. **24**(2): p. 229-245.

156. Banerjee, A., et al., *Increased Sensitivity to Binge Alcohol-Induced Gut Leakiness and Inflammatory Liver Disease in HIV Transgenic Rats.* PLoS One, 2015. **10**(10): p. e0140498.

157. Sarkar, S., et al., *Age- and ethanol concentration-dependent effects of acute binge drinking in the HIV-1 transgenic rat.* Alcohol Clin Exp Res, 2013. **37 Suppl 1**: p. E70-8.

158. Rosenstiel, P., et al., *Transgenic and infectious animal models of HIV-associated nephropathy.* J Am Soc Nephrol, 2009. **20**(11): p. 2296-304.

159. Thaney, V.E., et al., *Transgenic mice expressing HIV-1 envelope protein gp120 in the brain as an animal model in neuroAIDS research.* J Neurovirol, 2018. **24**(2): p. 156-167.

160. Hanna, Z., et al., *Transgenic mice expressing human immunodeficiency virus type 1 in immune cells develop a severe AIDS-like disease.* J Virol, 1998. **72**(1): p. 121-32.

161. Springer, R., C. Aparicio, and K. Mansky, *Mechanical Properties of HIV-Infected and Tenofovir-Treated Bone.* Journal of Dental Research, 2017. **96**(A:2170).

162. Lafferty, M.K., et al., *Elevated suppressor of cytokine signaling-1 (SOCS-1): a mechanism for dysregulated osteoclastogenesis in HIV transgenic rats.* Pathog Dis, 2014. **71**(1): p. 81-9.

163. Schouten, J., et al., *Cross-sectional comparison of the prevalence of age-associated comorbidities and their risk factors between HIV-infected and uninfected individuals: the AGEhIV cohort study.* Clin Infect Dis, 2014. **59**(12): p. 1787-97.

164. Yin, M.T. and J. Falutz, *How to predict the risk of fracture in HIV?* Curr Opin HIV AIDS, 2016. **11**(3): p. 261-7.

165. Hernandez, C.J. and T.M. Keaveny, *A biomechanical perspective on bone quality.* Bone, 2006. **39**(6): p. 1173-81.

166. McDonnell, P., P.E. McHugh, and D. O'Mahoney, *Vertebral osteoporosis and trabecular bone quality.* Ann Biomed Eng, 2007. **35**(2): p. 170-89.

167. Niu, F., et al., *Tat 101-mediated enhancement of brain pericyte migration involves platelet-derived growth factor subunit B homodimer: implications for human immunodeficiency virus-associated neurocognitive disorders.* J Neurosci, 2014. **34**(35): p. 11812-25.

168. Duvall, C.L., et al., *Impaired angiogenesis, early callus formation, and late stage remodeling in fracture healing of osteopontin-deficient mice.* J Bone Miner Res, 2007. **22**(2): p. 286-97.

169. Buie, H.R., et al., *Automatic segmentation of cortical and trabecular compartments based on a dual threshold technique for in vivo micro-CT bone analysis.* Bone, 2007. **41**(4): p. 505-15.

170. Street, J., et al., *Vascular endothelial growth factor stimulates bone repair by promoting angiogenesis and bone turnover.* Proc Natl Acad Sci U S A, 2002. **99**(15): p. 9656-61.

171. Turner, C.H. and D.B. Burr, *Basic biomechanical measurements of bone: a tutorial.* Bone, 1993. **14**(4): p. 595-608.

172. Jilka, R.L., *The relevance of mouse models for investigating age-related bone loss in humans.* J Gerontol A Biol Sci Med Sci, 2013. **68**(10): p. 1209-17.

173. Glatt, V., et al., *Age-related changes in trabecular architecture differ in female and male C57BL/6J mice.* J Bone Miner Res, 2007. **22**(8): p. 1197-207.

174. Bruggeman, L.A., et al., *Patterns of HIV-1 mRNA expression in transgenic mice are tissue-dependent.* Virology, 1994. **202**(2): p. 940-8.

175. Skowronski, J., D. Parks, and R. Mariani, *Altered T cell activation and development in transgenic mice expressing the HIV-1 nef gene.* EMBO J, 1993. **12**(2): p. 703-13.

176. Weng, X., et al., *CD4+ T cells from CD4C/HIVNef transgenic mice show enhanced activation in vivo with impaired proliferation in vitro but are dispensable for the development of a severe AIDS-like organ disease.* J Virol, 2004. **78**(10): p. 5244-57.

177. Fiume, G., et al., *Impairment of T cell development and acute inflammatory response in HIV-1 Tat transgenic mice.* Sci Rep, 2015. **5**: p. 13864.

178. Haffner-Luntzer, M., et al., *Mouse Models in Bone Fracture Healing Research.* Current Molecular Biology Reports, 2016. **2**(2): p. 101-111.

179. Nam, D., et al., *T-lymphocytes enable osteoblast maturation via IL-17F during the early phase of fracture repair.* PLoS One, 2012. **7**(6): p. e40044.

180. Behrends, D.A., et al., *Defective Bone Repair in C57Bl6 Mice With Acute Systemic Inflammation.* Clinical Orthopaedics and Related Research®, 2017. **475**(3): p. 906-916.

181. Rana, A.K., et al., *Delayed Bone Regeneration Is Linked to Chronic Inflammation in Murine Muscular Dystrophy.* Journal of Bone and Mineral Research, 2014. **29**(2): p. 304-315.

182. Albini, A., et al., *The angiogenesis induced by HIV-1 tat protein is mediated by the Flk-1/KDR receptor on vascular endothelial cells.* Nat Med, 1996. **2**(12): p. 1371-5.

183. Barillari, G. and B. Ensoli, *Angiogenic effects of extracellular human immunodeficiency virus type 1 Tat protein and its role in the pathogenesis of AIDS-associated Kaposi's sarcoma.* Clin Microbiol Rev, 2002. **15**(2): p. 310-26.

184. Basta, D., et al., *Angiogenic, lymphangiogenic and adipogenic effects of HIV-1 matrix protein p17.* Pathog Dis, 2015. **73**(8): p. ftv062.

185. Conroy, A.L., et al., *Altered angiogenesis as a common mechanism underlying preterm birth, small for gestational age, and stillbirth in women living with HIV.* Am J Obstet Gynecol, 2017. **217**(6): p. 684 e1-684 e17.

186. Beamer, W.G., et al., *Genetic variability in adult bone density among inbred strains of mice.* Bone, 1996. **18**(5): p. 397-403.

187. Devlin, M.J., et al., *Differential effects of high fat diet and diet-induced obesity on skeletal acquisition in female C57BL/6J vs. FVB/NJ Mice.* Bone Reports, 2018. **8**: p. 204-214.

188. Moran, M.M., et al., *Intramembranous bone regeneration differs among common inbred mouse strains following marrow ablation.* J Orthop Res, 2015. **33**(9): p. 1374-81.

189. UNAIDS, *Global AIDS Update*. 2016, Joint United Nations Programme on HIV/AIDS.

190. Piggott, D.A., K.M. Erlandson, and K.E. Yarasheski, *Frailty in HIV: Epidemiology, Biology, Measurement, Interventions, and Research Needs.* Curr HIV/AIDS Rep, 2016. **13**(6): p. 340-348.

191. Smit, M., et al., *Future challenges for clinical care of an ageing population infected with HIV: a modelling study.* Lancet Infect Dis, 2015. **15**(7): p. 810-8.

192. Yin, M.T. and T.T. Brown, *HIV and Bone Complications: Understudied Populations and New Management Strategies.* Curr HIV/AIDS Rep, 2016. **13**(6): p. 349-358.

193. Hernandez, C.J., G.S. Beaupre, and D.R. Carter, *A theoretical analysis of the relative influences of peak BMD, age-related bone loss and menopause on the development of osteoporosis.* Osteoporos Int, 2003. **14**(10): p. 843-7.

194. Burt, L.A., et al., *Lower Bone Density, Impaired Microarchitecture, and Strength Predict Future Fragility Fracture in Postmenopausal Women: 5-Year Follow-up of the Calgary CaMos Cohort.* J Bone Miner Res, 2018. **33**(4): p. 589-597.

195. Cooper, C., et al., *Review: developmental origins of osteoporotic fracture.* Osteoporos Int, 2006. **17**(3): p. 337-47.

196. Weitzmann, M.N., et al., *Bone Loss Among Women Living With HIV.* Curr HIV/AIDS Rep, 2016. **13**(6): p. 367-373.

197. Lelovas, P.P., et al., *The laboratory rat as an animal model for osteoporosis research.* Comp Med, 2008. **58**(5): p. 424-30.

198. Peng, J., et al., *The HIV-1 transgenic rat as a model for HIV-1 infected individuals on HAART.* J Neuroimmunol, 2010. **218**(1-2): p. 94-101.

199. CDC, *Guidelines for Survial Bleeding of Mice and Rats*, N.I.o.H.-O.o.A.C.a. Use, Editor. 2010.

200. Francisco, J.I., et al., *Relationship between age, skeletal site, and time post-ovariectomy on bone mineral and trabecular microarchitecture in rats.* J Orthop Res, 2011. **29**(2): p. 189-96.

201. Kim, B.T., et al., *The structural and hormonal basis of sex differences in peak appendicular bone strength in rats.* J Bone Miner Res, 2003. **18**(1): p. 150-5.

202. Erlandson, K.M., et al., *Bone Mineral Density Declines Twice as Quickly Among HIV-Infected Women Compared With Men.* JAIDS Journal of Acquired Immune Deficiency Syndromes, 2018. **77**(3): p. 288-294.

203. Gedmintas, L., et al., *Comparative risk of fracture in men and women with HIV.* J Clin Endocrinol Metab, 2014. **99**(2): p. 486-90.

204. Pietschmann, P., et al., *Osteoporosis: an age-related and gender-specific disease--a mini-review.* Gerontology, 2009. **55**(1): p. 3-12.

205. Adler, R.A., *Osteoporosis in men: a review.* Bone Res, 2014. **2**: p. 14001.

206. McLaurin, K.A., R.M. Booze, and C.F. Mactutus, *Selective developmental alterations in The HIV-1 transgenic rat: Opportunities for diagnosis of pediatric HIV-1.* J Neurovirol, 2017. **23**(1): p. 87-98.

207. Nemeth, C.L., et al., *Meloxicam blocks neuroinflammation, but not depressive-like behaviors, in HIV-1 transgenic female rats.* PLoS One, 2014. **9**(10): p. e108399.

208. Roscoe, R.F., Jr., C.F. Mactutus, and R.M. Booze, *HIV-1 transgenic female rat: synaptodendritic alterations of medium spiny neurons in the nucleus accumbens.* J Neuroimmune Pharmacol, 2014. **9**(5): p. 642-53.

209. Burge, R., et al., *Incidence and economic burden of osteoporosis-related fractures in the United States, 2005-2025.* J Bone Miner Res, 2007. **22**(3): p. 465-75.

210. Boutroy, S., et al., *In vivo assessment of trabecular bone microarchitecture by high-resolution peripheral quantitative computed tomography.* J Clin Endocrinol Metab, 2005. **90**(12): p. 6508-15.

211. Harvey, N.C., et al., *Trabecular bone score (TBS) as a new complementary approach for osteoporosis evaluation in clinical practice.* Bone, 2015. **78**: p. 216-24.

212. Yadav, A., et al., *HIV-1 transgenic rat CD4+ T cells develop decreased CD28 responsiveness and suboptimal Lck tyrosine dephosphorylation following activation.* Virology, 2006. **353**(2): p. 357-65.

213. Homji, N.F., et al., *Endotoxin-induced cytokine and chemokine expression in the HIV-1 transgenic rat.* J Neuroinflammation, 2012. **9**: p. 3.

214. Mauffrey, C., B.T. Barlow, and W. Smith, *Management of segmental bone defects.* J Am Acad Orthop Surg, 2015. **23**(3): p. 143-53.

215. Wu, N., et al., *Economic burden of illness among US patients experiencing fracture nonunion.* Orthopedic Research and Reviews, 2013. **5**: p. 21-33.

216. Harrison, W.J., C.P. Lewis, and C.B. Lavy, *Wound healing after implant surgery in HIV-positive patients.* J Bone Joint Surg Br, 2002. **84**(6): p. 802-6.

217. Harrison, W.J., C.B. Lavy, and C.P. Lewis, *One-year follow-up of orthopaedic implants in HIV-positive patients.* Int Orthop, 2004. **28**(6): p. 329-32.

218. Bahebeck, J., et al., *Implant orthopaedic surgery in HIV asymptomatic carriers: management and early outcome.* Injury, 2009. **40**(11): p. 1147-50.

219. Xu, G., et al., *Analysis of the surgical treatment of fracture in HIV positive patients: A clinical study.* Pak J Med Sci, 2017. **33**(6): p. 1449-1453.

220. Leow, J.M., et al., *The radiographic union scale in tibial (RUST) fractures: Reliability of the outcome measure at an independent centre.* Bone Joint Res, 2016. **5**(4): p. 116-21.

221. Yadav, A., et al., *Increased expression of suppressor of cytokine signaling-1 (SOCS-1): A mechanism for dysregulated T helper-1 responses in HIV-1 disease.* Virology, 2009. **385**(1): p. 126-33.

222. Oest, M.E., et al., *Quantitative assessment of scaffold and growth factor-mediated repair of critically sized bone defects.* J Orthop Res, 2007. **25**(7): p. 941-50.

223. Kolambkar, Y.M., et al., *An alginate-based hybrid system for growth factor delivery in the functional repair of large bone defects.* Biomaterials, 2011. **32**(1): p. 65-74.

224. Boerckel, J.D., et al., *Mechanical regulation of vascular growth and tissue regeneration in vivo.* Proc Natl Acad Sci U S A, 2011. **108**(37): p. E674-80.

225. Priddy, L.B., et al., *Spatiotemporal Gene Expression Patterns as a Function of BMP-2 Dose in Early Segmental Bone Defect Regeneration.* Tissue Engineering Part A, 2015. **21**: p. S148-S149.

226. Egermann, M., J. Goldhahn, and E. Schneider, *Animal models for fracture treatment in osteoporosis.* Osteoporos Int, 2005. **16 Suppl 2**: p. S129-38.

227. von Ruden, C. and P. Augat, *Failure of fracture fixation in osteoporotic bone.* Injury, 2016. **47 Suppl 2**: p. S3-S10.

228. Lissenberg-Thunnissen, S.N., et al., *Use and efficacy of bone morphogenetic proteins in fracture healing.* Int Orthop, 2011. **35**(9): p. 1271-80.

229. Boerckel, J.D., et al., *Effects of protein dose and delivery system on BMP-mediated bone regeneration.* Biomaterials, 2011. **32**(22): p. 5241-51.

230. McGinty, T., et al., *Does systemic inflammation and immune activation contribute to fracture risk in HIV?* Curr Opin HIV AIDS, 2016. **11**(3): p. 253-60.

231. Gibon, E., L. Lu, and S.B. Goodman, *Aging, inflammation, stem cells, and bone healing.* Stem Cell Res Ther, 2016. **7**: p. 44.

232. Gibon, E., et al., *Inflammation, ageing, and bone regeneration.* J Orthop Translat, 2017. **10**: p. 28-35.

233. Clark, D., et al., *Effects of Aging on Fracture Healing.* Curr Osteoporos Rep, 2017. **15**(6): p. 601-608.

234. Meyer, R.A., Jr., et al., *Young, adult, and old rats have similar changes in mRNA expression of many skeletal genes after fracture despite delayed healing with age.* J Orthop Res, 2006. **24**(10): p. 1933-44.

235. Meyer, R.A., et al., *Delayed union of femoral fractures in older rats:decreased gene expression.* BMC Musculoskelet Disord, 2001. **2**: p. 2.

236. Meyer, R.A., Jr., et al., *Age and ovariectomy impair both the normalization of mechanical properties and the accretion of mineral by the fracture callus in rats.* J Orthop Res, 2001. **19**(3): p. 428-35.

237. Ode, A., et al., *Interaction of age and mechanical stability on bone defect healing: an early transcriptional analysis of fracture hematoma in rat.* PLoS One, 2014. **9**(9): p. e106462.

238. Meyer, R.A., Jr., et al., *Gene expression in older rats with delayed union of femoral fractures.* J Bone Joint Surg Am, 2003. **85-A**(7): p. 1243-54.

239. Dutta, S. and P. Sengupta, *Men and mice: Relating their ages.* Life Sci, 2016. **152**: p. 244-8.

240. Sengupta, P., *The Laboratory Rat: Relating Its Age With Human's.* Int J Prev Med, 2013. **4**(6): p. 624-30.

241. Paiardini, M. and M. Muller-Trutwin, *HIV-associated chronic immune activation.* Immunol Rev, 2013. **254**(1): p. 78-101.

242. Ruffin, N., et al., *The impact of inflammation and immune activation on B cell differentiation during HIV-1 infection.* Front Immunol, 2011. **2**: p. 90.

243. Lorenzo-Redondo, R., et al., *Persistent HIV-1 replication maintains the tissue reservoir during therapy.* Nature, 2016. **530**(7588): p. 51-56.

244. Mzingwane, M.L. and C.T. Tiemessen, *Mechanisms of HIV persistence in HIV reservoirs.* Rev Med Virol, 2017. **27**(2).

245. Nowlan, N.C., et al., *Mechanobiology of embryonic skeletal development: Insights from animal models.* Birth Defects Res C Embryo Today, 2010. **90**(3): p. 203-13.

246. Young, S., et al., *Complications after intramedullary nailing of femoral fractures in a low-income country.* Acta Orthop, 2013. **84**(5): p. 460-7.

247. Garcia, P., et al., *Rodent animal models of delayed bone healing and non-union formation: a comprehensive review.* Eur Cell Mater, 2013. **26**: p. 1-12; discussion 12-4.

248. Agarwal-Harding, K.J., et al., *Estimating the global incidence of femoral fracture from road traffic collisions: a literature review.* J Bone Joint Surg Am, 2015. **97**(6): p. e31.

249. Young, S., et al., *Risk factors for infection after 46,113 intramedullary nail operations in low- and middle-income countries.* World J Surg, 2013. **37**(2): p. 349-55.

250. Hansen, L., et al., *Azidothymidine (AZT) leads to arterial stiffening and intima-media thickening in mice.* J Biomech, 2013. **46**(9): p. 1540-7.

251. Pan, G., et al., *AZT enhances osteoclastogenesis and bone loss.* AIDS Res Hum Retroviruses, 2004. **20**(6): p. 608-20.

252. Ofotokun, I., et al., *Role of T-cell reconstitution in HIV-1 antiretroviral therapy-induced bone loss.* Nat Commun, 2015. **6**: p. 8282.